AD_____

Award Number: DAMD17-99-1-9443

TITLE: Role of RAD6, a DNA Repair Gene, in Tumor Progression and Drug Resistance

PRINCIPAL INVESTIGATOR: Malathy P.V. Shekhar, Ph.D.

CONTRACTING ORGANIZATION: Wayne State University
Detroit, MI 48201

REPORT DATE: August 2003

TYPE OF REPORT: Final

PREPARED FOR: U.S. Army Medical Research and Materiel Command
Fort Detrick, Maryland 21702-5012

DISTRIBUTION STATEMENT: Approved for Public Release;
Distribution Unlimited

The views, opinions and/or findings contained in this report are those of the author(s) and should not be construed as an official Department of the Army position, policy or decision unless so designated by other documentation.

20040226 068

REPORT DOCUMENTATION PAGE

Form Approved
OMB No. 074-0188

Public reporting burden for this collection of information is estimated to average 1 hour per response, including the time for reviewing instructions, searching existing data sources, gathering and maintaining the data needed, and completing and reviewing this collection of information. Send comments regarding this burden estimate or any other aspect of this collection of information, including suggestions for reducing this burden to Washington Headquarters Services, Directorate for Information Operations and Reports, 1215 Jefferson Davis Highway, Suite 1204, Arlington, VA 22202-4302, and to the Office of Management and Budget, Paperwork Reduction Project (0704-0188), Washington, DC 20503

1. AGENCY USE ONLY (Leave blank)	2. REPORT DATE	3. REPORT TYPE AND DATES COVERED
	August 2003	Final (1 Jul 1999 - 1 Jul 2003)

4. TITLE AND SUBTITLE
Role of RAD6, a DNA Repair Gene, in Tumor Progression and Drug Resistance

5. FUNDING NUMBERS
DAMD17-99-1-9443

6. AUTHOR(S)
Malathy P.V. Shekhar, Ph.D.

7. PERFORMING ORGANIZATION NAME(S) AND ADDRESS(ES)
Wayne State University
Detroit, MI 48201

E-Mail: shekharm@kci.wayne.edu

8. PERFORMING ORGANIZATION REPORT NUMBER

9. SPONSORING / MONITORING AGENCY NAME(S) AND ADDRESS(ES)
U.S. Army Medical Research and Materiel Command
Fort Detrick, Maryland 21702-5012

10. SPONSORING / MONITORING AGENCY REPORT NUMBER

11. SUPPLEMENTARY NOTES
Original contains color plates: ALL DTIC reproductions will be in black and white

12a. DISTRIBUTION / AVAILABILITY STATEMENT
Approved for Public Release; Distribution Unlimited

12b. DISTRIBUTION CODE

13. ABSTRACT (Maximum 200 Words)

The goal of this IDEA award was to understand the role of Rad6B, a key mediator of postreplication DNA repair (PRR), in breast tumor progression and drug resistance. Results of our study demonstrated that Rad6B plays a critical role in maintenance of genomic integrity of human breast cells, as imbalances in Rad6B levels induced by experimental manipulation (and observed in human breast tumors) cause loss of cell polarity and genomic instability which correlate with alterations in chemosensitivity and PRR capacities. Rad6B forms supramolecular complexes with p53, p14ARF and Mdm2, and inclusion of p14ARF and Mdm2 into Rad6-p53 complexes is dependent upon exposure to DNA damaging agent. Recombinant Rad6B mediates monoubiquitination of p53. That monoubiquitinated p53 functions in DNA damage-induced response is evident as G2/M arrest and p53 response observed in normal MCF10A breast cells following DNA damage is associated with parallel increases in monoubiquitinated p53. Loss of cell polarity induced by Rad6B overexpression appears to be a result of dysregulation in Wnt and Rho signaling pathways. Samples accrued from patients post-chemotherapy shows differential distribution of Rad6 in cytoplasmic versus nuclear compartments, and our preliminary data suggest that recruitment of Rad6 into nucleus following chemotherapy may predict favorable treatment outcome.

14. SUBJECT TERMS
Postreplication repair, Rad6-p53 interaction, chemosensitivity, loss of cell polarity, regulation of expression, cDNA array

15. NUMBER OF PAGES
81

16. PRICE CODE

17. SECURITY CLASSIFICATION OF REPORT	18. SECURITY CLASSIFICATION OF THIS PAGE	19. SECURITY CLASSIFICATION OF ABSTRACT	20. LIMITATION OF ABSTRACT
Unclassified	Unclassified	Unclassified	Unlimited

Table of Contents

Cover.....1

SF 298.....2

Table of Contents.....3

Introduction.....4

Body.....4

Key Research Accomplishments.....10

Reportable Outcomes.....11

Conclusions.....12

References.....12

Appendices.....14

INTRODUCTION

The RAD6 group is concerned with 'post-replication' error-free and error-prone repair (1). The RAD6 gene encodes a 17 kDa protein (2) which is one of a group of ubiquitin conjugating (E2) enzymes (3)that covalently add ubiquitin to selected lysine residues. The RAD6 pathway appears to be regulated by posttranslational modification of target proteins with ubiquitin, which commits them to rapid proteolysis. The RAD6 gene of *Saccharomyces cerevisiae* is required for a variety of cellular functions including DNA repair, induced mutagenesis and sporulation (4, 5). *rad6* mutant phenotypic effects include slow growth, severe defects in induced mutagenesis, extreme sensitivity to UV, X-ray and chemical mutagens and hypersensitivity to antifolate drug metabolites (6,7). The diversity of the phenotypes of *rad6* mutants suggests that the RAD6 gene product is central to cell cycle regulation. RAD6 is highly conserved among eukaryotes. Two closely related human Rad6 homologues, HHR6A and HHR6B (human homologues of yeast RAD6), encode ubiquitin conjugating enzymes (E2) and complement the DNA repair and UV mutagenesis defects of the *S. cerevisiae rad6* mutant (8). HHR6A and HHR6B share 95% identical amino acid residues and are localized on human chromosome Xq24-q25 and 5q23-q31, respectively (9). Inactivation of the gene encoding HR6B in mice leads to male sterility (10).

The goals of our IDEA award were to determine whether aberrant activation of the RAD6-mediated stress response pathway is responsible: i) for the ability of malignant cells to resist cytotoxic chemotherapy and radiation, and/or ii) for increased aggressiveness of tumor following chemotherapy. Aberrant activation of the Rad6 pathway can potentially contribute to these phenotypes by increased error-free or error-prone translesion bypass postreplication repair pathways. Towards understanding the role of Rad6 in breast cancer progression and drug resistance, we had proposed to:

1. Compare the effects of wild type RAD6, mutant RAD6 (C88A) and antisense RAD6 in normal and metastatic human breast cancer cells with respect to *in vivo* growth, RAD6-associated ubiquitin conjugating activity, RAD6 distribution, sensitivity to chemotherapy (cisplatin, adriamycin, and radiation) and DNA repair efficiency.
2. Determine whether RAD6 expression correlates with breast tumor stage of progression and p53 status.
3. Determine whether RAD6 expression, patterns of distribution and activity can be used as a marker to predict response/resistance to chemotherapy.

BODY OF PROPOSAL

Tasks proposed in Aims 1 and 2 form the basis of two publications, three abstracts and a submitted manuscript.

Publication 1.
RAD6 overexpression induces centrosome amplification, abnormal mitosis, aneuploidy and transformation. Shekhar P.V.M., Lyakhovich A., Heng H., Visscher D.W. and Kondrat N. Cancer Res., 62:2115-2124, 2002.
In this article, we have a) characterized the structural and functional aspects of Rad6B gene in normal and cancerous breast cells, b) correlated Rad6 expression with breast tumor stage, c) measured ubiquitin conjugating activity of Rad6 in breast cells, d) evaluated the consequences of Rad6B overexpression in normal breast cells, e) evaluated Rad6 expression and distribution during mitosis, f) demonstrated ability of Rad6-overexpressing clones for anchorage-independent growth, and f) demonstrated importance of Rad6B in the maintenance of genomic stability.

Publication 2.
Supramolecular complex formation between Rad6 and proteins of p53 pathway during DNA damage-induced response. Lyakhovich, A and Shekhar, P.V.M. Mol. and Cell. Biol., 23: 2463-2475, 2003.
In this article, we have discussed a) regulation of Rad6 gene expression by DNA damaging agents, viz., cisplatin and adriamycin, b) interaction between Rad6 and p53, c) regulation of Rad6-p53 interaction by DNA damage-induced response, d) effect of adriamycin on expression and localization of Rad6, p53 and Mdm2 in normal breast cells, e) differences in stability and longevity of G2/M checkpoint in normal and metastatic human breast cells, f)

characterization of Rad6 ubiquitin conjugating activity: mono- versus poly-ubiquitination, and g) ability of Rad6 to monoubiquitinate p53, and h) DNA damage-induced P53 response is accompanied by an increase in levels of monoubiquitinated p53.

Submitted manuscript.
Chemosensitivity of human breast cells correlates with Rad6B expression and postreplication repair capacity. Shekhar P.V.M. and Lyakhovich A.
In this article, we have demonstrated: a) Rad6 expression is maximal during late S/G2 phase of cell cycle, b) induction of Rad6B gene expression by adriamycin, c) adriamycin-induced Rad6B gene expression is primarily regulated at the transcriptional level, d) overexpression of Rad6B gene confers resistance to cisplatin and adriamycin, e) depletion of Rad6B causes extreme sensitivity to cisplatin and adriamycin, f) DNA damage-induced response is accompanied by redistribution of Rad6 to the chromatin, and g) Rad6B-overexpressing human breast cells are postreplication repair-proficient as opposed to Rad6B-depleted cells that are postreplication repair-compromised.

***In vivo* characterization of Rad6B transfectants in nude mice.** This experiment has been initiated in June 2003 and is expected to be completed in September 2003. Completion of this aspect was delayed due to unforseen circumstances that included changes in personnel and personal reasons. The latter involved making emergency trips overseas to take care of ill and convalescing parents followed by an emergency trip upon demise of my parent.

Method. Nude mice were injected in the mammary fat pads with 1 x 10^7 cells suspended in Matrigel. The following cells were injected: MCF10A cells stably transfected with empty vector pCMV-neo, and three stable clones of MCF10A cells expressing exogenous Rad6B gene. Clones 1 and 5 express ~ 30-50 -fold higher levels of Rad6B as compared to vector control, and clone 2 expresses approximately similar levels of Rad6B as compared to vector controls. Lesions will be harvested (if present), and portions of the lesions will be fixed in formalin and paraffin-embedded for histological analysis, and remaining portions digested with collagenase for recovery of cells that will be used for evaluating expression levels of Rad6 and sensitivity to chemotherapeutic drugs. Results from *in vitro* assays (Rad6 expression and drug sensitivity) will be correlated with the morphology and histotypes of lesions produced, expression levels and distribution of Rad6, and expression and distribution of Rad18, p53, PCNA and Mdr-1 P-glycoprotein in the lesions. Since MCF10A-Rad6B clones 1 and 5 exhibit anchorage-independent growth and show aneuploidy, results on their ability to grow *in vivo* as a function of Rad6B levels are expected to yield intriguing information.

Rad6B overexpression induces loss of cell polarity. A striking consequence of constitutive Rad6B overexpression in normal human breast epithelial cells is generation of multinucleated cells, centrosome amplification, abnormal mitosis and aneuploidy. Our data suggest that multinucleated cells arise from 1) abnormal mitosis accompanied by defective cytokinesis, and 2) cell-cell fusion. In order to identify the molecular changes that perhaps contribute to genomic instability of Rad6B-overexpressing clones, we performed cDNA array analysis. mRNAs from vector-transfected MCF10A cells and MCF10A-Rad6B-overexpressing clone 5 cells were reverse transcribed in the presence of [α-^{32}P]-dCTP and hybridized to Atlas human cancer arrays (Clontech, Palo Alto, CA). The cancer arrays contain cDNAs for DNA repair, cell cycle, intermediate filaments, apoptosis, G-proteins, adhesion proteins, invasion and metastasis, and growth regulators (signal transduction). The membranes were analyzed with Atlas 2.0 software. Table 1 shows the results of differential expression of genes between MCF10A-neo and MCF10A-Rad6B clone 5 cells. It is interesting to note that the analysis revealed differential expression of several markers that have been reported to influence cell-cell interactions at the cell membrane. In particular, alterations in the Wnt signaling pathway appear to be an important feature in cells overexpressing Rad6B. The validity of the markers identified by cDNA array analysis was tested by Western blot analysis to determine if differences in mRNA levels reflected similar differences in steady-state levels of these proteins. Specifically, levels of E-cadherin, β-catenin, APC, RhoA,

Table 1. Analysis of differential gene expression in MCF10A versus MCF10A-Rad6 cells by cDNA expression array (Atlas Human Cancer Array).

	MCF10A-Rad6	MCF10A-Neo
5-10X		
keratin 1(epidermolytic hyperkeratosis)	7.2 ↑	
Dissheveled homolog 1 (segment polarity protein)	8.7 ↑	
cell division protein kinase (CDK4)	6.8 ↑	
cdc2-related protein kinase PISSLRE	6.2 ↑	
CD40 receptor associated factor 1	7 ↑	
ubiquitin conjugating enzyme (HHR6A/B)	6 ↑	
2 - 5X		
cdc42 GTPase	4 ↓	
nm23H1	4 ↑	
nm23H2S	3 ↓	
integrin β-8 precursor	4 ↑	
cysteine-rich FGF GLG1	4.7 ↑	
cell division protein kinase 6	4.9 ↑	
G1/S specific cyclin D1 (CCND1)	3.7 ↑	
APC	3.8 ↑	
rho-associated protein kinase p160ROCK	3.7 ↑	
cdc2-related protein kinase CHED	3.8 ↑	
ninjurin-1	3.4 ↑	
laminin 3 kDa receptor	3.4 ↑	
tyrosine-protein kinase receptor tyro3 precursor; rse, sky, dtk	3.3 ↑	
cyclin H (CCnH1); mO15 -associated protein	3 ↑	
desmocollin 3 + desmocollin 4	3 ↑	
VEGF	3 ↑	
G2/mitotic specific cyclin G1 (CCNG1)	3 ↑	
cell division control protein 2 homolog (cdc2); p34 protein	2.9 ↑	
caveolin-2	2.3 ↑	
caspase 10 precursor	2.5 ↑	
cadherin precursor-2	2 ↑	
cadherin -4 precursor	4 ↑	
cadherin-6 precursor	2 ↑	
cadherin-11 precursor	1.5 ↑	
cadherin-12 precursor	2 ↑	
wnt-5a	3 ↑	
Dissheveled 3	2 ↑	
EGFR	2 ↓	
replication factor C 38 kDa subunit (RFC38)	1.9 ↑	
β-catenin	2 ↓	

cdc42-GTPase and Rad6 were examined. Results of Western blot analysis revealed that MCF10A-Rad6 clone 5 cells expressed ~ 50-, 2-, and 7-fold higher levels of Rad6, E-cadherin, and APC proteins as compared to vector controls. However, no significant differences in steady-state levels of β-catenin and cdc42-GTPase proteins were detected by Western blot analysis (Fig. 1). Expression and distribution of Rad6, β-catenin, RhoA, RhoC and cdc42-GTPase proteins were examined by immunofluorescence staining. Results in Figs. 2 and 3 show that Rad6B overexpressing MCF10A cells not only express higher levels of RhoA and RhoC proteins but also show high levels of RhoA and RhoC in the nucleus. That Rad6B-overexpressing cells express not only display higher levels of total RhoA but also contain high levels of RhoA in the nucleus was confirmed by affinity pull-down (Rhotek beads) of total cell extracts, and fractionated cytosolic and nuclear extracts from vector control and Rad6B-overexpressing MCF10A cells (Fig. 4). These data also showed that majority of RhoA present in the nucleus of Rad6B-overexpressing cells are in their active GTP-bound state (data not shown). Rho family of GTPases, including RhoA has been implicated in establishment of epithelial planar polarity in Drosophila, a process mediated by the receptor Frizzled (Fz) and Wnt signaling pathway (11). Our data on nuclear RhoA signaling have formed the basis of two grant applications submitted by our collaborator (see Reportable outcomes).

Consistent with Western blot data, no differences in cdc42-GTPase were observed between vector control

and Rad6B-overexpressing MCF10A cells (data not shown). Similar detection of β-catenin by immunofluorescence staining revealed dramatic differences in levels and distribution pattern of β-catenin between vector control and Rad6B-overexpressing cells (Figs. 5 and 6). Whereas majority of β-catenin circumscribed the cell membranes of vector controls, β-catenin staining was diffuse and pervasive (Figs. 5 and 6), present in perinuclear and nuclear compartments, and associated with crinkled cell membranes in Rad6B-overexpression MCF10A cells (Fig. 5).

Detection of loss of cell polarity in Rad6B-overexpressing clones of MCF10A cells. Vector control or Rad6B-overexpressing MCF10A cells, clones 1 or 5 (100 x 10^3 cells) were suspended in Matrigel and plated in 8-well chamber slides. At 5 days, the Matrigel plugs were recovered from the chamber slides, fixed in buffered formalin and paraffin-embedded. Sections (6 μm) were analyzed for morphology and expression of Rad6, β-catenin, E-cadherin, RhoA, PCNA, and Epithelial mucin antigen (EMA) by H&E staining and immunohistochemistry, respectively. Whereas three-dimensional spheroids (acinar structures) formed by vector control MCF10A cells display polarized oraganization, contained fewer cells, and showed the presence of (or the beginning of formation) of central lumen (revealed by EMA staining), spheroids formed from Rad6b-overexpressing cells displayed loose clusters of nonpolarized cells with irregular or absence of central lumen (Fig. 7). High levels of Rad6 expression were observed in the nuclei, combined with higher levels of E-cadherin, β-catenin, PCNA and RhoA in Rad6-overexpressing clones as compared to empty vector-transfected MCF10A cells (Fig. 8, 9 and 10).

The integrity of epithelia relies upon formation and organization of epithelial cell junctions, and c ell junctions often become disrupted as tumors progress. Cell junctions can be divided into several classes: tight junctions establish the ion conducting channels and apical/basal sorting of epithelial cell layers, desmosomes link cell junctions to the intermediate filament network and adherens junctions provide a link to the actin cytoskeleton (12,13). Adherens junctions consist of membrane-spanning cadherin molecules, whose cytoplasmic domain interacts with β- and γ-catenin. α-catenin is recruited to adherens junctions through its interaction with β-catenin and links adherens junctions to the actin cytoskeleton. The Rho family of cytoskeletal regulators play a critical role in the maintenance of adherens junctions (12,13). Our results suggest that increase in cell-cell fusion (and genomic instability) induced by imbalances in Rad6B levels in normal MCF10A human breast epithelial cells probably arise from alterations in Wnt and Rho signaling pathways, mechanisms that have been implicated in regulation of adherens junctions and maintenance of epithelial cell polarity.

Aim 3. In order to determine if expression pattern of Rad6 can be used singly or in combination to predict response or resistance to chemotherapy, we retrospectively obtained pre- and post-treatment tissue samples from patients with locally advanced (clinical stages IIB and III) or limited Stage IV breast carcinoma who received preoperative chemotherapy containing adriamycin, taxol or taxotere, followed by surgical excision (mastectomy = 24; lumpectomy =10) at Harper Hospital in the Detroit Medical Center, Detroit, MI. Twenty four patients met these criteria.

Treatment response. Treatment response was based on the change in bi-dimensional tumor size (surface area) in the breast from the initial clinical examination to the surgical specimen examined macroscopically and microscopically. Clinical response was classified as complete (CR) if no palpable mass is present at the tumor site, partial response (PR) if the tumor response decreased 50% or more, and no response (NR) if no change was observed. Pathologic response is based solely on the surgical specimen and is classified as complete response (CR) if no tumor is found microscopically in the breast or axilla, partial response (PR) if tumor cells showed marked chemotherapy response with only minimal microscopic tumor involvement, and no response (NR) otherwise.

Immunohistochemistry and interpretation. Tissues were fixed in 10% buffered formalin and paraffin embedded. Four micron thick sections were cut and mounted on gelatin coated slides. Deparaffinized tissue sections were then immunostained with antibodies to Rad6, p53 (DO7), PCNA, Mdr-1 and Rad18. Rad18 has been recently included

in the study as Rad6 forms heterodimers with Rad18, and complexing with Rad18 has been reported to be important for DNA repair function of Rad6 (14). Following reaction with primary antibody, tissue sections were washed and incubated with the appropriate secondary antibody. Sections were washed, color developed with chromagen from the Vector ABC kit (Vector Labs), and counterstained with hematoxylin. All immunostains were reviewed by two pathologists (Dr. Dan Visscher and Dr. Nat Pernick). Interpretation was based on the target site of staining nuclear (p53, PCNA), cytoplasmic (Rad6) or nuclear plus cytoplasmic (Rad6), or cell membrane (Mdr-1). The frequency (<5%, 5-30%, 30-60%, >60%, >90% of tumor cells) and strength (strong, +++; moderate, ++; weak, +; or negative, -) of immunostaining was determined. Samples were deemed immunoreactive for Rad6 if >30% of tumor cells stained in cytoplasm or nucleus. Samples were deemed positive for p53 if >5-10% of nuclei of tumor cells stained for p53. There was inadequate tissue available on some of the pre-treatment core biopsies. Both pre- and post-treatment samples were immunostained for Rad6, p53, PCNA and Mdr-1. Change in expression is defined as a difference in immunostaining in nuclear versus cytoplasmic (for Rad6), or as a difference of at least 2 frequency levels (i.e., 5-30% to >60% for p53, Rad6, PCNA or Mdr-1) or a change in interpretation from positive to negative or negative to positive.

Results. Results from staining with Rad6, p53, PCNA and P-glycoprotein Mdr-1 antibodies and treatment outcome are shown in Table 2. Statistical analysis of data are being carried out by Biostatistics Core Facility of Karmanos Cancer Institute and is expected to be completed by the end of August, 2003.

Table 2. Expression ofRad6, p53, PCNA and P-gp Mdr-1, and treatment outcome in pre- and post-neoadjuvant chemotherapy cases

Case #	**Rad6** Nuclear	Cytoplasmic	**P53** Nuclear	**PCNA**	**P-gp**	**Response** Clinical	Pathologic
1A 1B	+ -	++ +	++ (10-30%) - to +	+ + (60%)	+/- to + - to +/-	NR	PR
2A 2B	+ -	++ +++	+/- to+(5-10%) +/- to +++	+ to ++ ++ (60-90%)	+ to +++	NR	NR
3A 3B	+/- ++	+ +	- + (<5%)	- +/- to +(5%)	+ to ++	CR	PR
4A 4B	No tissue +/-	+/-	- to +/- (<5%)	+/- (5-30%)	+ to ++	PR	PR
5A 5B	+/- +++	+/- ++	- -	- -	++ (>50%)	CR	CR
6A 6B	- +	- +/-	+ to ++ (5-10%) - to ++	+/- - to + (30-60%)	+ to ++ (>90%)	PR	PR
7A 7B	No tissue ++ (>90%)	+	-	+/- to + (60%)	+ to ++ (60-90%)	CR	CR
8A 8B	No tissue -	++ (90%)	+	++ (60-90%)	+/- to + (5-30%)	NR	NR
9A 9B	minimal tissue +	++ (>90%)	-	++ (>90%)	+ to ++ (10-30%)	NR	NR

10A 10B	- -	++ (60-90%) +/- (>90%)	++ +/- (30-60%)	+ (30-60%)	+/- to +	PR	NR
11A 11B	- -	++ (>90%) +/- (diffuse)	+ -	+/- (only focally 5-30%)	+ to ++ (50%)	PR	PR
12A 12B	+ (focally positive 5-30%) ++	+ ++	- - to +	- + (>60%)	+/- to +	PR	PR
13A 13B	No tissue - to +/-	- to +/- (60-90%)	- to + (60-90%)	+ to ++ (60-90%)	+/- to +	PR	PR
14A 14B	No tissue + (10-30%)	++ (30-60%)	+/-	+ (5-30%)	+ (5-30%)	PR	NR
15A 15B	+ (>10%) -	- + to ++ (90%)	- to + ++ (60-90%)	+ (60%) + to ++ (>60%)	+ to ++ (50%)	NR	NR
16A 16B	No tissue ++ to +++	++ (>60%)	-	-	+ to ++ (50%)	CR	PR
17A 17B	- -	+ (60-90%) + to ++ (60-90%)	+/- -	+ (5%) + to ++ (90%)	+ (10-30%)	PR	PR
18A 18B	- (tumor) + (stroma) -	- ++ to +++	- ++ (60-90%)	- ++ (60-90%)	++ (60-90%)	PR	NR
19B	++ (apoptotic nuclei)	+ (60-90%)	+/-	++ (60-90%)	+ to ++ (5-30%)	PR	PR
20B	- to + (>90%)	++ (>5%)	++ (60-90%)	+/- to + (30-60%)	+/- to + (5-30%)	NR	NR
21B	++ (focally)	+ to ++ (>90%)	-	+ to ++ (60-90%)	+ to ++ (60-90%)	PR	PR

A, represents pre-treatment cores; B, represents, post-treatment samples.

***In situ* hybridization analysis of Rad6B mRNA expression.** Since the antibody used for detection of Rad6 protein cannot distinguish between Rad6A and Rad6B homologues that are ~97% similar, we will perform *in situ* hybridization analysis using antisense Rad6B specific RNA probe. TA-cloning vector containing a 250 bp Rad6B-specific sequence just upstream of the first ATG codon will be transcribed in the sense and antisense directions using T7 and Sp6 specific RNA polymerases and digoxigenin-labeled UTP. Tissue sections recovered from specimens with complete, partial and no-response will be hybridized with antisense and sense (negative control) RNA probes, washed and presence of hybridizing signals detected following incubation in HRP-conjugated anti-digoxigenin antibody. Evaluation of data from immunohistochemical and *in situ* hybridization analysis will confirm the therapeutic utility of Rad6B for predicting response/resistance to chemotherapeutic drugs.

Promoter analysis of Rad6B gene. Since we have reported differences in levels of Rad6B mRNA expression levels between normal and cancerous human breast cells, we have begun to characterize regulatory sequences in the 5' UTR of the Rad6B gene. Luciferase reporter plasmids encoding various lengths of 5' UTR have been subcloned into pGL3-Basic vector and expression of luciferase in control (basal) and adriamycin-treated MCF10A, MCF-7 and MDA-MB-231 cells are examined by transient transfection assays. Data will be analyzed to see if i) there are differences in basal activity between normal and cancerous cells, and ii) there are differences in sensitivity and regulation by adriamycin. After initial analysis, a more refined series of constructs will be made to further define the key regulatory sequences and the transcription factors that control promoter activity. Using SSCP analysis, we have found that only one of the alleles of Rad6B is transcribed in normal and cancerous human breast cells. We are in the process of determining if methylation plays a role in silencing of one of the alleles, as the Rad6B promoter contains a trinucleotide tract of CpG repeats that exhibit slight variations in length among various breast cell lines. Examination of mechanisms regulating transcriptional and posttranscriptional control of Rad6B gene in human breast cells is the basis for a grant application that has been submitted to NIH.

KEY RESEARCH ACCOMPLISHMENTS

1. Rad6 expression levels are low and predominantly cytoplasmic in normal and nontumorigenic breast tumors and cell lines, whereas Rad6 levels are high and predominantly nuclear in tumorigenic and metastatic breast tumors and cell lines.
2. Rad6B mRNA is wild type and no significant differences in ubiquitin conjugating activity are observed between normal and cancerous mammary cells.
2. Constitutive overexpression of Rad6B in normal breast cells induces multinucleation, centrosome amplification, abnormal mitosis, aneuploidy and confers ability for anchorage independent growth.
5. Rad6B forms supramolecular complexes with p53 and proteins of the p53 pathway following exposure to DNA damaging drugs.
6. Rad6B functions in monoubiquitination of p53 and inclusion of Mdm2 is essential for its polyubiquitination.
7. DNA damage-induced p53 response is accompanied by increase in monoubiquitinated p53.
8. Rad6 expression is maximal during late S/G2 phases of the cell cycle in normal MCF10A cells.
9. Using *in vivo* cross-linking experiments, we have shown that majority of Rad6 present in the nucleus is not associated with chromatin in untreated MCF10A cells. However, upon exposure to cisplatin or adriamycin, majority of Rad6 is redistributed to the chromatin. In cells exposed to the DNA damaging agent, P53, PCNA, Rad18 and Rad6 are found to be associated with the chromatin in the same fractions.
10. MCF10A cells stably overexpressing ectopic Rad6B exhibit resistance to adriamycin and cisplatin. This ability to tolerate DNA damage correlates with its ability to convert nascent strands of DNA in damaged cells to high molecular weight DNA (Post replication-repair proficient). MCF10A cells expressing antisense Rad6B are hypersensitive to DNA damaging drugs. These cells are deficient in their ability to convert nascent DNA strands to high molecular weight DNA (PRR-deficient).
11. Preliminary data suggest that the strength and frequency of nuclear Rad6 expression relative to cytoplasmic reactivity when used in conjunction with strength and frequency of p53 nuclear reactivity may correlate with treatment response.
12. Alterations in Wnt and Rho signaling pathways appear to contribute to loss of cell polarity and induction of genomic instability in Rad6B-overexpressing breast cells.
13. Rad6B expression is monoallelic. Our preliminary analysis indicate that methylation of the CpG island in the Rad6B promoter may play an important role in regulation of Rad6B expression in breast cells.

REPORTABLE OUTCOMES

Funding from the Department of Defense has immensely helped further understanding of the role of Rad6B gene in human breast carcinogenesis. Although the presence of human homologues of yeast Rad6 has been known for several years, very little research was focused on understanding this important gene. I am very grateful for the funding. Results of our work have revealed several important clues to understanding mechanisms that cause loss of cell polarity, induce genomic instability, initiate tumorigenesis, mediate sensitivity to DNA damaging drugs, and intervene/aggravate malignant progression.

1. We have characterized the validity, utility and specificity of our Rad6 antibody.
2. MCF10A-Rad6B clones, MCF10A-a/s Rad6B clones.
3. Shekhar, P.V.M., Lyakhovich, A, Heng, H., Visscher, D.W. and Kondrat, N. RAD6 overexpression induces centrosome amplification, abnormal mitosis, aneuploidy and transformation. Cancer Res., 62:2115-2124,2002. (Appendix 1).
4. Supramolecular complex formation between Rad6 and proteins of p53 pathway during DNA damage-induced response. Lyakhovich, A and Shekhar, P.V.M. Mol. and Cell. Biol., 23: 2463-2475, 2003 (Appendix 2).
5. Chemosensitivity of human breast cells correlates with Rad6 expression and postreplication repair capacity. Shekhar P.V.M. and Lyakhovich A. Manuscript submitted (Appendix 3).
6. Correlation between RAD6 expression/function and metastatic potential. Shekhar, P.V.M., Wang, H., Pethe, V. & Werdell, J. Proc. AACR, 40:1029, 1999.
7. Upregulation of RAD6 expression in human breast cancer: effects of RAD6 overexpression in human breast epithelial cells. Shekhar, P.V.M., Visscher, D.W. & Kondrat, N. Proc Amer Assoc Cancer Res., 42, 2001.
8. Rad6 participates in DNA damage-induced response by regulating stability of p53. Lyakhovich A. & Shekhar, P.V.M. Proc Amer Assoc Cancer Res., 43, 2002 (abstract selected for AACR award from Pharmacia).
9. Rad6, an important mediator in the maintenance of genomic integrity. Shekhar, P.V.M., Lyakhovich, A. and Visscher, D.W. Era of Hope, Department of Defense, 2002.
10. Regulation of Rad6 expression during cell cycle and in response to DNA damage. Shekhar P.V.M. Proc AACR, 44, 251, 2003.
11. Molecular regulation of Rad6 expression and activity; PI, R01, NIH, Revised application will be submitted in Nov, 2003.
12. Apoptosis and Genomic Instability: When Excessive Cell Death is Detrimental, PI, Department of Defense, submitted May 2003.
13. Targeting Nuclear Actin Regulation for Cancer Therapy; Co-Investigator (Ratner, PI), R21, NIH, submitted June 2003.
14. Nuclear Actin and its Regulators as Therapeutic Targets in Breast; Co-Investigator (Ratner, PI), Department of Defense, submitted May 2003.
15. Rad6 expression, a marker for therapeutic response. Manuscript and abstract will be submitted as soon as the statistical analysis is completed.
16. Monoallelic expression of Rad6B: Regulation by methylation of the noncoding trinucleotide CpG repeat tract. Abstract and manuscript expected to be submitted in three months.
17. Dysregulation in Wnt and Rho signaling pathways contribute to loss of cell polarity in Rad6B-overexpressing human breast cells. Manuscript in preparation.

Personnel supported by the grant.

1. Noelle Kondrat; 2. Dr. Alex Lyakhovich; 3. Dr. Daniel Visscher; 4. Dr. Davis Cheng

CONCLUSIONS

Rad6 plays an important role in maintaining genomic integrity of human breast cells. Imbalances in the levels of Rad6B causes loss of cell polarity and genomic instability that correlate with alterations in sensitivity to chemotherapeutic drugs and postreplication DNA repair capacities. Rad6B forms supramolecular complexes with p53, p14ARF and Mdm2, and inclusion of p14ARF and Mdm2 into Rad6-p53 complexes is dependent upon exposure to DNA damaging agent. Rad6 mediates monoubiquitination of p53, and the p53 response observed following DNA damage is associated with parallel increases in monoubiquitinated p53. Loss of cell polarity induced by Rad6B overexpression appears to be a result of dysregulation in Wnt and Rho signaling pathways. Rad6 staining shows differential distribution in cytoplasmic versus nuclear compartments in samples accrued from patients following post-chemotherapy. Our preliminary data suggest that recruitment of Rad6 into the nuclei following chemotherapy may predict favorable treatment outcome.

REFERENCES

1. Lawrence, C.W. The RAD6 DNA repair pathway in *Saccharomyces cerevisiae*: What does it do, and how does it do it? *BioEssays* 16, 253-258 (1994).
2. Reynolds, P., Weber, S. & Prakash, L.. RAD6 gene of *Saccharomyces cerevisiae* encodes a protein containing a tract of 13 consecutive aspartates. *Proc. Natl. Acad. Sci. USA* 82,168-172 (1985).
3. Jentsch, S., McGrath, J.P.& Varshavsky, A. The yeast DNA repair gene RAD6 encodes a ubiquitin-conjugating enzyme. *Nature* 329,131-134 (1987).
4. Lawrence, C.W. Mutagenesis in *Saccharomyces cerevisiae*. *Adv. Genetics* 21.:173-254 (1982).
5. Haynes, R.H. & Kunz, B.A. In: The Molecular Biology of the Yeast *Saccharomyces cerevisiae*: Life Cycle and Inheritance (Strathern J, jones E and Broach J, eds.) pp. 371-414, Cold Spring Harbor Laboratory, Cold Spring Harbor, NY (1981).
6. Prakash, S., Sung, P. & Prakash, L. The Eukaryotic Nucleus, eds. Straus P.R. & Wilson S.H. (Telford Press, Caldwell NJ) Vol I, pp. 275-292 (1990).
7. Goebl, M.G., Yochem. J., Jentsch, S., McGrath, J.P., Varshavsky, A. & Byers, B. The yeast cell cycle gene CDC34 encodes a ubiquitin conjugating enzyme. *Science* 241,1331-1335 (1988).
8. Koken, M.H.M., Reynolds, P., Jaspers-Dekker, I., Prakash, L., Prakash, S., Bootsma, D., & Hoeijmakers, J.H.J. Structural and functional conservation of two human homologs of the yeast DNA repair gene RAD6. *Proc. Natl. Acad. Sci. USA* 88, 8865-8869 (1991).
9. Koken, M.H., Smith, E.M., Jaspers-Dekker, I., Oostra, B.A., Hagemeijer, A., Bootsma, D., & Hoeijmakers, J.H. Localization of two human homologs, HHR6A and HHR6B, of the yeast DNA repair gene RAD6 to chromosomes Xq24-q25 and 5q23-q31. *Genomics* 12, 447-453, (1992).
10. Roest, H.P., van Klaveren, J., de Wit, J., van Gurp, C.G., Koken, M.H., Vermey, M., van Roijen, J.H., Hoogerbrugge, J.W., Vreeburg, J.T., Baarends, W.M., Bootsma, D., Grootegoed, J.A., & Hoeijmakers, J.H. Inactivation of the HR6B ubiquitin-conjugating DNA repair enzyme in mice causes male sterility associated with chromatin modification. *Cell* 86, 799-810 (1996).
11. Strutt, D.I., Weber, U., & Mlodzik M. The role of RhoA in tissue polarity and Frizzled signaling. *Nature* 387, 292-29 (1997).
12. Yap, A.S., Brieher, W.M., & Gumbiner, B.M. Molecular and functional analysis of cadherin-based adherens junctions. *Ann. Rev. Cell. Dev. Biol.* 13, 119-146 (1997).
13. Fukata, M. & Kabuchi, K. Rho family GTPases in cadherin-mediated cell-cell adhesion. *Nature Rev. Mol.*

Cell. Biol. 2, 887-897 (2001).

14. Bailly, V., Lamb, J., Sung, P., Prakash, S., & Prakash, L. Specific complex formation between yeast Rad6 and Rad18 proteins: a potential mechanism for targeting Rad6 ubiquitin conjugating activity to DNA damage sites. *Genes & Dev.*, 8, 811-820 (1994).

APPENDIX COVER SHEET

FIGURES 1-10

Appendix 1: Shekhar et al, Cancer Res., 2002
Appendix 2. Lyakhovich and Shekhar, Mol. Cell. Biol, 2003
Appendix 3. Shekhar and Lyakhovich, ms submitted (37 pages)

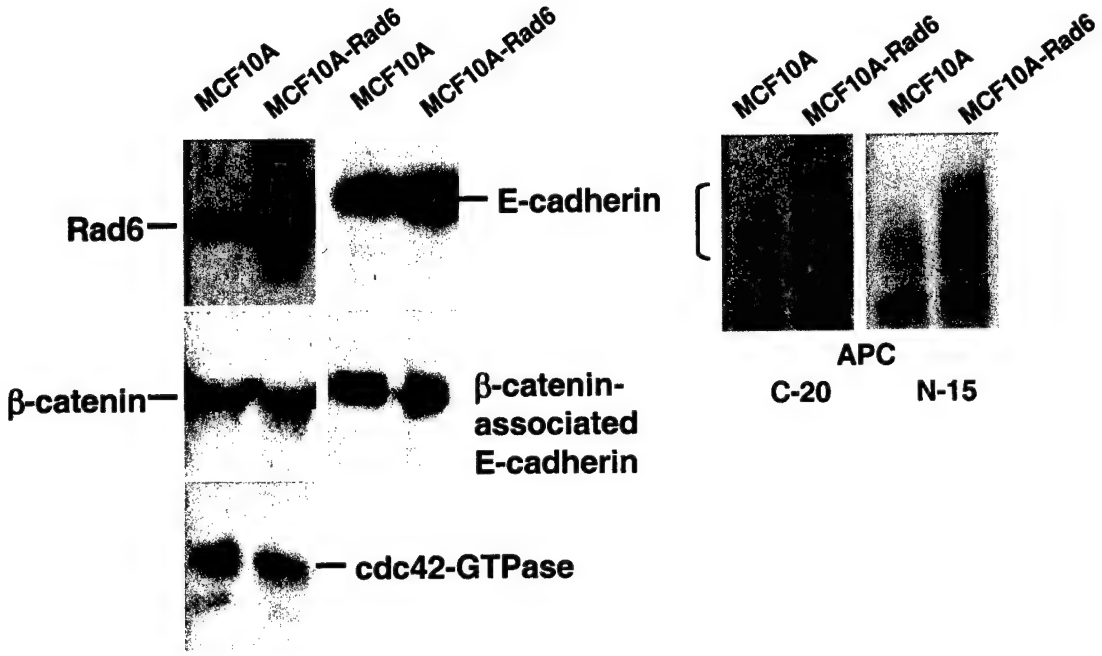

Fig. 1. Western blot analysis of steady-state levels of Rad6, E-cadherin, β-catenin, E-cadherin associated with β-catenin, cdc42-GTPase, and APC proteins. E-cadherin associated with β-catenin was detected by immunoprecipitating cell extracts with β-catenin monoclonal antibody followed by Western blot analysis with E-cadherin-specific monoclonal antibody. APC proteins were detected by antibodies C-20 and N-15 that recognize epitopes at the C- and N-termini, respectively. Although no appreciable differences in β-catenin immunoprecipitable E-cadherin were detected between vector control and Rad6-overexpressing MCF10A cells, slight differences in the size of E-cadherin is detected, although the significance of this is not clear at present.

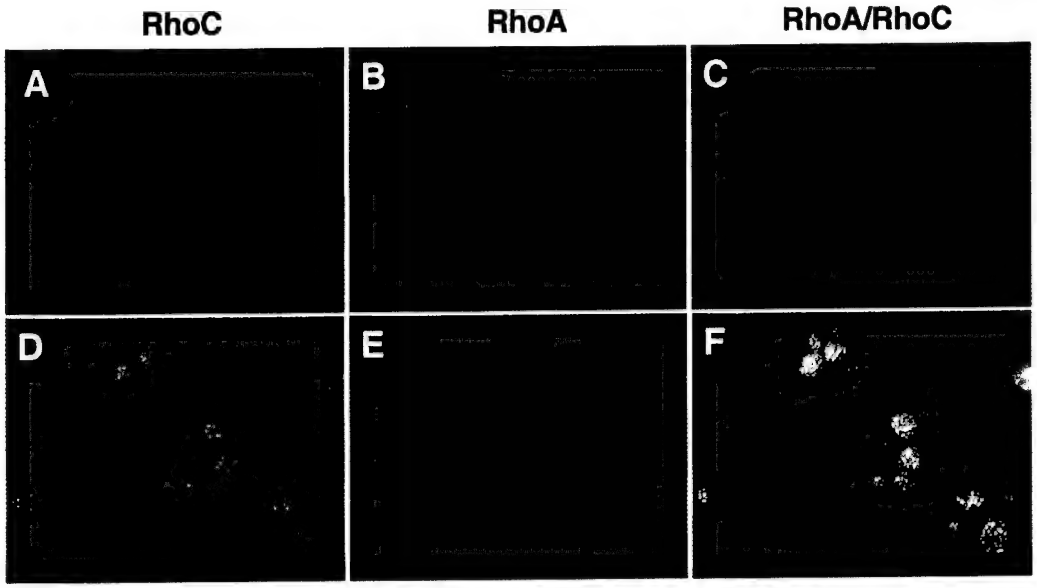

Fig. 2. Detection of RhoA and RhoC proteins in vector control (A-C) and Rad6B-overexpressing (D-F) MCF10A cells by immunofluorescence microscopy. Note the presence of high levels of Rho proteins and pleimorphic nuclei (detected by DAPI) in Rad6B-overexpressing cells. Magnification X100.

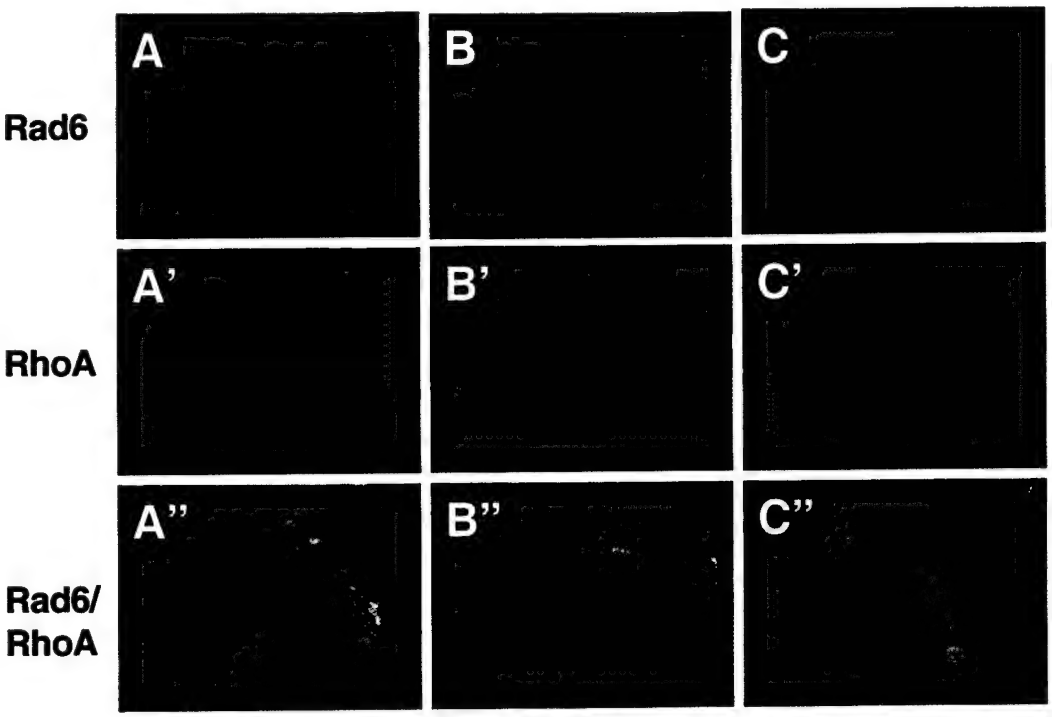

Fig. 3. Detection of Rad6 and RhoA in Rad6B-overexpressing MCF10A cells by immunofluorescence microscopy. Note the presence of high levels of Rad6 and RhoA in the nuclei. Also note the segregatioon of genetic material from a tripolar spindle (B, B', B").

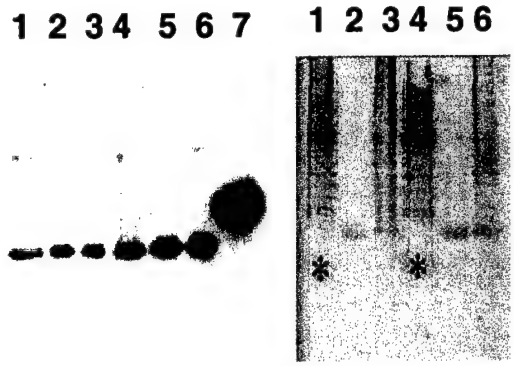

Fig. 4. Detection of RhoA from vector control and Rad6B-overexpressing MCF10A cells by pull-down assays on Rhotek affinity beads. Lanes 1-3, total cell extract, cytoplasmic, and nuclear fractions of vector control cells, respectively. Lanes 4-6, total cell extract, cytoplasmic, and nuclear fractions of Rad6B-overexpressing MCF10A cells, respectively. Lane 7, GST-tagged RhoA (Positive control). The Coomassie stained blot on the right shows that similar levels of total protein were loaded and that the differences in RhoA levels are not due to loading variations.

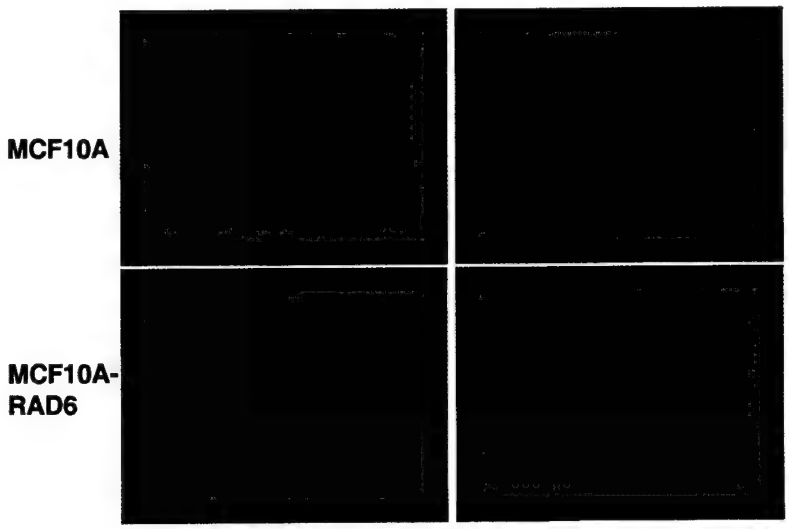

Fig. 5. Detection of β-catenin in vector control and Rad6B-overexpressing MCF10A cells by immunofluorescence microscopy. Note the difference in sizes of cells, the presence of defined β-catenin staining in vector control versus presence of crinkled membranes, diffuse and pervasive β-catenin staining, and presence of β-catenin in the nucleus. Also, note the presence of nuclei that are localized asymetrically in Rad6-overexpressing cells. Magnification, X100.

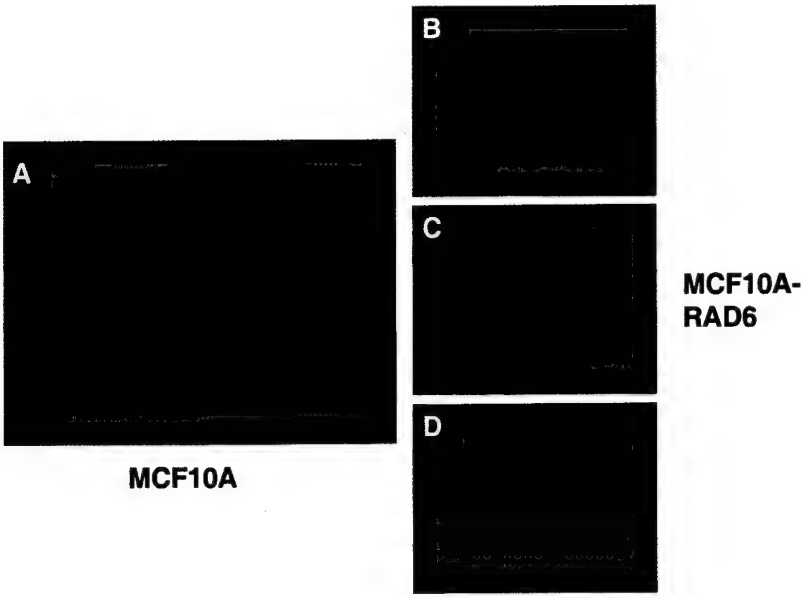

Fig. 6. Localization of β-catenin by immunofluorescence microscopy. Note the presence of higher levels of β-catenin, and alterations at the cell membrane (revealed by β-catenin staining) in Rad6-overexpressing cells that probably contribute to increased rates of cell-cell fusions seen in MCF10A-Rad6B cells. Magnification X100.

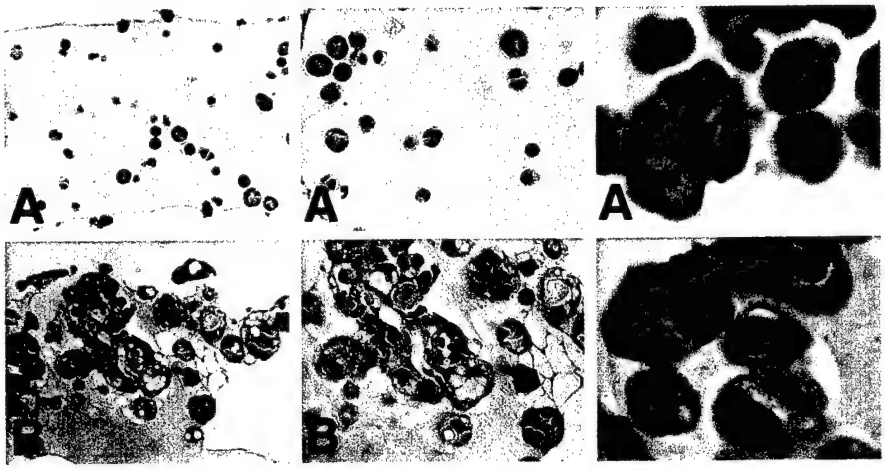

Fig. 7. Spheroids formed from vector control (A, A', A") and MCF10A-Rad6B (B, B', B") cells grown in reconstituted basement membrane. A, A', B, B', represent H&E staining; A" and B", staining with Epithelial mucin antigen-specific antibody. Note the formation of well polarized spheroids containing fewer cells (A and A') as compared to non-polarized clusters containing several cells (B and B'). Also, note the presence of EMA-staining on the cell membranes and formation of a central lumen in panel A". Note the absence of such staining and lack of similar lumen formation panel B". Magnification, X 25, A and B; X 40, A' and B'; and X 100, A" and B".

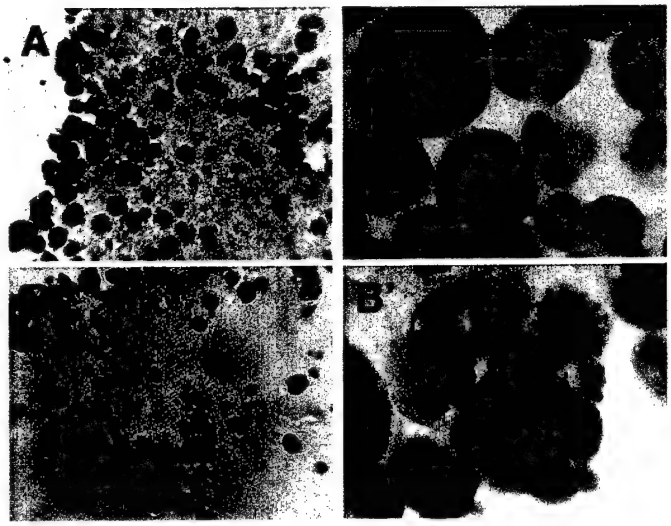

Fig. 8. Immunocytochemical analysis of Rad6 protein expression in spheroids formed from vector control (A and A') and Rad6B-overexpressing MCF10A (B and B') cells. Note the presence of significantly high levels of Rad6 in MCF10A-Rad6 cells. Also, note the presence of high levels of Rad6 in cells containing pleimorphic and apoptotic nuclei (indicated by arrows in B'). Magnification, X 10X, A and B; X 100, A' and B'.

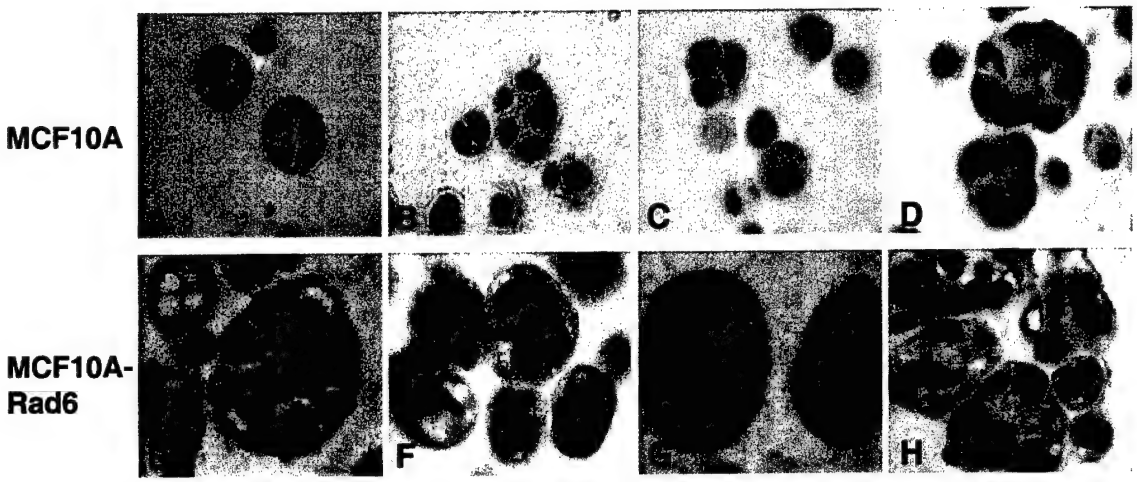

Fig. 9. Immunocytochemical analysis of E-cadherin, β-catenin and PCNA expression in spheroids formed from vector control (MCF10A) and MCF10A-Rad6B cells. A and E, E-cadherin; B and F, β-catenin; C and G, RhoA; D and H, PCNA. Note the presence of higher levels of E-cadherin, β-catenin, RhoA and PCNA in MCF10A-Rad6B cells as compared to control MCF10A cells. Magnification, X100.

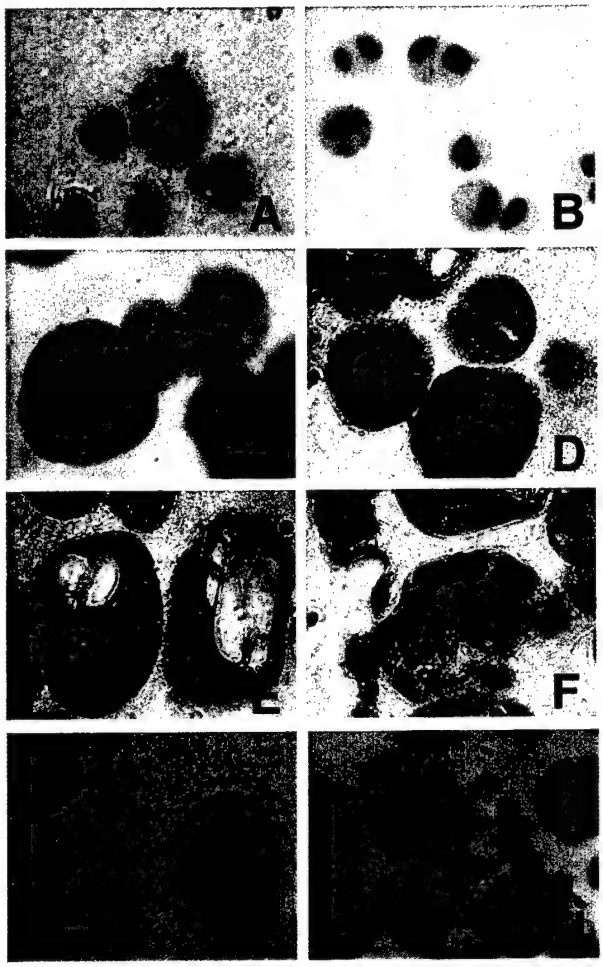

Fig. 10. Immunocytochemical analysis of β-catenin in spheroids formed from MCF10A and MCF10A-Rad6B cells. Panels A-F, staining with unphosphorylated β-catenin monoclonal antibody; Panels G and H, staining with serine phosphorylated β-catenin antibody. Compare the dramatic differences in spheroid structures (revealed by β-catenin staining) formed from parental versus Rad6B-overexpressing MCF10A cells. Note, loss of polarity, presence of pleimorphic nuclei, apoptotic nuclei (F) and the criss-cross staining of β-catenin in MCF10A-Rad6B cells (C-F). Note the lack of immunoreactivity to phosphorylated β-catenin
in MCF10A-Rad6B cells (panel H) and the presence of weak immunoreactivity in vector control MCF10A cells (panel G). This indicates the presence of active β-catenin in MCF10A-Rad6B cells. Magnification, X100.

[CANCER RESEARCH 62, 2115–2124, April 1, 2002]

Rad6 Overexpression Induces Multinucleation, Centrosome Amplification, Abnormal Mitosis, Aneuploidy, and Transformation[1]

Malathy P. V. Shekhar,[2] Alex Lyakhovich, Daniel W. Visscher, Henry Heng, and Noelle Kondrat

Breast Cancer Program, Karmanos Cancer Institute [M. P. V. S., A. L., D. W. V., N. K.], Department of Pathology [M. P. V. S., D. W. V., H. H.], and Center for Molecular Medicine and Genetics [H. H.], Wayne State University School of Medicine, Detroit, Michigan 48201

ABSTRACT

We have isolated by differential RNA display a cDNA that is up-regulated in metastatic mammary tumor lines. This cDNA corresponds to HR6B, the yeast homologue of Rad6, a ubiquitin-conjugating enzyme, and a key player in postreplication repair and induced mutagenesis in the yeast. We show that Rad6 protein expressed in metastatic tumor lines is wild type and functional, because it is able to catalyze the transfer of ubiquitin to histone H2b and is predominantly localized in the nucleus as compared with cytoplasmic localization in normal or nonmetastatic mammary cells. This pattern of Rad6 protein expression/localization is not restricted to breast cancer cell lines, because human breast carcinomas display similar patterns of Rad6 up-regulation and nuclear localization suggesting that deregulation in expression of Rad6 may be an important step in transformation to malignant phenotype. Constitutive overexpression of exogenous human HR6B cDNA into normal-behaving MCF10A human breast epithelial cells induced cell-cell fusion that resulted in generation of multinucleated cells, centrosome amplification, multipolar mitotic spindles, aneuploidy, and ability for anchorage-independent growth. Double immunofluorescence labeling experiments demonstrated the colocalization of Rad6 protein with γ-tubulin on centrosomes. This physical association of Rad6 with centrosomes is maintained throughout the interphase and mitotic phases of the cell cycle. The Rad6 protein exhibits notable alterations in distribution during interphase and mitotic stages of the cell cycle that are compatible with its function as a transcription factor. These findings suggest that Rad6 is an important ubiquitin-conjugating enzyme that may play a significant role in the maintenance of genomic integrity of mammalian cells and that an imbalance in the levels and activity of Rad6 could lead to chromosomal instability and transformation *in vitro*.

INTRODUCTION

Mutagenesis is considered to be a major pathogenetic factor in the progression of human epithelial neoplasia because mutations are thought to inactivate cellular defenses against uncontrolled proliferation and cell migration. Some of these mutations are likely to have occurred during physiological cell replication as a result of rare failures to correct DNA synthesis errors (1). High accuracy is maintained by the combined action of mechanisms that include 3′ to 5′ exonuclease editing of mismatched nucleotide insertions, DNA polymerase preference for correct base-pairs, and postreplication mismatch repair. Despite demonstration of numerous genomic alterations in human breast carcinoma cells, little is known about the mechanisms(s) responsible for genetic instability.

The Rad6 group is concerned with postreplication or "error-prone" repair (2). The *Rad6* gene encodes a M_r 17,000 protein (3), which is one of a group of ubiquitin-conjugating (E2) enzymes (4) that covalently add ubiquitin to selected lysine residues. The Rad6 pathway appears to be regulated by post-translational modification of target proteins with ubiquitin, which commits them to rapid proteolysis. The *Rad6* gene of *Saccharomyces cerevisiae* is required for a variety of cellular functions including DNA repair, induced mutagenesis, and sporulation (5, 6). *rad6* mutant phenotypic effects include slow growth, severe defects in induced mutagenesis, extreme sensitivity to UV, X-ray, and chemical mutagens, and hypersensitivity to antifolate drug metabolites (7). The diversity of the phenotypes of *rad6* mutants suggests that the *Rad6* gene product is central to cell cycle regulation. All of the functions performed by the Rad6 protein appear to result from ubiquitination, because replacement of the conserved Cys 88 with serine produces a totally null phenotype. Although all of the E2s characterized to date are structurally related, they fall into several functionally distinct categories. The yeast CDC34 (UBC3) E2 is required for G_1 to S phase transition of the cell cycle (8), whereas the yeast Rad6/UBC2/E2 is involved in a variety of processes including DNA repair, mutagenesis, and cell proliferation (6).

Rad6 is highly conserved among eukaryotes. Two closely related human DNA repair genes, *HHR6A* and *HHR6B* (human homologues of yeast Rad6), encode ubiquitin-conjugating enzymes (E2), and complement the DNA repair and UV mutagenesis defects of the *S. cerevisiae rad6* mutant (9). HHR6A and HHR6B share 95% identical amino acid residues and are localized on human chromosome Xq24-q25 and 5q23-q31, respectively (10). Inactivation of the gene encoding the mammalian homologue of yeast Rad6, *HR6B*, in mice leads to male sterility (11). Experiments described here show for the first time that HR6B is overexpressed in mouse and human breast cancer lines and tumors, and that constitutive overexpression of HR6B induces formation of multinucleated cells, centrosome amplification, abnormal mitosis, aneuploidy, and transformation.

MATERIALS AND METHODS

Mouse Mammary Metastasis Model. Tumor sublines 67, 168, 66cl4, 4T07, and 4T1 were isolated from a single spontaneously arising mammary tumor from the Balb/cfC3H mouse (12). The subpopulations were classified based on their ability to metastasize spontaneously from the orthotopic site. Subline 66cl4 spontaneously metastasizes to the lung via the lymphatics, whereas subline 4T1 spontaneously metastasizes to the lung and liver via the hematogenous route (12). Sublines 67, 168FAR, and 4T07 are highly tumorigenic but fail to metastasize from primary lesions through different end points in the dissemination; however, injection of 4T07 cells into the tail vein results in the formation of tumor nodules in the lung and liver (13).

Human Breast Epithelial Cell Lines. MCF10A, MCF10AT, MCF10ADCIS.com, MCF-7, and MDA-MB-231 cells were also used. MCF10A cells are normal-behaving human breast epithelial cells that lack tumorigenicity in nude mice and are unable to support anchorage-independent growth (14), whereas MCF10AT and MCF10ADCIS.com are T24-*Ha-ras*-transformed MCF10A cells that produce preneoplastic (15) or DCIS[3] (16) lesions, respectively, when implanted in immunodeficient mice. MCF-7 (tumorigenic) and MDA-MB-231 (metastatic) human breast cancer cells were

Received 6/29/01; accepted 1/28/02.

The costs of publication of this article were defrayed in part by the payment of page charges. This article must therefore be hereby marked *advertisement* in accordance with 18 U.S.C. Section 1734 solely to indicate this fact.

[1] Supported by United States Army Medical Research and Materiel Command Grant DAMD17-99-I-9443 (to M. P. V. S.); and NIH Grant CA22453 (Cancer Center Support Grant to the Karmanos Cancer Institute).

[2] To whom requests for reprints should be addressed, at Breast Cancer Program, Karmanos Cancer Institute, 110 East Warren Avenue, Detroit, Michigan 48201. Phone: (313) 833-0715, extensions 2326/2259; Fax: (313) 831-7518; E-mail: shekharm@karmanos.org.

[3] The abbreviations used are: DCIS, ductal carcinoma *in situ*; Gas, growth arrest-specific; RT-PCR, reverse transcription-PCR; GAPDH, glyceraldehyde-3-phosphate dehydrogenase; HRP, horseradish peroxidase; CFE, colony-forming efficiency; PCNA, proliferating cell nuclear antigen.

obtained from Cell Resource Core of Karmanos Cancer Institute or purchased from American Type Culture Collection (Manassas, Virginia), respectively.

Cell Culture. Mouse mammary tumor sublines were grown in DMEM supplemented with 5% FCS, 5% newborn calf serum, 1 mM nonessential amino acids, 2 mM L-glutamine, 100 units/ml penicillin, and 100 μg/ml streptomycin. MCF10A and MCF10AT cells were maintained in DMEM/F-12 medium supplemented with 2.5% horse serum, 0.02 μg/ml epidermal growth factor, 0.5 μg/ml hydrocortisone, 10 μg/ml of insulin, 0.1 μg/ml cholera toxin, 100 units/ml penicillin, and 100 μg/ml streptomycin. MCF10ADCIS.com and MDA-MB-231 cells were grown in DMEM supplemented with 10% FCS, and MCF-7 cells were maintained in DMEM/F-12 supplemented with 5% FCS and 10 μg/ml insulin.

mRNA Differential Display. Total cellular RNA was isolated using the TRIzol reagent kit (Life Technologies, Inc., Grand Island, NY) following the manufacturer's protocol. Before mRNA differential display, DNase I treatment was performed on the RNA samples using the Message Clean kit (GenHunter Corp., Nashville, TN) and differential display of cDNA fragments was performed essentially as described by Liang *et al.* (17). The radioactive PCR products were electrophoresed on 6% acrylamide-8 M urea gels in Tris-borate EDTA buffer (pH 8.0) at 35 W for 3 h, and the gel was dried and subjected to autoradiography. Selected bands were identified, and the corresponding slices on the dried gels were excised and eluted by incubation in 50 μl of 10 mM Tris-HCl-1 mM EDTA buffer (pH 8.0) at 60°C for 1 h. Gel pieces containing differentially displayed bands of interest were reamplified by PCR, subcloned into pCR-telomeric repeat amplification protocol vector and sequenced using primers provided in the pCR-telomeric repeat amplification protocol cloning system (GenHunter Corp.). *Gas1* (18) and the HR6B/E2B/Rad6 cDNAs were isolated using 5′-AGGTGACCGT-3′ (AP3) and $T_{11}C$ primers for PCR amplification (GenHunter Corp.).

Full-length HR6B cDNAs were amplified by RT-PCR from RNAs of 168FAR, 66cl4, and 4T1 tumor sublines, and normal BALB/c mouse liver using the forward and reverse primers 5′-AGCTGCGGAGCATGTCG-3′ (+17/+33) and 5′-AAGGATGAGCAGACCAGG-3′ (+574/+553; Accession no. NM_009458), respectively. PCR amplification was performed for 25 cycles at 95°C for 1 min, 52°C for 2 min, and 72°C for 3 min. The PCR products were additionally characterized by Southern blot analysis using: (*a*) the 240-bp cDNA fragment isolated from differential display; and (*b*) a full-length HHR6B cDNA prepared from the normal human breast epithelial cell line MCF10A using primers +330/+348 and +935/+914 (Accession no. M74525). The amplified cDNAs were sequenced by Cyclist DNA sequencing kit (Stratagene, La Jolla, CA) and sequence data subjected to similarity search at nucleotide and amino acid levels using the GenBank databases.

RT-PCR Analysis of HR6B/E2B/Rad6 Expression. Total RNAs (2 μg) from 67, 168FAR, 4T07, 4T1, and 66cl4 tumor sublines were digested with RNase-free DNase I and reverse transcribed using random hexamers and Superscript II (Life Technologies, Inc., Rockville, MD). Relative levels of HR6B mRNA expression were determined by RT-PCR using primers +17/+33 and +114/+97 (Accession no. NM_009458) as forward and reverse primers, respectively, and conditions that yielded a detectable PCR product using the minimum number of amplification cycles. In addition to the primers for the *HR6B* gene, a set of primers designed to recognize GAPDH cDNA was used in each reaction as an internal control for the amount of cDNA tested. The GAPDH-specific primers were forward, 5′-CATTGACCTCAACTACATGGT-3′ (+186/+206) and reverse, 5′-GGATCTCGCTCCTGGAAGA-3′ (+320/+302; Accession no. XM_006959). The PCR products were separated by agarose gel electrophoresis, transferred, and blots probed with the full-length HR6B (PCR amplified using primers +17/+33 and +509/+493; Accession no. NM_009458) and GAPDH cDNAs as the probes. The relative intensities of the HR6B and GAPDH hybridizable bands were quantitated by densitometry (Model 300A densitometer; Molecular Dynamics, Sunnyvale, CA).

Preparation of Rad6 Antibody and Western Blotting. Antibody to Rad6 was generated by multiple immunization of New Zealand White rabbits with a synthetic peptide (K plus amino acid residues 131–152; Accession no. NM_009458) that is conserved 100% in mouse and human HR6B, and 91% in human HR6A. For Western blotting, cell lysates from exponentially growing mouse and human breast cells were prepared in 10 mM Tris-HCl (pH 7.5), 150 mM NaCl, 1% Triton X-100, 1 mM phenylmethylsulfonyl fluoride, 1 μg/ml each of leupeptin, pepstatin, antipain, and 1 mM sodium orthovanadate, and proteins (50 μg) from each lysate were separated by SDS-PAGE and transblotted onto Immobilon P membranes. The blots were stained with anti-Rad6 antibody. After detection, blots were stripped and reprobed with a rabbit polyclonal Gas1 protein antibody, a kind gift from Dr. G. Del Sal (International Center for Genetic Engineering and Biotechnology, Consortium for Interuniversity, Biotechnology Laboratories, Trieste, Italy). Loading of protein was monitored by reprobing stripped membranes with mouse anti-β-actin antibody. Rad6 (and Gas1) and β-actin protein bands were visualized with antirabbit or antimouse IgG coupled to HRP, respectively, using enhanced chemiluminescence kit (Amersham, Arlington Heights, IL). The relative amounts of Rad6 (HR6A/HR6B) protein(s) to β-actin bands were quantitated with a scanner-densitometer (Molecular Dynamics).

Immunofluorescence Microscopy. For immunofluorescence staining, mouse mammary tumor sublines 67, 168FAR, 66cl4, and 4T1, and MCF10A human breast epithelial cells were grown on coverslips and fixed in methanol: acetone (1:1, v/v) at −20°C. Cells were preincubated with 2% horse serum/PBS and incubated with anti-Rad6 antibody. To assess centrosome number or colocalization of Rad6 with centrosomes, vector-transfected and Rad6-overexpressing MCF10A clones fixed in methanol-acetone were stained with mouse monoclonal antibody to γ-tubulin (Zymed Labs, San Francisco, CA), or a 1:1 mixture of anti-Rad6 antibody plus γ-tubulin antibody. Rad6 and γ-tubulin were detected with FITC-conjugated goat antirabbit IgG and Texas Red-conjugated goat antimouse IgG, respectively, and scored for the number of centrosomes. Nonbinding mouse or rabbit IgG was used as a control in all of the double-labeling experiments. Slides were counterstained with 4′,6-diamidino-2-phenylindole (Molecular Probes), and the number of abnormal mitoses was determined at ×100 magnification and expressed as a percentage of the total number of mitotic nuclei per 300 nuclei scored. Representative cells at different stages during mitosis were also scored to evaluate Rad6 expression and localization. All of the images were collected on a Olympus BX-4 fluorescence microscope equipped with Sony high resolution/sensitivity CCD video camera.

Immunohistochemistry. Cryostat or formalin-fixed, paraffin-embedded human breast carcinoma tissue sections were incubated with anti-Rad6 antibody followed by biotinylated antirabbit IgG secondary antibody and HRP-conjugated streptavidin. Nuclei were counterstained with hematoxylin. Control sections were stained with secondary antibody only.

Rad6-associated Histone H2B Ubiquitination Activity. Cell extracts of mouse tumor sublines 67, 168FAR, 4T07, 66cl4, and 4T1 containing equivalent amounts of total protein (100 μg) were immunoprecipitated with anti-Rad6 antibody or with an equivalent amount of normal rabbit IgG. Immune complexes were pelleted after incubation with protein A/G-Sepharose, washed in lysis buffer [10 mM Tris-HCl (pH 7.5), 150 mM NaCl, 1% Triton X-100, 1 mM phenylmethylsulfonyl fluoride], and the washed pellets rinsed with reaction buffer [50 mM Tris-HCl (pH 7.5), 50 mM KCl, 5 mM $MgCl_2$, 2 mM ATP, 0.2 mM DTT, 100 μg/ml BSA]. The rinsed pellets were resuspended in the same buffer supplemented with 0.5 μg Histone H2B (Sigma Chemical Co., St. Louis, MO), 0.5 μg ubiquitin (Sigma Chemical Co.), and 0.2 μg ubiquitin activating enzyme, E1 (Boston Biochem, Boston, MA) and incubated for 30 min at 30°C. Some reactions were performed with the same assay buffer but lacking ATP. The reaction mixtures were run on reducing 17% polyacrylamide gels, electroblotted, and subjected to Western analysis with mouse antiubiquitin antibody (Zymed Labs). Ubiquitinated histone H2B and free ubiquitin were visualized with antimouse IgG coupled to HRP using an enhanced chemiluminescence kit (Amersham Corp.).

Generation of Stable HHR6B Transfectants and Analysis. Full-length wild-type HHR6B cDNA was subcloned into the *Bam*HI site of the mammalian expression vector pCMVneo (Promega Corp., Madison, WI) for high-level expression under the transcriptional control of the cytomegalovirus promoter. Circular plasmid DNA (either empty vector or sample construct) was transfected into MCF10A cells by Mirus Trans IT-I transfection reagent (PanVera Corp., Madison, WI). Stable transfectants were selected by resistance to G418 selection (500 μg/ml) for 3 weeks. Selected resistant clones were isolated, expanded, and maintained in the presence of G418. Expression of the transfected gene was monitored by RT-PCR with primers specific for the vector and the exogenous gene on DNase-treated RNA samples, Northern, and Western blot analysis.

Growth in Soft Agar. Vector-transfected or HHR6B-overexpressing MCF10A clones (2×10^4 cells) were seeded in 2 ml of 0.33% agar in

DMEM-F12-supplemented medium as described above for propagation of MCF10A cells. This suspension was layered over 1 ml of 0.9% agar medium base layer and dishes incubated at 37°C in 5% CO_2/95% O_2 for 4 weeks with twice weekly medium changes. All of the cultures were examined 24 h after plating, and cell aggregates that might bias final results were marked. Plates with >10 aggregates were discarded. CFE was calculated by dividing the number of colonies >50 μm (sized using a calibrated ocular grid) by the number of cells seeded. Ten microscopic fields were counted to calculate the total number of colonies/well from the whole well (19). Reported values are the average count from triplicate wells. The number of colonies in different size ranges (50–100 μm and >100 μm) was calculated in the same manner.

SKY. The probe mixture containing 24 differentially labeled, chromosome-specific painting probes and Cot-1-blocking DNA (SKY kit; Applied Spectral Imaging, Carlsbad, CA) was denatured and hybridized to denatured metaphase chromosomes (20, 21) according to the protocol recommended by the manufacturer. After hybridization and washing, the chromosomes were counterstained with DAPI. Image acquisitions were performed using a SD200 Spectracube system mounted on a Zeiss Axioskop microscope with a custom designed optical filter (SKY-1; Chroma Technology, Brattleboro, VT). The emission spectra were then converted to the pseudocolors matching the fluorochrome combinations of each chromosome. For parental MCF10A and each clone, at least 9–10 metaphases were analyzed.

Statistical Analysis. Specific differences between parental vector-transfected MCF10A cells and HHR6B-overexpressing MCF10A cells were examined by Student's *t* test for centrosome numbers, or number of cells containing multiple/giant nuclei or showing abnormal mitosis. Statistical significance was determined using Student's *t* test with $P < 0.005$ considered as statistically significant.

RESULTS

Isolation and Sequence Analysis of Rad6. Taking advantage of a genetically related mouse mammary metastasis model system, we compared the cDNAs differentially displayed from mRNAs of mouse mammary tumor subpopulations 67, 168FAR, 66cl4, 4T07, and 4T1 of variant metastatic capacities. Two cDNAs that were overabundantly expressed or down-regulated in the most metastatic cell line, 4T1, were isolated and additionally characterized by sequence and expression analysis (Fig. 1*a*). A BLAST search for sequence homologues in the GenBank database revealed that the abundantly expressed 240-bp cDNA is the mouse homologue of the yeast ubiquitin-conjugating enzyme Rad6 and matched 93% and 100% with the human *HR6B* (Accession no. M74525) and mouse *E2B* (Accession no. NM_009458) genes, respectively, whereas the down-regulated 290-bp cDNA matched 100% with the mouse gene *Gas1* (18).

HR6B mRNA and Protein Are Overexpressed in Metastatic Mammary Tumor Cells. To test whether the pattern that appeared on differential display fingerprints faithfully reflects the real expression profile of HR6B/E2B transcript in the mouse mammary tumor subpopulations, 20 μg total RNA isolated from sublines 67, 168FAR, 66cl4, 4T07, and 4T1 cells were subjected to Northern analysis using the 240-bp Rad6 cDNA as the probe. Weakly hybridizing signals were detected, suggesting the presence of very low steady-state levels of HR6B mRNA in these cells. For RT-PCR analysis of HR6B expression, oligonucleotide primers designed (encompassing base 17–574) to amplify the entire coding region were used. A 558-bp fragment was detected in all of the tumor sublines, and the identity of the 558-bp fragment was confirmed by Southern blot hybridization to both the 240-bp Rad6 cDNA (isolated from differential display) and the full-length human HR6B cDNA amplified from MCF10A cellular RNA (data not shown). The relative levels of HR6B mRNA expression in the mouse mammary tumor sublines were confirmed by RT-PCR using primers for the mouse Rad6 (+17/+33 and +114/+97) and GAPDH cDNAs (+186/+206 and +320/+302), and PCR conditions that yielded detectable products with a minimum number of cycles. Results of RT-PCR (Fig. 1*b*) are in agreement with those from differential display (Fig. 1*a*). HR6B mRNA levels in 4T07 and 4T1 cells were ~35-fold higher than line 67, and approximately 15–20-fold, respectively, higher than lines 168FAR and 66cl4 (Fig. 1*b*).

Cell lysates prepared from mouse mammary tumor sublines (67, 168FAR, 4T07, 66cl4, and 4T1) or human breast cells MCF10A (normal), MCF10AT (preneoplastic), MCF10ADCIS.com (DCIS lesions), MCF-7 (tumorigenic), and MDA-MB-231 (metastatic) were subjected to SDS-PAGE and Western blot analysis with rabbit anti-Rad6 antibody. As expected for the mouse HR6B/E2B/Rad6 protein, the antibody recognized a M_r 17,000 protein from all of the cell extracts. Levels of the Rad6 protein detected in the lysates of mouse tumor sublines are in agreement with those observed by RT-PCR (Fig. 1*b*). The 66cl4, 4T07, and 4T1 cells expressed ~10-, 15-, and 25-fold higher steady-state levels of Rad6 protein, respectively, when compared with lines 67 and 168FAR (Fig. 1*c*). The human HR6A and

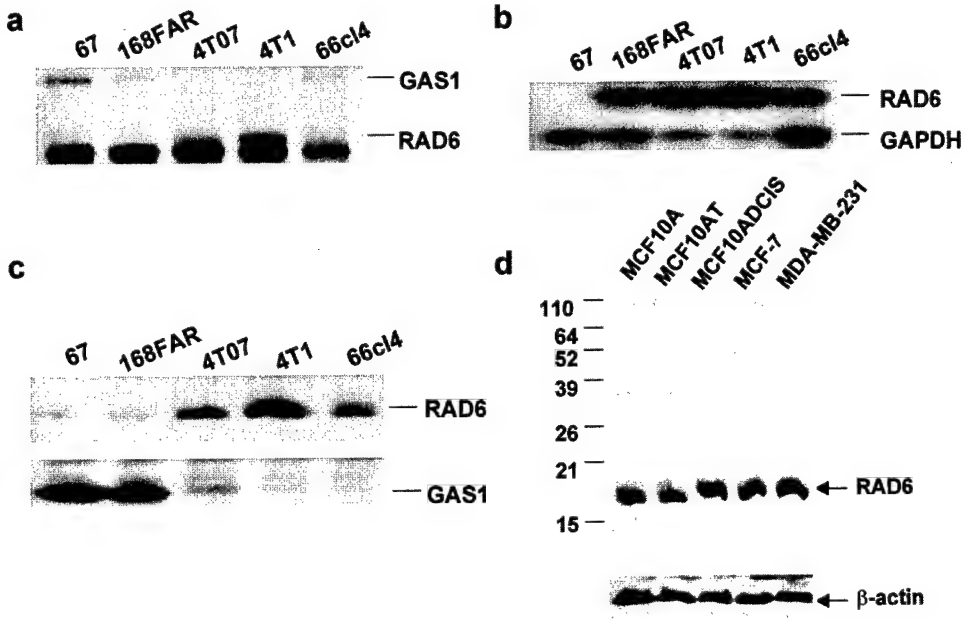

Fig. 1. HR6B/E2B/Rad6 mRNA and HR6A/B protein expression in mouse mammary tumor subpopulations and human breast cancer cells. *a*, differential display analysis of mRNAs from mouse mammary tumor sublines with variant metastatic capacity. Note that expression levels of a second differentially displayed cDNA GAS1, using the same primer set, exhibited an inverse relationship with HR6B expression. *b*, RT-PCR analysis of HR6B in mouse mammary tumor sublines. *c* and *d*, Western blot analysis of Rad6. Because the antibody may not distinguish the two forms of very closely related HR6A and HR6B proteins, immunoreactive Rad6 proteins detected with this antibody are referred to as Rad6 rather than HR6A or B. Membranes from *c* and *d* were stripped and reprobed with anti-Gas1 or anti-β-actin antibody, respectively.

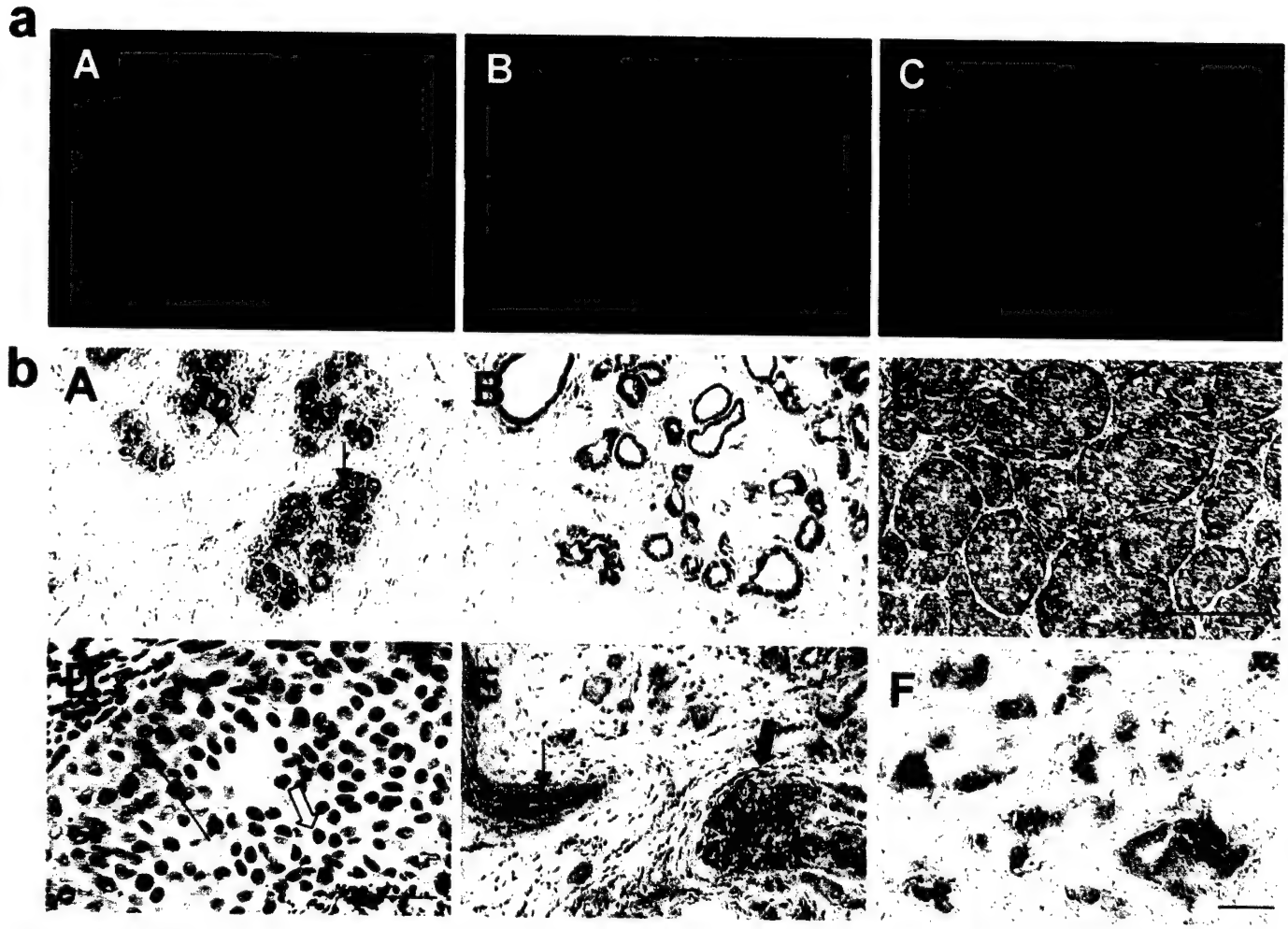

Fig. 2. Immunofluorescence localization of Rad6 in mouse and human mammary epithelial cells. *a*, Rad6 is predominantly localized in the cytoplasm with punctate or diffuse nuclear staining in normal-behaving MCF10A (*A*) or nonmetastatic 168FAR (*B*) cells as opposed to prevalent and intense staining in nuclei of metastatic 4T1 cells (*C*). *Bars*, 10 μm. *b*, immunostaining of Rad6 in human breast tumors. Ducts of normal breast (*A*) and normal mammary epithelium adjacent to tumor (*E*) show Rad6 that is localized in the lumen (⇐); breast tissues with adenosis exhibit moderate Rad6 immunoreactivity (*B*); and breast tumors with DCIS (*C* and *D*) or invasive cancer (➡; *E* and *F*) exhibit intense Rad6 staining. *D* and *F*, higher magnifications of a DCIS and malignant breast tumor, respectively. Whereas Rad6 immunostaining is localized in the cytoplasm of cells from normal or benign breast tissues, note the presence of distinct patterns of Rad6 distribution in a DCIS: cytoplasmic staining (*long black arrow*) in the peripheral cells *versus* nuclear staining (⇒) in the core (*D*). *A*, *B*, *C*, and *E*, *bars*, 10 μm; *D* and *F*, *bar*, 4 μm.

HR6B proteins share 95% identical amino acid residues. Because the synthetic peptide used for generation of the HR6B antibody differs from HR6A by only two amino acid residues, levels of Rad6 protein expressed by HR6A and B forms are not distinguishable. Thus, the M_r 17,000 immunoreactive protein(s) detected in the human cells are referred to as Rad6 rather than HR6A or B. Western blot analysis of human breast cells revealed approximately 3–4-fold higher levels of Rad6 protein in MCF10ADCIS.com, MCF-7, and MDA-MB-231 breast cancer cells as compared with MCF10A and MCF10AT cells after normalizing for loading with β-actin antibody (Fig. 1*d*).

Overexpressed HR6B mRNA Is Wild Type. HR6B cDNAs were amplified by RT-PCR from 67 (low Rad6 expressor), 4T1 (Rad6 overexpressor), and normal BALB/c mouse liver using primers designed to yield full-length HR6B cDNAs as described in "Materials and Methods." The amplified cDNAs were subjected to direct sequence analysis, and sequences of 67 and 4T1 Rad6 cDNAs compared with those from the normal mouse liver. No alterations were detected (data not shown), and the sequence matched 100% to that reported for the mouse HR6B/E2B/Rad6 mRNA indicating that the Rad6 overexpressed in the highly metastatic subline 4T1 is wild type.

Immunocytochemical Localization of Rad6 Protein in Mammary Tumor Cells and Human Breast Carcinomas. Results of immunofluorescence microscopy not only confirmed the abundant presence of Rad6 protein in metastatic 4T1 cells (Fig. 1*c*) but also showed a dramatic difference in cellular distribution of Rad6 between normal, nonmetastatic and metastatic breast epithelial cells. Whereas MCF10A and 168FAR cells show predominant localization of Rad6 in the cytoplasm with diffuse or punctate staining in the nucleus, Rad6 protein is predominantly localized as large aggregates in the nuclei of metastatic 4T1 cells (Fig. 2*a*).

Immunohistochemical localization of Rad6 was performed on cryostat and paraffin-embedded sections from 30 human breast carcinoma tissues and five human breast DCIS lesions, respectively. Examples of the results obtained are shown in Fig. 2*b*. Low levels of Rad6, predominantly localized in the lumen, were observed in the ducts of normal breast (Fig. 2*b*, *panel A*), and in ducts of normal mammary epithelium adjacent to tumor (Fig. 2*b*, *panel E*). Breast tissues with adenosis revealed moderate Rad6 immunoreactivity (Fig. 2*b*, *panel B*). In contrast to weak Rad6 staining in normal breast epithelium, breast tumors with DCIS (Fig. 2*b*, *panels C* and *D*) or invasive cancer (Fig. 2*b*, *panels E* and *F*) exhibited intense Rad6 reactivity. Whereas Rad6 immunostaining is localized in the cytoplasm of cells from normal or benign breast tissues, it is interesting to note that a significant proportion of DCIS and invasive breast carcinomas exhibited nuclear immunoreactivity. Among focally to strongly immunoreactive tumors, tumor cell staining was cytoplasmic in 5 (2,

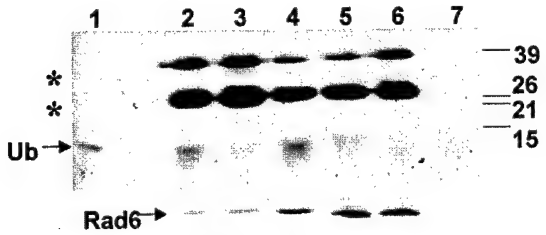

Fig. 3. Ubiquitin-conjugating activity of endogenous Rad6 in mouse mammary tumor sublines of variant metastatic capacities. Total cell lysates containing 100 μg protein from tumor sublines 67 *(Lane 2)*, 168FAR *(Lane 3)*, 4T07 *(Lane 4)*, 4T1 *(Lanes 1, 5* and *7)*, or 66cl4 *(Lane 6)* were immunoprecipitated with anti-Rad6 antibody *(Lanes 2–7)* or with an equivalent amount of corresponding nonimmune IgG *(Lane 1)* and subjected to ubiquitin conjugation assay in the presence of ATP *(Lanes 1–6)* or absence of ATP *(Lane 7)* as described in "Materials and Methods." Positions of mono- and di-ubiquitinated histone H2b are indicated by * beside position of unconjugated ubiquitin. The *blot* on the *bottom* is a Western blot analysis of cell extracts with anti-Rad6 antibody.

stage I; 3, stage II), nuclear in 2 (stage III), and combined nuclear and cytoplasmic in 4 (1, stage 1; 1, stage II; and 2, stage III).

Ubiquitin-conjugation Activity of Rad6 Protein in Tumor Cells. To determine whether the mouse tumor sublines of variant metastatic capacities and Rad6 expressions differed in their Rad6-mediated ubiquitin-conjugating activity, we tested the ability of Rad6 immunoprecipitated from cell lysates to ubiquitinate histone H2b. Results of Fig. 3 demonstrate both the validity of the anti-Rad6 antibody and the presence of functionally active Rad6 in the extracts of tumor sublines as immunoprecipitable Rad6 from all of the tumor sublines, regardless of their metastatic capacity, had the ability to conjugate one or two molecules of ubiquitin to histone H2b. However, contrary to expected results, metastatic sublines exhibited lower histone ubiquitin-conjugating activity as compared with nonmetastatic sublines that was not proportional to levels of endogenous Rad6. The histone ubiquitin-conjugating activity is dependent on Rad6 enzymatic activity, because assays performed in the absence of ATP or extracts immunoprecipitated with the corresponding normal IgG fail to conjugate ubiquitin to histone.

Stable HHR6B Expression in Normal MCF10A Cells. To determine the effect of constitutive overexpression of HHR6B, normal behaving breast epithelial cell line MCF10A was stably transfected with HHR6B expression construct. Rad6 expression levels in the G418-selected clones were evaluated by Western blot analysis, RT-PCR using primers specific to the vector and the exogenous gene, and Northern analysis. All of the clones overexpressed HHR6B mRNA as compared with MCF10A cells containing the empty vector (data not shown); however, of the six clones analyzed for Rad6 protein expression, four clones showed overexpression of Rad6 protein that ranged from approximately 10–50-fold higher levels than those of vector-transfected MCF10A cells (Fig. 4*a*). Clones 1 and 5 overexpressing Rad6 mRNA (50-fold higher than vector-transfected parental cells) and protein displayed an increase in the number of cells exhibiting nuclear pleiomorphism, multinucleated phenotypes, and supernumerary nucleoli (Fig. 4*b*). The generations of multinucleated cells are probably the result of both abnormal mitosis and cell-cell fusion. Evidence for the latter event is deduced from the observation that adjacent nuclei of two or more Rad6-overexpressing cells are found frequently to polarize toward one another apparently promoting cell-cell fusion with the cell membranes separating them often becoming less prominent (Fig. 4*b*). It is interesting to note that whereas parental MCF10A cells showed no cells with polarized nuclei on day 4 of plating, Rad6-overexpressing clones 1 or 5 frequently displayed cells with two or more polarized nuclei that widely ranged from 5 to 25%, which is probably reflective of dynamic cell behavior. Quantitative analysis of multinucleated cells revealed that in contrast to parental MCF10A cells that had <0.4% of cells containing multiple or giant nuclei, both Rad6-overexpressing clones 1 (14.5 ± 4; $P < 0.005$) and 5 (25.2 ± 8.9; $P < 0.001$) exhibited a significant increase in the percentage of cells containing multiple or giant nuclei. Although a proportion of these cells undergo senescence, the majority retained their proliferative capacity as observed by expression of PCNA (Fig. 4*c*). Colocalization of Rad6 with PCNA (Fig. 4*c*) was observed in some cells implicating the intimate association that Rad6, a DNA repair protein, might have with DNA replication factors during the S phase of the cell cycle.

Constitutive Overexpression of HHR6B Protein Induces Centrosome Amplification and Abnormal Mitosis. Because HHR6B-overexpressing MCF10A clones exhibited an abnormal increase in the number of multinucleated cells and cells with pleiomorphic nuclei, we tested whether these cells displayed alterations in centrosome number. Quantitative scoring of centrosomes with anti-γ-tubulin antibodies in mitotic and nonmitotic nuclei revealed the presence of supernumerary centrosomes in constitutively HHR6B-overexpressing MCF10A clones 1 and 5 as compared with cells transfected with the empty vector. Whereas ~98% of parental MCF10A cells contained two or three centrosomes per cell, ~25% of HHR6B-overexpressing clones displayed more than four centrosomes per cell including a significant proportion with >10 centrosomes in clone 5 (Fig. 5, *a* and *b*). These cells contained either a single giant nucleus or multiple multilobed nuclei. Double immunofluorescence labeling and image-merging experiments demonstrated colocalization of Rad6 with centrosomes in interphase cells and at each spindle pole in mitosis (Fig. 5*c*). Centrosome amplification observed in HHR6B-overexpressing clones was associated with a 4–8 fold increase in the number of multipolar mitosis (more than three and up to six spindle poles) as compared with MCF10A cells transfected with control vector (Fig. 6, *a* and *b*).

Rad6 Protein Is Not Associated with Mitotic Condensed Chromosomes. Because Rad6-overexpressing clones exhibit a greater tendency for abnormal mitosis, we determined whether Rad6 protein was associated with mitotic condensed chromosomes. Dividing MCF10A or HHR6B-overexpressing MCF10A cells were fixed and stained for Rad6, and representative cells at different stages during mitosis were examined. Rad6 is distributed fairly uniformly throughout the interphase nuclei either diffusely with notable exclusion from the nucleolus during G_0/G_1 phases (Fig. 7, *panel A*) or focally concentrated in the nucleolus during S and/or G_2-phases (Fig. 7, *panel B*). On entry into mitosis, *i.e.,* after the breakdown of the nuclear membrane, Rad6 diffuses throughout the cytoplasm, and the pattern of fluorescence corresponds to the shape of the cell. However, the fluorescence from Rad6 is clearly reduced in correspondence to the volume occupied by the condensed chromosomes indicating that Rad6 is not associated with DNA during mitosis (Fig. 7, *panels C–F*). After cell division and reformation of nuclear membranes (Fig. 7, *panels G* and *H*), Rad6 protein is redistributed throughout the nucleus suggesting that the protein is concentrated in the nuclei by passage through the nuclear membrane.

HHR6B Overexpression Induces Aneuploidy as Evidenced by SKY. To determine whether the multinucleated phenotypes and abnormal mitosis observed in HHR6B-overexpressing MCF10A cells (Fig. 4) correlated with chromosomal rearrangements, HHR6B-overexpressing clones 1 and 5, and the parental vector-transfected MCF10A cells were analyzed separately by SKY. Although clones 1 and 5 retained the translocation markers t(5;9), t(19;6), and t(3;17), and trisomy 20 observed in parental cells, it is interesting to note that both the HHR6B-overexpressing clones exhibited a tendency to lose chromosomes, because their chromosomal numbers ranged from 42–48 for clone 1 and 31–48 for clone 5 as compared with 46–48 for vector-transfected MCF10A cells (Table 1). Several new aberrations

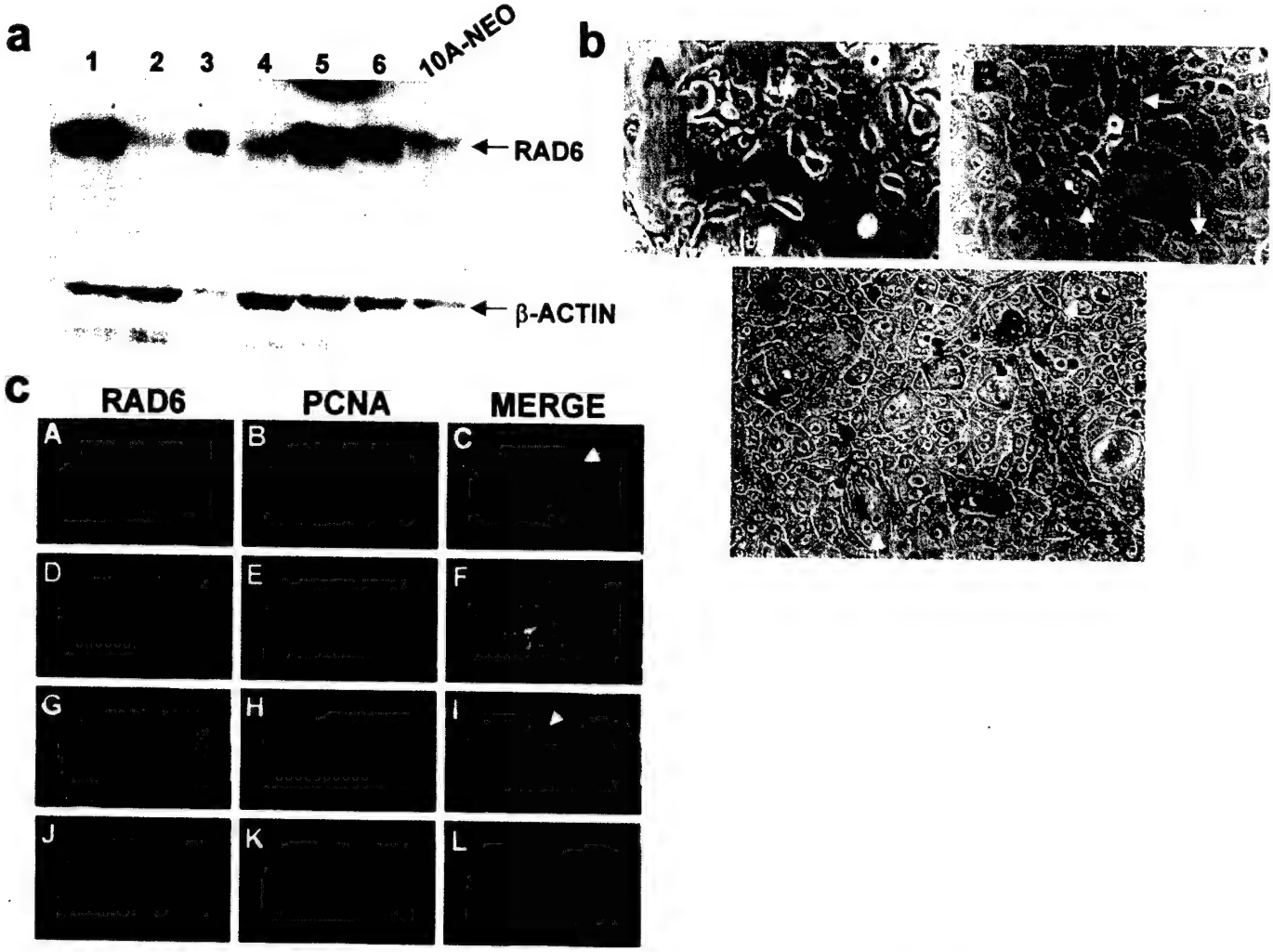

Fig. 4. Effects of constitutive overexpression of HHR6B. *a*, analysis of Rad6 protein expression in the vector-neo control and HHR6B-neo transfectants of MCF10A cells. *Lanes 1–6* represent six independent clones of HHR6B-transfected MCF10A cells selected by G418 selection. Variations resulting from loading differences were monitored by stripping and reprobing the membrane with anti-β-actin antibody. *b*, overexpression of HHR6B protein induces formation of multinucleated cells. *A*, *B*, and *C* are phase contrast micrographs of control (vector-neo) and HHR6B-overexpressing (Rad6-neo, clone 5) MCF10A cells. In contrast to control MCF10A cells that show centrally localized nuclei with two to three nucleoli per cell (*A*), HHR6B-overexpressing cells (*B* and *C*) demonstrate presence of polarized nuclei (➡) that appear to promote cell fusion with resultant formation of cells with multiple (*short white arrow*), pleiomorphic (*long white arrow*), or giant (*long black arrow*) nuclei often containing supernumerary nucleoli (*short black arrow*). Note the presence of apoptotic nuclei in cells containing multiple nuclei (▲). *C*, confluent morphologies of confluent HHR6B-overexpressing MCF10A cells. *Bars*, 1 μm. *c*, immunofluorescence analysis of Rad6 and PCNA expression in HHR6B-overexpressing MCF10A clone 5 and parental MCF10A cells. HHR6B-overexpressing MCF10A clones exhibit intense Rad6 staining in cytoplasmic and nuclear subcompartments of both singly nucleated (*A*) and multinucleated (*D* and *G*) cells. *B*, *E*, and *H* demonstrate proliferative potential of singly and multinucleated HHR6B-overexpressing cells, and *C*, *F*, and *I* show colocalization of Rad6 and PCNA. Note the absence of colocalization of Rad6 and PCNA in *C* (*short white arrow*) indicating the presence of cell cycle-regulated alterations in Rad6-PCNA interactions. Also, note the presence of nuclei of various sizes (*F* and *I*) and elimination of distinct nuclear entity from a multinucleated cell (*long white arrow*). *Panels J–L* represent Rad6 and PCNA localization in parental MCF10A cells. Note colocalization of Rad6 with PCNA in a dividing MCF10A cell. *Bars*, 10 μm.

not observed in parental cells were also found. These included translocations 6;9, 16;1 in 100% of clone 1 and trisomy 1 in 40% of mitotic clone 5 cells.

HHR6B-overexpressing MCF10A Clones Exhibit Anchorage-independent Growth. The HHR6B transfectants were characterized in regard to *in vitro* growth and their potential for transformation. Consistent with previous reports (14), results from soft agar assays showed that the vector-transfected MCF10A cells failed to form colonies in soft agar even if grown for longer periods of time. On the other hand, HHR6B-transfected MCF10A cells grew in soft agar as discrete colonies. Under the conditions used in our experiments, HHR6B-overexpressing MCF10A clone 1 had a CFE of ~10% with 50% of the colonies ranging 50–100 μm in diameter. HHR6B-overexpressing clone 5 had a CFE of 40% with ~60% of the colonies ranging from 50–100 μm and a third of them with diameter >100 μm. Interestingly, whereas a majority of the colonies formed by clone 5 cells remained viable and proliferative, colonies formed by clone 1 exhibited an increase in tendency to undergo apoptosis. These data suggest that constitutive Rad6 overexpression confers the ability for anchorage independent growth; however, continued survival and proliferation of the colonies are dependent on additional chromosomal alterations incurred by cells.

DISCUSSION

Using a well-characterized mouse mammary metastasis model system, we have demonstrated for the first time that the yeast homologue of Rad6, a ubiquitin-conjugating enzyme and a key player in postreplication repair and induced mutagenesis in the yeast, is overexpressed in metastatic tumor sublines and exhibit predominant localization in the nuclei of metastatic cells as compared with prevalent cytoplasmic distribution in nonmetastatic or normal mammary cells. This abnormal pattern of Rad6 protein expression/localization is not restricted to breast cancer cell lines, because human breast carcinomas (DCIS and

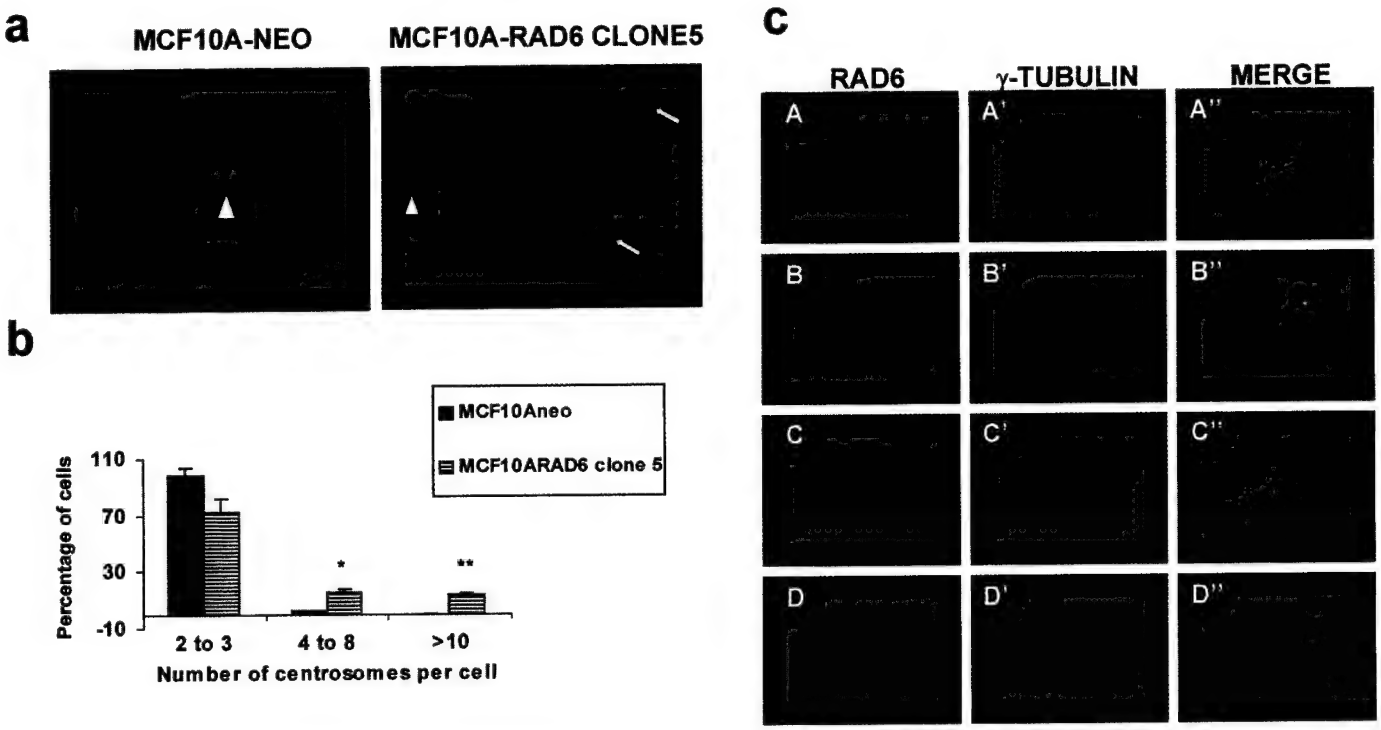

Fig. 5. Centrosome amplification induced by HHR6B overexpression. *a,* vector control (MCF10A-neo) and HHR6B-overexpressing MCF10A (clone 5) cells were stained for centrosomes with a mouse monoclonal antibody to γ-tubulin. *Arrowheads* indicate a cell with normal centrosome number; *arrow* indicates cells with abnormal centrosome number. Because the centrosomes are on different planes, it is not always possible to reveal all centrosomes or centrosomes with equal staining intensity on the same focal plane. *Bars,* 10 μm. *b,* summary of centrosome number amplification induced by HHR6B overexpression. Number of centrosomes were counted in MCF10A cells stably transfected with empty vector or vector containing HHR6B. Data are expressed as the means of four independent determinations; *bars,* ± SE. *, $P < 0.005$; **$P < 0.001$. *c,* localization of Rad6 with centrosomes during interphase and mitosis. MCF10A cells were fixed and stained for Rad6, γ-tubulin, and DNA with DAPI, and representative cells at different stages during cell cycle were examined. Rad6 colocalizes with γ-tubulin within centrosomes during interphase (*A, A'*, and *A''*), prophase (*B, B'*, and *B''*), metaphase (*C, C'*, and *C''*), and anaphase (*D, D', D''*) phases of mitosis. Image-merging analysis of Rad6 and γ-tubulin staining patterns is shown at the *right.* Note that fluorescence from Rad6 is clearly reduced in correspondence to the volume occupied by condensed chromosomes indicating that Rad6 protein is not associated with DNA during mitosis. *Bars,* 10 μm.

invasive cancers) display similar patterns of Rad6 up-regulation and nuclear localization suggesting that deregulation in expression of Rad6 may be an important step in transformation to malignant phenotype.

Because the antibody used in our studies probably fails to distinguish between HR6A and B forms of Rad6, it is not clear whether the elevated levels of Rad6 protein observed in metastatic cells are derived from either one or both forms of *Rad6* genes. It is also not clear whether the high levels of Rad6 protein and its predominant (aberrant?) localization in the nuclear subcompartment is indicative of its role as a direct contributor of genomic instability and, hence, progression, or whether the presence of elevated levels of Rad6 simply reflect the increased mutation rates in malignant tumors. Interestingly, Rad6 protein exhibits notable alterations in its distribution in the interphase and mitotic nuclei that is compatible with its function as a transcription factor. Stable constitutive overexpression of HHR6B in near diploid normal-behaving MCF10A cells resulted in generation of multinucleated cells, abnormal centrosome numbers, multipolar mitosis, and transformation *in vitro*. Although the mechanism(s) responsible for generation of multinucleated cells (*i.e.,* abnormal mitosis and/or cell-cell fusion) are yet to be determined, one possibility is that high levels of Rad6 may mediate increased ubiquitin-mediated degradation of proteins on cell membrane.

Whereas a small subset of cancers exhibit genetic instability primarily at the nucleotide level, most breast cancers exhibit instability at the chromosomal level resulting in losses and gains of whole chromosomes, or large portions thereof (22, 23). That Rad6 overexpression results in aneuploidy is confirmed by SKY analysis, because HHR6B-overexpressing clones 1 and 5 were found to have fewer chromosomes ranging from 42–48 or 31–48, respectively, than the parental vector-transfected MCF10A cells that had 46–48 chromosomes. Generation of aneuploidy appears to be an initiation step in these cells, because the parental MCF10A cells are near-diploid and lack the ability to support anchorage-independent growth in soft agar (14). In contrast, Rad6-overexpressing MCF10A cells exhibit a deviation from the normal number of chromosomes, and show centrosome amplification, multipolar mitosis, and the ability to grow in soft agar. Because the clones analyzed overexpress up to 50-fold greater levels of Rad6 than vector-transfected parental cells and ~10-fold greater levels than breast cancer cell lines, it will be interesting to verify whether cells expressing ectopic Rad6 at levels observed in breast cancer cell lines exhibit aneuploidy and whether these effects can be negated by overexpression of mutant *rad6*.

Aneuploidy is the predominant class of genomic instability found in breast, colorectal, prostate, and other solid cancers in general (24–27). Given the relationship of centrosome function to cell polarity and to maintenance of genomic integrity, understanding the mechanisms that lead to aberrant centrosomes, their interaction with specific proteins, and the degree and nature of centrosomal defects may have predictive value in regard to patient prognosis. Centrosome amplification or dysregulation in centrosome duplication results in assembly of aberrant mitotic spindles that result in misegregation of chromosomes and aneuploidy (28). That Rad6 may play an important role in the maintenance of genomic integrity is strengthened by the observation that it is associated with centrosomes throughout the interphase and mitotic phases of the cell cycle, and displays striking changes in its distribution during different stages of the cell cycle. A noteworthy

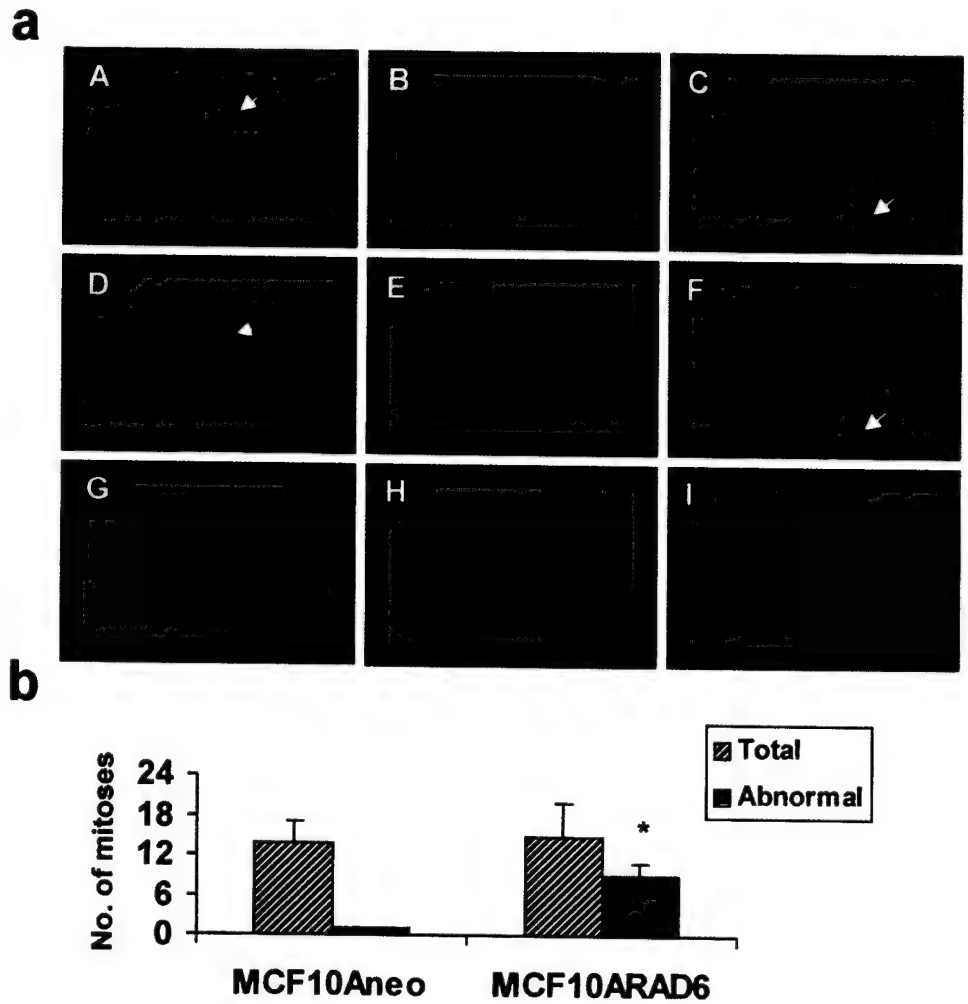

Fig. 6. Abnormal mitosis in HHR6B-overexpressing MCF10A cells. *a*, HHR6B-overexpressing MCF10A clone 5 cells were fixed and stained for γ-tubulin (*red; A–C, E,* and *G–I*) or DNA with DAPI (*blue; D–F*), and mitotic cells with established spindle poles were examined. *Arrows* indicate cells with normal bipolar spindle (*A, D, C,* and *F*). Note the presence of monopolar (*C*), tetrapolar (*B, E,* and *H*), tripolar (*G*), and hexapolar (*I*) spindles. Image-merging of γ-tubulin and DNA staining is shown in *E*. *Bars*, 10 μm. *b*, summary of aberrant mitoses induced by HHR6B overexpression. Multipolar (*abnormal*) mitosis (3 and >3 spindle poles) were counted in vector-control (*MCF10A-neo*) and HHR6B-overexpressing (*MCF10A-Rad6* clone 5), and results expressed relative to the total number of mitotic nuclei scored from 300 cells. Data are the means of three independent determinations; *bars*, ± SD. *, $P < 0.005$.

consequence of Rad6 overexpression is abnormal mitosis. It is conceivable that the loss of chromosome(s) evidenced by SKY analysis resulted from multidirectional forces impacted on a single chromosome in a multipolar spindle (29). Consequently, the daughter cells would receive abnormal numbers of chromosomes and become aneuploid as supported by our SKY data. These data show that HHR6B overexpression can cause aberrant chromosomal partitioning at mitosis culminating in a catastrophic loss or gain of chromosomes that result in either cell death or survival through malignant transformation.

Centrosomes are abnormal in number, form, and function in a number of human tumors although the mechanisms by which

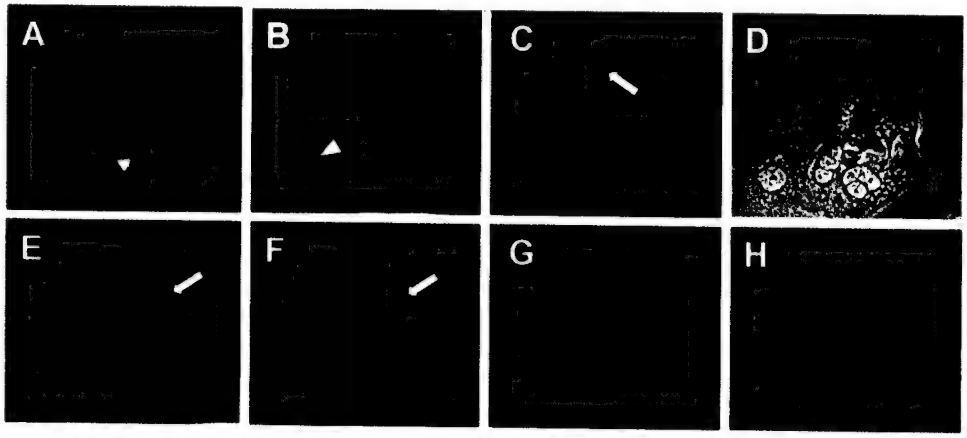

Fig. 7. Rad6 protein is not associated with mitotic condensed chromosomes. Dividing MCF10A (*A* and *E–H*) or HHR6B-overexpressing MCF10A (*B–D*) cells were fixed and stained for Rad6, and representative cells at interphase (*A*, G_0/G_1; *B*, S/G_2) and different stages during mitosis (metaphase, *C* and *D*; anaphase, *E* and *F*; and telophase, *G* and *H*) were examined. Note the exclusion of Rad6 from the nucleolus in *A* (←) and its appearance in the nucleolus in B (△), which coincides with its colocalization with PCNA (Fig. 4*c*). Also note that after the breakdown of the nuclear membrane, Rad6 is distributed uniformly throughout the cytoplasm, and the pattern of green fluorescence corresponds to the shape of the cell. However, the fluorescence from Rad6 is clearly reduced in correspondence to the volume occupied by condensed chromosomes (⇨), indicating that Rad6 is not associated with DNA during mitosis. After cell division and reformation of nuclear membranes (*G* and *H*), note that Rad6 is redistributed uniformly throughout the nucleus. *D* is a phase contrast micrograph of *C*.

Table 1 *SKY analysis of vector-control versus HHR6B-overexpressing clones of MCF10A cells*[a]

	MCF10A-neo		MCF10A-Rad6 clone 5		MCF10A-Rad6 clone 1	
Mitotic figure	Chromosome no.	Extra chromosome	Chromosome no.	Extra chromosome	Chromosome no.	Extra chromosome
1	47	20(3)	47	20(3)	46	20(3),14(1)
2	48	20(3), 10(3)	48	20(3), 1(3)	46	20(3),13(1)
3	46	20(3), 10(1)	43	20(3), 22(1), 21(1), 18(3), 13(1), 7(1), 6(1), 3(1), 1(3)	41	20(3),15(1),10(1),9(1), 8(1),6(1),2(1)
4	46	20(3), 3(1)	48	20(3), 1(3)	48	20(3),6(3)
5	47	20(3)	48	20(3), 19(3)	45	20(3),18(0)
6	48	20(3), 1(3)	38	20(3), 19(1), 15(1), 14(1), 12(1), 11(1), 8(1), 7(1), X(0)	47	20(3)
7	47	20(3)	40	20(3), 19(0), 16(1), 10(1), 5(1), 3(1), X(1)	48	20(3),6(3)
8	47	20(3)	39	20(3), 21(1), 18(1), 13(1), 12(1), 11(1), 8(1), 6(3), 5(1), 3(1), 1(1)	44	20(3),15(1),11(1),10(1), 4(3),3(1)
9	47	20(3)	31	partial	45	20(3),14(1),5(1)

[a] Alterations involving chromosomal translocations are not shown here.

centrosomal anomalies arise is unknown. Phosphorylation of centrosomal proteins in *Drosophila* (29) and vertebrates (30, 31) have been reported to influence microtubule nucleation and dynamics at the centrosomes (32). In mammalian cells, cdc2, NIMA, and PLK1 kinases have been implicated in centrosome duplication, maturation, and separation (33–36). Because Rad6 protein is associated with centrosomes throughout the interphase and mitotic phases of the cell cycle, Rad6 protein may play an important regulatory role via regulated ubiquitination and proteolytic degradation of centrosomal proteins. Thus, an imbalance in the levels of Rad6 protein in the cell or that associated with centrosomes could lead to defects in centrosome duplication, maturation, and function, which could induce aneuploidy. Taken together, these data suggest that centrosomes may provide a platform for assembly and functioning of several activities, and that alteration or dysregulation in the activities of specific molecules could directly impact centrosome function as part of tumorigenic process. Identification of natural substrates of Rad6 on centrosomes will help in understanding its role in maintenance of centrosome structure and function, the disruption of which could result in anomalous centrosome amplification and chromosome segregation in tumor cells. These may, in turn, provide new insights in development of new drugs for therapy of tumors with chromosome instability.

In summary, our findings suggest that Rad6 is an important ubiquitin-conjugating enzyme that may play a significant role in the maintenance of genomic integrity of mammalian cells and that an imbalance in the levels and activity of Rad6 could lead to chromosomal instability and transformation *in vitro*.

ACKNOWLEDGMENTS

We thank Dr. G. Del Sal for kindly providing the Gas1 antibody. We also thank Dr. Gloria Heppner for critical reading of the manuscript and helpful suggestions.

REFERENCES

1. Minnick, D. T., and Kunkel, T. A. DNA synthesis errors, mutators and cancer. Cancer Surv., *28:* 3–20, 1996.
2. Lawrence, C. W. The Rad6 DNA repair pathway in *Saccharomyces cerevisiae*: what does it do, and how does it do it? Bioessays, *16:* 253–258, 1994.
3. Reynolds, P., Weber, S., and Prakash, L. Rad6 gene of *Saccharomyces cerevisiae* encodes a protein containing a tract of 13 consecutive aspartates. Proc. Natl. Acad. Sci. USA, *82:* 168–172, 1985.
4. Jentsch, S., McGrath, J. P., and Varshavsky, A. The yeast DNA repair gene RAD6 encodes a ubiquitin-conjugating enzyme. Nature (Lond.), *329:* 131–134, 1987.
5. Lawrence, C. W. Mutagenesis in *Saccharomyces cerevisiae*. Adv. Genet., *21:* 173–254, 1982.
6. Haynes, R. H., and Kunz, B. A. Life cycle and inheritance. *In:* J. Strathern, E. Jones, and J. Broach (eds.), The Molecular Biology of the Yeast *Saccharomyces cerevisiae*, pp. 371–414. Cold Spring Harbor, NY: Cold Spring Harbor Laboratory, 1981.
7. Prakash, S., Sung, P., and Prakash, L. The eukaryotic nucleus. P. R. Straus and S. H. Wilson (eds.), Vol I, pp. 275–292. Caldwell, NJ: Telford Press, 1990.
8. Goebl, M. G., Yochem. J., Jentsch, S., McGrath, J. P., Varshavsky, A., and Byers, B. The yeast cell cycle gene CDC34 encodes a ubiquitin conjugating enzyme. Science (Wash. DC), *241:* 1331–1335, 1988.
9. Koken, M. H. M., Reynolds, P., Jaspers-Dekker, I., Prakash, L., Prakash, S., Bootsma, D., and Hoeijmakers, J. H. J. Structural and functional conservation of two human homologs of the yeast DNA repair gene RAD6. Proc. Natl. Acad. Sci. USA, *88:* 8865–8869, 1991.
10. Koken, M. H., Smith, E. M., Jaspers-Dekker, I., Oostra, B. A., Hagemeijer, A., Bootsma, D., and Hoeijmakers, J. H. Localization of two human homologs, HHR6A and HHR6B, of the yeast DNA repair gene RAD6 to chromosomes Xq24–q25 and 5q23–q31. Genomics, *12:* 447–453, 1992.
11. Roest, H. P., van Klaveren, J., de Wit, J., van Gurp, C. G., Koken, M. H., Vermey, M., van Roijen, J. H., Hoogerbrugge, J. W., Vreeburg, J. T., Baarends, W. M., Bootsma, D., Grootegoed, J. A., and Hoeijmakers, J. H. Inactivation of the HR6B ubiquitin-conjugating DNA repair enzyme in mice causes male sterility associated with chromatin modification. Cell, *86:* 799–810, 1996.
12. Miller, F. R., Miller, B. E., and G. H. Heppner. Characterization of metastatic heterogeneity among subpopulations of a single mouse mammary tumor. Invasion Metastasis, *3:* 22–31, 1983.
13. Aslakson, C. J., and F. R. Miller. Selective events in the metastatic process defined by analysis of the sequential dissemination of subpopulations of a mouse mammary tumor. Cancer Res., *52:* 1399–1405, 1992.
14. Soule, H., Maloney, T. M., Wolman, S. R., Peterson, W. D. Jr., Brenz, R., McGrath, C. M., Russo, J., Pauley, R. J., Jones, R. F., and S. C. Brooks. Isolation and characterization of a spontaneously immortalized human breast epithelial line, MCF10. Cancer Res., *50:* 6075–6086, 1990.
15. Shekhar, M. P., Nangia-Makker, P., Wolman, S. R., Tait, L., Heppner, G. H., and Visscher, D. W. Direct action of estrogen on sequence of progression of human preneoplastic breast disease. Am. J. Pathol., *152:* 1129–1132, 1998.
16. Miller, F. R., Santner, S. J., Tait, L., and Dawson, P. J. MCF10DCIS.com xenograft model of human comedo ductal carcinoma *in situ*. J. Natl. Cancer Inst., *92:* 1185–1186, 2000.
17. Liang, P., Averboukh, L., and Pardee, A. B. Distribution and cloning of eukaryotic mRNAs by means of differential display: refinements and optimization. Nucleic Acids Res., *21:* 3269–3275, 1993.
18. Del Sal, G., Ruaro, M. E., Philipson, L., and Schneider, C. The growth arrest-specific gene, gas1, is involved in growth suppression. Cell, *70:* 595–607, 1992.
19. Shekhar, P. V., Werdell, J., and Basrur, V. S. Environmental estrogen stimulation of growth and estrogen receptor function in preneoplastic and cancerous human breast cell lines. J. Natl. Cancer Inst., *89:* 1774–1782, 1997.
20. Heng, H. H., and Tsui, L. C. Modes of DAPI banding and simultaneous *in situ* hybridization. Chromosoma (Berl.), *102:* 325–332, 1993.
21. Liu, G., Lu, W., Bremer, S., Hameister, H., Schreiner, B., Hughes, M., and Heng, H. H. Spectral karyotyping of mouse cell line WMP2. Cytogenet. Cell Genet., *90:* 271–274, 2000.
22. Lengauer, C., Kinzler, K. W., and Vogelstein, B. Genetic instabilities in human cancers. Nature (Lond.), *396:* 643–648, 1998.
23. Duesberg, P. H., Rausch, C., Rasnick, D., and Hehlmann, R. Genetic instability of cancer cells is proportional to their degree of aneuploidy. Proc. Natl. Acad. Sci. USA, *95:* 13692–13697, 1998.
24. Hartwell, L., Weinert, T., Kadyk, L., and Garvik, B. Genomic integrity and cancer. *In:* B. Stillman (ed.), Cell Cycle Checkpoints, Vol. LIX, pp. 259–263. Plainview, NY: Cold Spring Harbor Laboratory, 1994.
25. Mitelman, F., Johansson, B., and Mertens, F. Catalog of Chromosome Aberrations in Cancer. New York, NY: Wiley, 1998.

26. Lengauer, C., Kinzler, K., and Vogelstein, B. Genetic instability in colorectal cancers. Nature (Lond.), *386:* 623–627, 1997.
27. Hartwell, L. Defects in a cell cycle check point may be responsible for the genomic instability of cancer cells. Cell, *71:* 543–546, 1992.
28. Dowsy, S. The centrosome–a tiny organelle with big potential. Nat. Genet., *20:* 104–106, 1998.
29. Kellogg, D. R., Oegama, K., Raff, J., Schneider, K., and Alberts, B. M. CP60: a microtubule associated protein that is localized to the centrosome in a cell cycle-specific manner. Mol. Biol. Cell, *6:* 1673–1684, 1995.
30. Vandre, D. D., Davis, F. M., Rao, P. N., and Borisy, G. G. Phosphoproteins are components of mitotic microtubule organizing centers. Proc. Natl. Acad. Sci. USA., *81:* 4439–4443, 1984.
31. Taagepera, S., Campbell, M. S., and Gorbsky, G. J. Cell cycle-regulated localization of tyrosine and threonine phosphoepitopes at the kinetochores of mitotic chromosomes. Exp. Cell Res., *221:* 249–260, 1995.
32. Verde, F., Berrez, J. M., Antony, C., and Karsenti, E. Taxol-induced microtubule asters in mitotic extracts of *Xenopus* eggs: requirement for phosphorylated factors and cytoplasmic dynein. J. Cell Biol., *112:* 1177–1187, 1991.
33. Buendia, B., Draetta, G., and Karsenti, E. Regulation of the microtubule nucleating activity of centrosomes in *Xenopus* egg extracts: role of cyclin A-associated protein kinase. J. Cell Biol., *116:* 1431–1442, 1992.
34. Fry, A. M., Meraldi, P., and Nigg, E. A. A centrosomal function for the human Nek2 protein kinase, a member of the NIMA family of cell cycle regulators. EMBO J., *17:* 470–481, 1998.
35. Nigg, E. A., Blangy, A., and Lane, H. A. Dynamic changes in nuclear architecture during mitosis: on the role of protein phosphorylation in spindle assembly and chromosome segregation. Exp. Cell Res., *229:* 174–180, 1996.
36. Lane, H. A., and Nigg, E. A. Antibody microinjection reveals an essential role for human polo-like kinase 1 (Plk 1) in the functional maturation of mitotic centrosomes. J. Cell Biol., *135:* 1701–1713, 1996.

MOLECULAR AND CELLULAR BIOLOGY, Apr. 2003, p. 2463–2475 Vol. 23, No. 7
0270-7306/03/$08.00+0 DOI: 10.1128/MCB.23.7.2463–2475.2003
Copyright © 2003, American Society for Microbiology. All Rights Reserved.

Supramolecular Complex Formation between Rad6 and Proteins of the p53 Pathway during DNA Damage-Induced Response

Alex Lyakhovich[1] and Malathy P. V. Shekhar[1,2]*

Breast Cancer Program, Karmanos Cancer Institute,[1] and Department of Pathology,[2] Wayne State University School of Medicine, Detroit, Michigan 48201

Received 19 June 2002/Returned for modification 23 July 2002/Accepted 1 January 2003

The HR6A and -B genes, homologues of the yeast Rad6 gene, encode ubiquitin-conjugating enzymes that are required for postreplication repair of DNA and damage-induced mutagenesis. Using surface plasmon resonance, we show here that HR6 protein (referred as Rad6) physically interacts with p53. Analysis of proteins coimmunoprecipitated with Rad6 antibody from metabolically labeled normal MCF10A human breast epithelial cells not only confirmed Rad6-p53 interactions in vivo but also demonstrated for the first time that exposure of MCF10A cells to cisplatin or adriamycin (ADR) induces recruitment of p14ARF into Rad6-p53 complexes. Further analysis of ADR-induced p53 response showed that stable Rad6-p53-p14ARF complex formation is associated with a parallel increase and decrease in monoubiquitinated and polyubiquitinated p53, respectively, and arrest in G_2/M phase of the cell cycle. Interestingly, the ADR-induced suppression of p53 polyubiquitination correlated with a corresponding decline in intact Hdm2 protein levels. Treatment of MCF10A cells with MG132, a 26S proteasome inhibitor, effectively stabilized monoubiquitinated p53 and rescued ADR-induced downregulation of Hdm2. These data suggest that ADR-induced degradation of Hdm2 occurs via the ubiquitin-proteasome pathway. Rad6 is present in both the cytoplasmic and nuclear compartments of normal MCF10A cells, although in response to DNA damage it is predominantly found in the nucleus colocalizing with ubiquitinated p53, whereas Hdm2 is undetectable. Consistent with in vivo data, results from in vitro ubiquitination assays show that Rad6 mediates addition of one (mono-) to two (multimono-) ubiquitin molecules on p53 and that inclusion of Mdm2 is essential for its polyubiquitination. The data presented in the present study suggest that Rad6-p53-p14ARF complex formation and p53 ubiquitin modification are important damage-induced responses that perhaps determine the fidelity of DNA postreplication repair.

Postreplication DNA repair is believed to function during and after DNA synthesis when unrepaired lesions in the template strand induce stalling of the DNA replication assembly, thereby causing gaps in the newly synthesized strand. The postreplication repair system is composed of two separate processes, error-free and error-prone, that are jointly regulated by the Rad6 gene and are designed to promote the completion of DNA synthesis (30). Error-prone recovery entails a mutagenic bypass of damaged sites by a specialized DNA polymerase dedicated to translesion synthesis (30), whereas error-free recovery involves bypass by template switching and/or gap filling by recombination, although the mechanism of error-free repair has not been fully understood (30, 31).

The Rad6 gene encodes a 17-kDa protein that belongs to a group of ubiquitin-conjugating enzymes (E2) that covalently adds ubiquitin to specific lysine residues of a substrate protein (24, 53). All functions performed by Rad6 appear to result from ubiquitination since replacement of the conserved Cys88 with serine produces a totally null phenotype (55, 56). Mutations in Rad6 confer extreme sensitivity toward a variety of DNA-damaging agents but are defective in damage-induced mutagenesis (43). Rad6 is highly conserved among eukaryotes. Two closely related human DNA repair genes, HHR6A and HHR6B (human homologues of yeast Rad6), encode ubiquitin-conjugating enzymes and complement the DNA repair and UV mutagenesis defects of the *Saccharomyces cerevisiae rad6* mutant (26). HHR6A and HHR6B share 95% identical amino acid residues and are localized on human chromosome Xq24-q25 and 5q23-q31, respectively (27). In *S. cerevisiae*, error-free and error-prone lesion bypass require Rad6 and Rad18 genes (8, 41, 58, 59). Rad18 is a zinc finger protein with single-stranded DNA-binding activity and forms a complex with Rad6 (3–5). Recently, a human homolog of Rad18 has been identified that encodes for a 54-kDa protein and forms stable protein complexes with both HHR6A and HHR6B when coexpressed in yeast (61). However, proteins relevant to DNA repair that are ubiquitinated by Rad6 remain unknown.

Proteasomal degradation of key regulatory proteins control physiological events involving cell cycle, differentiation, DNA repair, apoptosis, and immune responses (18). Ubiquitination of a protein involves three separate enzymatic activities designated E1 (ubiquitin-activating enzyme), E2 (ubiquitin-conjugating enzyme), and E3 (ubiquitin ligase [9, 18, 19]). Ubiquitin is first activated through a covalent thiol ester linkage to E1. The activated ubiquitin is transferred to one of the several different ubiquitin-conjugating enzymes (E2) in an ATP-dependent manner. E2 then functions in combination with an E3 ligase to transfer ubiquitin to the target protein. The final ubiquitin transfer results in an isopeptide bond between the carboxyl-terminal Gly of ubiquitin and the ε-amino group of a Lys residue on the target protein. Whereas monoubiquitination may serve as targeting or localization signal (52), further conjugation of ubiquitin, usually to Lys48 of the previous ubiq-

* Corresponding author. Mailing address: Breast Cancer Program, Karmanos Cancer Institute, 110 East Warren Ave., Detroit, MI 48201. Phone: (313) 833-0715, ext. 2326. Fax: (313) 831-7518. E-mail: shekharm@karmanos.org.

uitin moiety, results in the formation of polyubiquitin chains that labels the substrate for selective degradation by the 26S proteasome (10, 12, 14). Different E2s can function with a given E3. Thus, the formation of different E2-E3 complexes may provide additional levels of substrate specificity (29).

The tumor suppressor p53 is a latent and highly labile transcription factor that is mutated in 50% of human tumors mainly by missense mutation in the DNA-binding region. It plays a central role in maintaining genomic integrity by coordinating cell cycle (25), DNA repair (16), and programmed cell death in response to DNA damage (32, 49). In normal cells, p53 is present at very low levels; however, in response to DNA damage, wild-type p53 accumulates in the nucleus and coordinates a change in the balance of gene expression leading to growth arrest or apoptosis, events that prevent the growth or survival of damaged cells. Signals arising from cellular stresses trigger a complex series of regulatory events in the p53 pathway that lead to increased stability of p53 and activation of its biochemical functions (15). The stability and half-life of p53 are tightly regulated by Mdm2 and the ubiquitin-proteasome pathway (2, 16, 28). Binding of Mdm2 to the amino terminus of p53 (amino acid residues 19 to 26) represses p53 transcriptional activity (38, 39), promotes ubiquitination of p53 by acting as the E3 ubiquitin ligase, and targets p53 to the cytoplasm for 26S proteasome-dependent degradation (17). Disruption of p53-Mdm2 complexes is a pivotal event during the induction of p53 and is sufficient to invoke p53-mediated gene expression and cell cycle arrest (48). The increase in p53 is thought to result from p14ARF binding to the Mdm2, which interferes with p53-Mdm2 complex formation and proteasome degradation by inhibiting the E3 ubiquitin ligase activity of Mdm2 (23, 28, 35).

Here we show that Rad6 functions in cells after exposure to DNA-damaging agents by forming supramolecular complexes with p53 and p14ARF that correlate with p53 stability. Adriamycin (ADR)-induced p53 response in normal MCF10A human breast epithelial cells is accompanied by an increase in monoubiquitinated p53 and a simultaneous decrease in p53 polyubiquitination that is coincident with Hdm2 downregulation via the ubiquitin-proteasome pathway. The stable Rad6-p53 interaction observed is not unique to MCF10A cells since it is also seen after ADR treatment, albeit only temporarily, in metastatic MDA-MB-231 human breast cancer cells that express mutant p53. Results from in vitro ubiquitination assays show that Rad6 mediates limited addition of ubiquitin molecules on p53, and inclusion of Mdm2 is essential for extending the ubiquitin chains. The data presented in the present study suggest that (i) p53 ubiquitination is an important and regulated damage-induced modification and (ii) the accuracy of postreplication DNA repair process may be determined by the stability of supramolecular complexes formed between Rad6 and proteins of the p53 pathway.

MATERIALS AND METHODS

Cell lines, cell culture, and drug treatment. MCF10A cells are normal-behaving pseudodiploid cells that lack tumorigenicity in nude mice and are unable to support anchorage-independent growth (50). The metastatic human breast cancer cell line MDA-MB-231 harbors an R280K mutation in p53 (T. Soussi, p53 mutation database [http://p53.curie.fr/]) and was purchased from the American Type Culture Collection (Manassas, Va.). MCF10A cells were maintained in Dulbecco modified Eagle medium (DMEM)–F-12 medium supplemented with 2.5% horse serum, 0.02 μg of epidermal growth factor, 0.5 μg of hydrocortisone/ml, 10 μg of insulin/ml, 0.1 μg of cholera toxin/ml, 100 U of penicillin/ml, and 100 μg of streptomycin/ml. MDA-MB-231 cells were grown in DMEM supplemented with 10% fetal calf serum. Cells were treated with ADR (inhibition concentration [IC_{50}] = 0.1 μg/ml for MCF10A or 0.5 μg/ml for MDA-MB-231) for 1 h, rinsed, and replaced with fresh medium to allow recovery for 0 to 72 h. For p53 or Hdm2 ubiquitination, the proteasome inhibitor MG132 (Calbiochem, San Diego, Calif.) was added to a final concentration of 25 μM to the culture media of untreated or ADR-treated cells 3 h before lysates were prepared.

Metabolic labeling and immunoprecipitation. Control or cisplatin-treated (5 μg/ml for 6 h) MCF10A cells (5×10^6 cells per 100-mm dish) were incubated in methionine-free DMEM–2% dialyzed fetal bovine serum supplemented with 100 μCi of [L-^{35}S]-methionine (specific activity, 1,083 Ci/mmol; NEN Life Science Products). Cells were labeled for 3 h, after which the monolayers were gently rinsed twice with phosphate-buffered saline and lysed with lysis buffer (10 mM Tris-HCl, pH 7.5; 150 mM NaCl; 1% Triton X-100; 1 mM phenylmethylsulfonyl fluoride; 5 μg of leupeptin, aprotonin, pepstatin, and chymostatin/ml; 1 mM sodium orthovanadate). Aliquots of lysates containing equivalent amounts of [^{35}S]methionine incorporated into trichloroacetic acid-insoluble material (10^7 cpm) were immunoprecipitated by incubating them overnight with Rad6 antibody or nonimmune rabbit immunoglobulin G (IgG). Immune complexes were pelleted by incubating them with protein A/G-agarose and washed several times with lysis buffer. Rad6-immunodepleted lysates and total cellular lysates were subjected to immunoprecipitation with p53 Ab421 antibody, and immune complexes similarly recovered with protein A/G-agarose. Bound proteins were solubilized in sodium dodecyl sulfate (SDS) buffer and subjected to SDS-polyacrylamide gel electrophoresis (PAGE). Gels were either processed for Western blot analysis with polyclonal p53 CM-1 antibody or for fluorography.

Antibodies, immunoprecipitation, and Western blot analysis. Control or ADR-treated MCF10A cells harvested after 0-, 2-, 4-, 8-, 24-, 48-, or 72-h recovery periods were lysed as described above, and aliquots of lysates containing 100 μg of protein were then either subjected to Western blot analysis of Rad6, Rad18, p53, p14ARF, Hdm2, and β-actin or to immunoprecipitation with Rad6 antibody. Immune complexes were pelleted with protein A/G-agarose, washed, and subjected to SDS-PAGE after solubilization in SDS sample buffer under reducing or nonreducing conditions. For reprecipitation experiments, immune complexes resulting from immunoprecipitation with Rad6 antibody were boiled in 100 μl of 50 mM Tris-HCl (pH 7.5)–1% SDS–5 mM dithiothreitol (DTT), diluted 10-fold in lysis buffer, and reprecipitated with antibodies to p53, p14ARF, Mdm2, or Rad18. p53, p14ARF, Hdm2, or Rad18 proteins coprecipitated with Rad6 antibody were detected by Western blot analysis with pAb421, p14ARF, Mdm2, or Rad18 antibody, respectively. To examine effects of the 26S proteasome inhibitor MG132 on p53 ubiquitination, cell extracts were immunoprecipitated with p53 pAb421 antibody, followed by Western blot analysis with p53 CM-1, and antibodies that specifically recognize ubiquitin-protein conjugates (FK2) or polyubiquitinated proteins (FK1) but not free ubiquitin. Effects of MG132 on Hdm2 ubiquitination were determined by Western blot analysis with Mdm2 antibody. Protein bands were visualized after reaction with appropriate anti-rabbit IgG, anti-mouse IgG, or anti-mouse IgM coupled to horseradish peroxidase by using ECL kit (Amersham, Arlington Heights, Ill.). The relative steady-state levels of HHR6A/HHR6B, Rad18, p14ARF, p53, or Hdm2 to β-actin bands were quantitated with a scanner-densitometer (model 300A densitometer; Molecular Dynamics, Sunnyvale, Calif.). Antibody to Rad6 was generated by multiple immunizations of New Zealand White rabbits with a synthetic peptide (K plus amino acid residues 131 to 152; accession no. NM_009458) that is conserved 100% in mouse and human HR6B and 91% in human HR6A (46). Since the antibody is unable to distinguish between HR6A and -B forms of Rad6, the 17-kDa proteins detected by this antibody are referred to as Rad6. p53 CM-1 polyclonal antibody was purchased from Novocastra Laboratories, Ltd. (Newcastle upon Tyne, United Kingdom); p53 pAb421 and pAb1801 antibodies recognize epitope on amino acids 372 to 382 and amino acids 46 to 55, respectively; Mdm2 antibody recognizes an epitope in the N terminus of Mdm2 and was purchased from Oncogene Science (Cambridge, Mass.). Other antibodies used were specific for human Rad18 (Imgenex, San Diego, Calif.), ubiquitin (Zymed Labs, San Francisco, Calif.), ubiquitin-protein conjugates (FK2) and polyubiquitin-protein conjugates FK1 (Affiniti Research Products, Ltd., Mamhead Castle, United Kingdom), p14ARF, and β-actin (Oncogene Science).

Immunofluorescence microscopy. Control or ADR-treated MCF10A cells were grown on coverslips and fixed in methanol-acetone (1:1 [vol/vol]) at −20°C. Cells were preincubated with 2% horse serum–phosphate-buffered saline and then incubated with anti-Rad6 antibody. To assess colocalization and/or regulation by ADR of Rad6, p53, or Hdm2 expression, cells were stained with a 1:1

mixture of Rad6 and p53 pAb421 antibodies, pAb421 and ubiquitin antibodies, or Rad6 and Mdm2 antibodies. Cells were washed, and Rad6, ubiquitin, p53, or Hdm2 was detected with fluorescein isothiocyanate (FITC)-conjugated goat anti-rabbit IgG or Texas red-conjugated goat anti-mouse IgG. Nonbinding mouse or rabbit IgG was used as a control in all double-labeling experiments. All images were collected on a Olympus BX-4 fluorescence microscope equipped with Sony high-resolution/sensitivity charge-coupled device video camera.

Surface plasmon resonance assay. p53-Rad6 interaction studies were carried out by using a BIAcore 3000 surface plasmon resonance instrument (BIAcoreAB, Uppsala, Sweden). All of the experiments were carried out at 25°C by using a constant flow rate (5 μl/min) of running buffer. Glutathione *S*-transferase (GST)-tagged p53, a gift from H. Yasuda (School of Life Science, Tokyo University of Pharmacy and Life Science, Tokyo, Japan) was affinity purified on a glutathione-conjugated Sepharose 4B column and covalently attached to CM5 sensor chip surface by the standard amine coupling procedure. Reactive sites remaining on the surface were blocked by reaction with ethanolamine. Various concentrations (50 to 1,000 nM) of human recombinant Rad6 (UbcH2; BostonBiochem, Boston, Mass.) prepared in 35-μl portions were sequentially injected into 20 mM HEPES–150 mM NaCl–3.4 mM EDTA–0.05% Tween 20 (pH 7.4) through the flow cell. Between experiments, the sensor chips were regenerated by washing them with two pulses of 20 mM HCl, followed by an EXTRACLEAN procedure that was done as recommended by the manufacturer. For competition assays, GST-p53 was immobilized on the sensor chip, and Rad6 (400 nM) was injected, followed by the immediate injection of various dilutions of Rad6 antibody or corresponding normal rabbit serum (1:500, 1:2,000, 1:5,000, or 1:10,000) by the coinjection mode. In some experiments, anti-Rad6 antibody (1:500) or bovine serum albumin (BSA; 400 nM) was injected over the chip containing immobilized GST-p53 in the absence of Rad6. Sensorgrams were prepared and globally fit by using nonlinear least-squares analysis and numerical integration of the differential rate equations by using the SPRevolution software package. Sensorgrams were generated after subtraction of the signal due to nonspecific binding of Rad6 to the control chip. Duplicate injections were made and the response units reported are the average of two injections.

Ubiquitination assay. Reactions were performed in the presence or absence of 0.5 μg of affinity-purified GST-Mdm2 (generous gift from H. Yasuda) in mixtures containing 100 ng of E1, 0.5 μg of Rad6 (BostonBiochem), 0.5 μg of purified GST-p53, and 10 μg of ubiquitin in 20 mM Tris-HCl (pH 7.6)–50 mM NaCl–4 mM ATP–10 mM $MgCl_2$–0.2 mM DTT for 2 h at 30°C. Reactions were also performed in the absence of Rad6 to determine the specific effects of Rad6 on p53 ubiquitination. Reactions were terminated and resolved by SDS-PAGE on 6% or 8 to 16% gradient gels under reducing and nonreducing conditions. Ubiquitinated p53 products were visualized by Western blot analysis with p53 CM-1-, ubiquitin-, or polyubiquitin-specific antibodies.

Flow cytometry. Control or ADR-treated MCF10A and MDA-MB-231 cells were trypsinized into single cell suspension, fixed in ice-cold 70% ethanol, and stored at 4°C until required. Before analysis, cells were resuspended in 100 μg of RNase A (Promega Corp., Madison, Wis.)/ml, 40 μg of propidium iodide/ml, and phosphate-buffered saline. Analysis was performed on a Becton Dickinson fluorescence-activated cell sorter (FACScan).

Deubiquitinating enzyme assay. Deubiquitinating enzyme activity in control and ADR-treated MCF10A cells exposed to MG132 was measured according to the method of Dang et al. (13). Briefly, aliquots of cell extracts containing 25 μg of protein were incubated in assay buffer (50 mM HEPES–0.5 mM EDTA [pH 7.8] containing 0.1 mg ovalbumin/ml and 1 mM DTT) at room temperature for 30 min to allow DTT-mediated activation of isopeptidase T and UCH-L3 prior to the addition of predetermined concentration (25 nM) of Ub-AMC (BostonBiochem). Reaction progress was monitored by measuring the increase in fluorescence emission at 460 nm (λ_{ex} = 380 nm) that accompanies cleavage of AMC from Ub-AMC by using a Hitachi 2000 fluorescence spectrophotometer. The specificity of ubiquitin-hydrolyzing activity measured in cell extracts was confirmed by preincubating reactions with a 10-fold excess of ubiquitin aldehyde, a ubiquitin hydrolase inhibitor (BostonBiochem).

RESULTS

Treatment with a DNA-damaging agent stabilizes de novo interaction of Rad6 with p53 and p14ARF proteins. To determine the effects of DNA damage on de novo expression of Rad6, normal MCF10A cells treated with cisplatin (5 μg/ml) or untreated were metabolically labeled with [^{35}S]methionine and analyzed for Rad6 expression by immunoprecipitation with

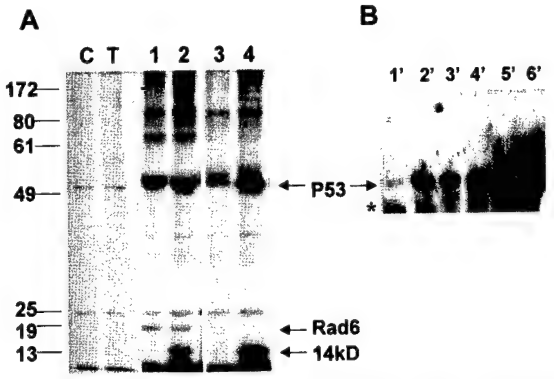

FIG. 1. De novo interaction between Rad6 and p53. Exponentially growing MCF10A cells were either untreated or treated with 5 μg of cisplatin/ml for 6 h and then incubated in methionine-free DMEM supplemented with 100 μCi of [^{35}S]methionine for 3 h. Equivalent amounts of [^{35}S]methionine-labeled trichloroacetic acid-precipitable proteins were immunoprecipitated with anti-Rad6 antibody or normal IgG, and immune complexes were pelleted by incubating with protein A/G-agarose. Rad6-immunodepleted lysates were subjected to a second immunoprecipitation with p53 pAb421 antibody, and immune complexes were similarly recovered with protein A/G-agarose. Bound proteins were resolved by SDS-PAGE, followed by fluorography (A) or Western blot analysis with p53 CM-1 antibody (B). (A) Lanes C and T, control and cisplatin-treated cell extracts, respectively, precipitated with normal IgG; lanes 1 and 2, control and cisplatin-treated cell extracts, respectively, immunoprecipitated with anti-Rad6 antibody; lanes 3 and 4, immunoprecipitation of Rad6-depleted supernatants from control and cisplatin-treated cells, respectively, with pAb421 antibody. (B) Lanes 1′ to 4′, p53 CM-1 reactivity of corresponding lanes 1 to 4 of panel A; lanes 5′ and 6′, p53 CM-1 reactivity of pAb421 immunoprecipitated control and cisplatin-treated cell extracts, respectively. Positions of Rad6, p14ARF, and p53 are indicated. Note the presence of p14ARF coprecipitating with both Rad6 (lane 2) and p53 (lane 4) antibodies only in cisplatin-treated cells.

anti-Rad6 antibody. Control immunoprecipitations were performed with equivalent amounts of normal rabbit IgG. Whereas nonimmune IgG did not precipitate 17-kDa proteins from control or cisplatin-treated lysates of MCF10A cells (Fig. 1A, lanes C and T), immunoprecipitation with Rad6 antibody caused similar levels of de novo-synthesized Rad6 to immunoprecipitate from both control and cisplatin-treated MCF10A cells (Fig. 1A, lanes 1 and 2). Besides immunoprecipitating Rad6, the Rad6 antibody effectively coprecipitated a protein doublet of ~53 kDa from both control and treated cells (Fig. 1A, lanes 1 and 2). Since functional interactions between p53 and several key proteins involved in DNA repair have been reported (7, 37, 60), we determined the identity of the 53-kDa protein to be p53 by subjecting the proteins immunoprecipitated by Rad6 antibody (Fig. 1A, lanes 1 and 2) and those reimmunoprecipitated from Rad6-immunodepleted supernatants by p53 pAb421 antibody (Fig. 1A, lanes 3 and 4) to Western blot analysis with p53 CM-1 antibody (Fig. 1B, lanes 1′ to 4′). The relative levels of p53 recovered from Rad6 immunoprecipitates (Fig. 1B, lanes 1′ and 2′) versus Rad6-immunodepleted supernatants (Fig. 1B, lanes 3′ and 4′) were determined by comparing total p53 levels detected from corresponding samples without prior immunoprecipitation with Rad6 antibody (Fig. 1B, lanes 5′ and 6′). The data from Fig. 1B show that, whereas in the control cells ca. 80% of p53 was present in Rad6-immunodepleted supernatants, >50% of p53

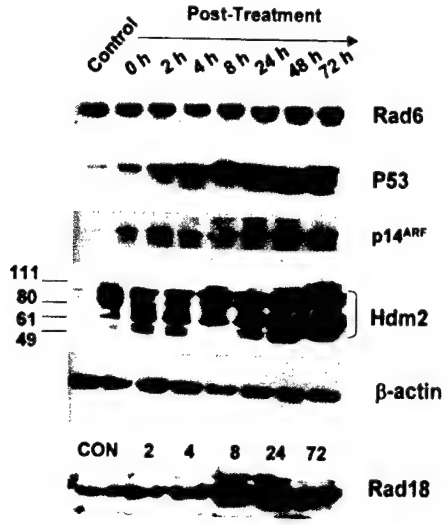

FIG. 2. Effects of ADR on steady-state levels of Rad6, Rad18, p53, p14ARF, and Hdm2 proteins. MCF10A cells were treated with ADR (0.1 μg/ml) for 1 h, and the cultures were washed and replaced with fresh drug-free medium to allow for recovery. Cell lysates were prepared from control (untreated) and ADR-treated cells at the indicated time periods of recovery. Aliquots of cell lysates containing 100 μg of total protein were subjected to SDS-PAGE and Western blot analysis. Immunoblots were reacted with antibodies to Rad6, p53 pAb421, p14ARF, Mdm2, Rad18, or β-actin as discussed in Materials and Methods.

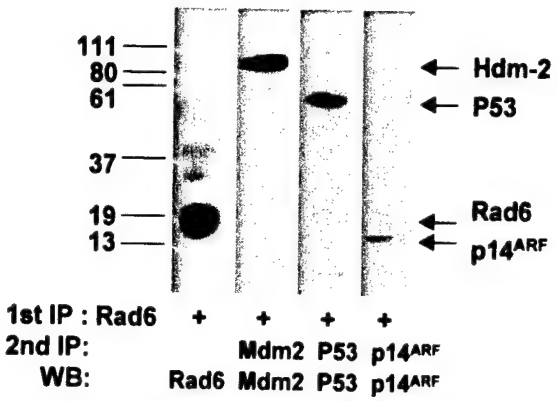

FIG. 3. Rad6 interacts with p53, p14ARF, and Hdm2. ADR-treated MCF10A cell extracts (200 μg of protein) prepared at 8 h of recovery were subjected to immunoprecipitation with anti-Rad6 antibody. Immune complexes were pelleted with protein A/G-agarose, boiled, and reprecipitated with antibodies to p53 pAb421, p14ARF, or Mdm2 as described in Materials and Methods. Coprecipitating p53, p14ARF, or Hdm2 were detected by Western blot analysis with antibodies to p53 (pAb1801), p14ARF, or Mdm2. The positions of Hdm2, p53, and p14ARF that coprecipitated with Rad6 are indicated.

was found to be associated with Rad6 after exposure to the drug. That a physical interaction, perhaps regulated by DNA-damaging agent, occurs between Rad6 and p53 is further confirmed by coprecipitation of a 14-kDa protein, identified to be p14ARF by Western blot analysis (data not shown and Fig. 5B), by both Rad6 and p53 antibodies from only cisplatin-treated MCF10A cells (Fig. 1A, lanes 2 and 4).

Regulation of Rad6, p53, p14ARF, Hdm2, and Rad18 protein levels by ADR treatment. Since results from Fig. 1 demonstrated a potential de novo interaction regulated by cisplatin between Rad6, p53, and p14ARF, we examined the regulation of Rad6, Rad18, p53, p14ARF, and Hdm2 steady-state levels in normal MCF10A cells after exposure to ADR, a potent anthracycline and topoisomerase II inhibitor that is one of the most widely used cancer chemotherapeutic drugs. MCF10A cells were either left untreated or treated with predetermined IC_{50} dose of ADR (0.1 μg/ml) for 1 h; cells were rinsed, and cultures were incubated with fresh drug-free medium. Cell lysates were prepared from untreated samples and at 0-, 2-, 4-, 8-, 24-, 48-, and 72-h recovery periods after exposure to the drug and then analyzed for Rad6, Rad18, p53, p14ARF, and Hdm2 steady-state levels relative to β-actin by Western blot analysis. As shown in Fig. 2, an increase in Rad6 levels was evident at 8 h of recovery and steadily increased by 24 to 72 h posttreatment to approximately two- to fivefold-higher levels relative to the untreated control lysates. Steady-state levels of Rad18 protein exhibited a similar regulation profile by ADR treatment and reached approximately four- to sixfold-higher levels relative to the untreated control cells by 8 to 72 h of treatment (Fig. 2). Both p14ARF and p53 exhibited dramatic and steady increases that were evident immediately after exposure to ADR. Levels of p14ARF were enhanced 5-fold relative to untreated control lysates at 0 h of recovery and steadily increased to ~15-fold by 48 to 72 h posttreatment (Fig. 2). The p53 expression pattern after ADR exposure mirrored the p14ARF profile; however, levels of p53 were upregulated and were maintained at ca. 25- to 40-fold-higher levels relative to the controls in the period from 4 to 72 h after recovery from drug exposure. Induction of p53 was accompanied by a simultaneous increase in the appearance of p53 as a doublet band, a finding that may indicate a posttranslational modification of p53 (Fig. 2). Although the steady-state levels of Hdm2 exhibited a modest increase after drug treatment, maintenance of higher levels of intact Hdm2 is probably impaired by the simultaneous accumulation of several lower-molecular-weight Mdm2-immunoreactive proteins (Fig. 2). These data suggest that ADR significantly enhances Rad6, Rad18, p14ARF, and p53 proteins with only modest effects on Hdm2 levels.

Intact p53, p14ARF, and Hdm2 proteins are physically complexed with Rad6. Since our data from Fig. 1 and 2 have demonstrated physical interactions between de novo-synthesized Rad6, p53, and p14ARF in cisplatin-treated cells and similar ADR-mediated inductory effects on Rad6, p14ARF, and p53 proteins, respectively, we investigated whether Rad6 exists in vivo as part of a supramolecular complex with proteins of the p53 pathway in ADR-treated MCF10A cells. MCF10A lysates prepared at 8 h of recovery after ADR treatment were subjected to immunoprecipitation with Rad6 antibody. Lysates prepared at 8 h posttreatment showed that Rad6, p53, p14ARF, Hdm2, and Rad18 are all upregulated (Fig. 2). Rad6 immunoprecipitates were washed, boiled, and diluted 10-fold prior to reprecipitation with p53 pAb421, p14ARF, Mdm2, or Rad18 antibodies. The results (Fig. 3) indicated the presence of immunoprecipitable Hdm2, p53, and p14ARF in Rad6-immunoprecipitated proteins from ADR-treated MCF10A cells. A similar analysis of control MCF10A lysates failed to reveal detectable amounts of p53, p14ARF, or Hdm2 in Rad6-immunoprecipitated proteins (data not shown). These data

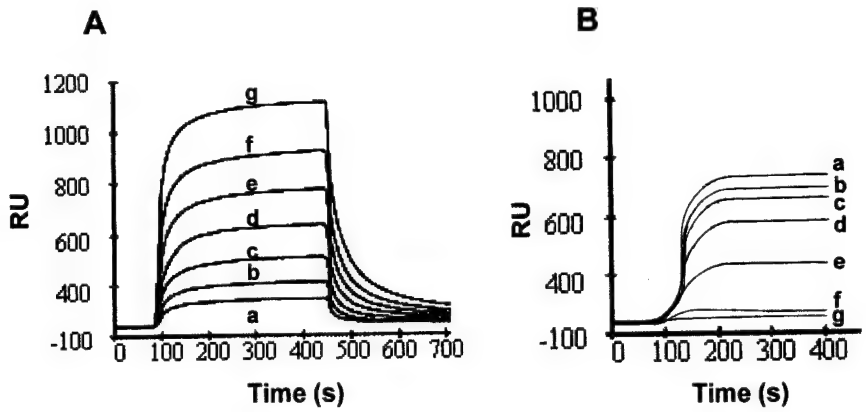

FIG. 4. Rad6 binds to p53 in vitro. (A) Affinity-purified p53-GST was immobilized on a BIAcore 3000 sensor chip, and various concentrations of Rad6 protein were injected over the chip surface. Curves a to g represent binding curves obtained with 50, 100, 200, 300, 400, 600, and 1,000 nM concentrations, respectively. (B) GST-p53 immobilized chip was injected with 400 nM Rad6; this step was immediately followed by injection of various dilutions of anti-Rad6 antibody by the coinjection mode. Curve a represents Rad6 binding in the absence of antibody; curves b to e represent Rad6 binding in the presence of 1:10,000, 1:,5000, 1:2,000, and 1:500 dilutions of anti-Rad6 antibody; curves f and g represent the binding of 400 nM BSA or a 1:500 dilution of anti-Rad6 antibody alone, to immobilized GST-p53 chip.

suggest the presence of a weak interaction between Rad6 and proteins of the p53 pathway in untreated MCF10A cells and that drug-induced effects on p53, p14ARF, and Hdm2 levels perhaps stabilize their interaction with Rad6. Rad18 was not detectable in Rad6 immunoprecipitates from both control and ADR-treated MCF10A lysates, and the majority of Rad18 was detected in Rad6-immunodepleted supernatants (data not shown). Amino acid residues 141 to 149 at the carboxyl terminus of Rad6 are essential for Rad18 binding (5); thus, immunoprecipitation with the Rad6 antibody, which recognizes an epitope on amino acids 138 to 152, could occlude Rad6 interaction with Rad18.

Rad6-p53 interactions by surface plasmon resonance assay. Our data from metabolic-labeling and immunoprecipitation experiments (Fig. 1 and 3) demonstrated the existence of physical interactions between endogenous Rad6 and p53 proteins. Surface plasmon resonance was used to verify whether there is a direct interaction between p53 and Rad6 proteins or whether this association is dependent on the presence of extraneous cellular factors. As shown in Fig. 4A, Rad6 showed a dose-dependent increase in binding to immobilized GST-p53, suggesting that Rad6-p53 interaction occurred independently of cellular factors. The k_{on} was determined from the association phase of binding of Rad6 to immobilized p53 by using the sensorgrams obtained with different concentrations of the soluble component and was 2.6×10^5 M^{-1} s^{-1}. Similarly, k_{off} was calculated from the dissociation phase and was 9.4×10^{-3} s^{-1}. These data suggest that Rad6 complexes readily with p53, and the apparent K_d (k_{off}/k_{on}) value 3.6×10^{-8} M is in the range of strong interactions. In order to further determine the specificity of the Rad6-p53 interaction, the effects of various amounts of anti-Rad6 antiserum or the corresponding normal rabbit serum were tested on binding of Rad6 (400 nM) to immobilized GST-p53. As shown in Fig. 4B, coinjection of Rad6 antibody caused a dose-dependent inhibition in the binding of Rad6 to immobilized GST-p53. Whereas the injection of Rad6 antibody at 1:10,000, 1:5,000, 1:2,000, or 1:500 produced 7, 15.5, 25.2, or 44% inhibition of Rad6 binding to GST-p53, respectively (Fig. 4B), similar coinjection of normal rabbit serum failed to alter Rad6 binding to immobilized GST-p53 (data not shown). Direct injection of Rad6 antibody (1:500) or BSA into immobilized p53 failed to elicit binding, further confirming the specificity of binding reactions (Fig. 4B).

Normal breast epithelial cells exhibit ADR-mediated stabilization of Rad6 complexed p53. Since our data from Fig. 3 have shown a direct interaction between Rad6 and proteins of the p53 pathway, we examined the effects of ADR on the stability of molecular complexes formed between Rad6 and p53 in normal MCF10A and metastatic MDA-MB-231 breast cells. MDA-MB-231 and MCF10A cells were chosen since they express mutant (T. Soussi, [http://p53.curie.fr/]) and wild-type (47) p53, respectively. MCF10A cell lysates prepared from untreated cells and at 0, 4, 24, and 72 h in the recovery period after ADR treatment were subjected to immunoprecipitation with Rad6 antibody, and immune complexes resolved by SDS-PAGE were assessed by Western blot analysis with antibodies to p53 or p14ARF. Complex formation was tested under both nonreducing and reducing conditions to determine whether variations in size and immunoreactivity to specific proteins are detectable. Consistent with ADR-induced regulation of p14ARF steady-state levels (Fig. 2), the results (Fig. 5A) showed that no Rad6-immunoprecipitable p14ARF was detectable in the control MCF10A cell lysates. However, upon exposure to the drug, Rad6-immunoprecipitable p14ARF was detectable immediately after treatment and was localized to an ~150-kDa band. By 4 h posttreatment, p14ARF immunoreactivity was observed as a broad band spanning ca. 100 to 150 kDa, and by 24 h the majority of p14ARF immunoreactivity was increasingly localized to the 100-kDa band (Fig. 5A). Analysis of the corresponding immunoprecipitates in the presence of β-mercaptoethanol not only confirmed the presence of p14ARF in Rad6-immunoprecipitable complexes but also corroborated DNA damage-induced effects on p14ARF recruitment and formation of Rad6-p14ARF complexes observed in Fig. 1.

Similar analysis of Rad6-p53 interaction in MCF10A cell

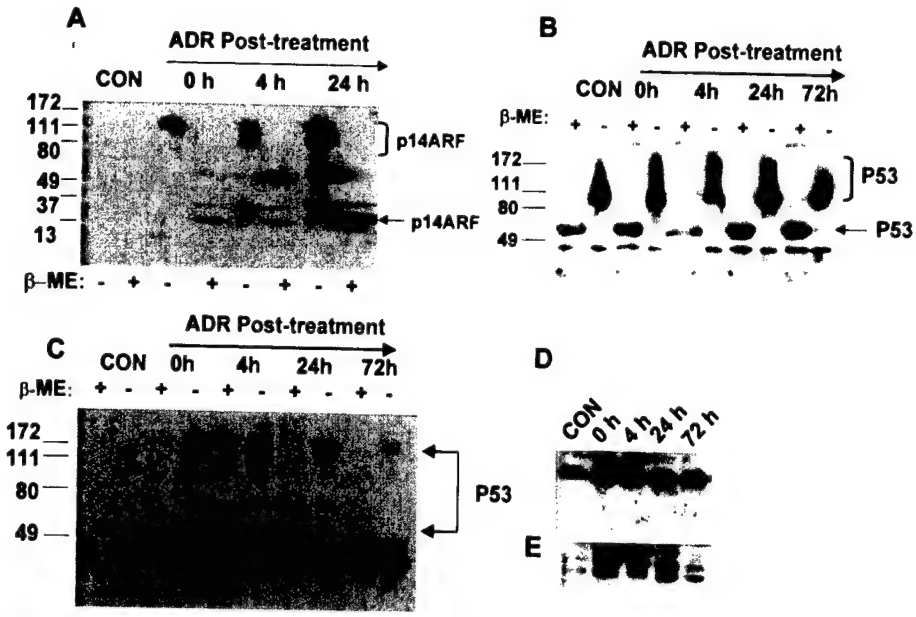

FIG. 5. Effect of ADR on Rad6-p53-p14ARF interactions. MCF10A (A and B) or MDA-MB-231 (C, D, and E) cells were treated with ADR for 1 h, and cultures were rinsed and incubated with drug-free medium as described in Materials and Methods. At the indicated periods of recovery, aliquots of cell extracts containing equivalent amounts of total protein were subjected to immunoprecipitation with anti-Rad6 antibody (A to D) or immunoblotted with pAb421 without prior immunoprecipitation (E). Immune complexes were resolved by SDS-PAGE under reducing and nonreducing conditions as indicated and then analyzed by immunoblotting with p14ARF (A), pAb421 (B and C), or Rad6 (D) antibody. The positions of p14ARF and p53 in immune complexes are indicated.

extracts from untreated control and 0, 4, 24, and 72 h after ADR treatment revealed the presence of Rad6-immunoprecipitable pAb421-immunoreactive p53 both in control and ADR-treated cells (Fig. 5B). These data suggest that Rad6-p53 interaction in MCF10A cells, unlike that observed with p14ARF, is not contingent upon exposure to drug. Rad6-immunoprecipitable p53 was found to be present as a broad smear spanning ca. 100 to 150 kDa (Fig. 5B). Analysis of the corresponding immunoprecipitates under reducing conditions confirmed the presence of p53 in Rad6-p53 (Fig. 5B).

Although equivalent amounts of antibody and total cellular proteins were included in each immunoprecipitation, it is interesting that the sizes of molecular complexes formed not only reflect a supershift caused by antibody reaction but also the stability of interactions between Rad6, p53, and p14ARF. This is evident from regulation of Rad6-p53 complex formation observed in ADR-treated metastatic MDA-MB-231 breast cancer cells (Fig. 5C). Analysis of Rad6-p53 interaction in metastatic MDA-MB-231 cell extracts from untreated controls and 0, 4, 24, and 72 h after ADR treatment, revealed the presence of detectable Rad6-immunoprecipitable pAb421-immunoreactive p53 in an ~160-kDa band only in drug-exposed cells (Fig. 5C). These data suggest that, unlike in normal MCF10A cells, exposure to the DNA-damaging drug is required to enhance and/or stabilize Rad6-p53 interaction in metastatic MDA-MB-231 cells (Fig. 5C). Interestingly, unlike in MCF10A cells, in which stable complexes of Rad6-p53 were detectable at least up to 72 h after ADR treatment, a 75% decrease in Rad6-immunoprecipitable p53 was observed at 24 h posttreatment, and by 72 h negligible p53 reactivity was seen under nonreducing conditions (Fig. 5C). The presence of p53 in Rad6-immunoprecipitable complexes was confirmed not only by the immunoreactivity of the complex with p53 antibody but also by derivation under reducing conditions of p53-immunoreactive 53-kDa band in amounts that were proportional to that present in complexes under nonreducing conditions (Fig. 5C). The reduction in the amounts of Rad6-p53 complexes observed at 24 and 72 h after ADR treatment was not due to inefficient immunoprecipitation by Rad6 antibody, since Western blot analysis of corresponding Rad6 immunoprecipitates showed significant amounts of Rad6 in all samples (Fig. 5D). In contrast, Western analysis of p53 steady-state levels showed p53 induction in ADR-treated samples at 0, 4, and 24 h and significant reduction at 72 h posttreatment (Fig. 5E). These data indicate that, although ADR-induced p53 response is associated with an upregulation in interaction between Rad6 and p53 in metastatic MDA-MB-231 cells, prolonged maintenance of Rad6-complexed p53 in metastatic MDA-MB-231 cells is impaired, in contrast to the situation in normal MCF10A cells.

ADR induces Hdm2 degradation via the ubiquitin-proteasome pathway. Since the results of Fig. 2 showed ADR to exert dramatic inductory effects on Rad6, p53, and p14ARF accumulation and modest stimulatory and/or degradation-inducing effects on Hdm2 in MCF10A cells, we investigated whether ADR-induced decline in Hdm2 occurs via the ubiquitin-proteasome pathway. Lysates of control and ADR-treated MCF10A cells were subjected to immunoprecipitation with Mdm2 antibody, and immune complexes resolved by SDS-PAGE under nonreducing conditions were analyzed by Western blotting with antibodies to ubiquitin or Mdm2. The results (Fig. 6A) demonstrated the presence of a prominent Mdm2-immunoreactive band at ~172 kDa during early periods of recovery (0 to 4 h) after ADR treatment that was not detect-

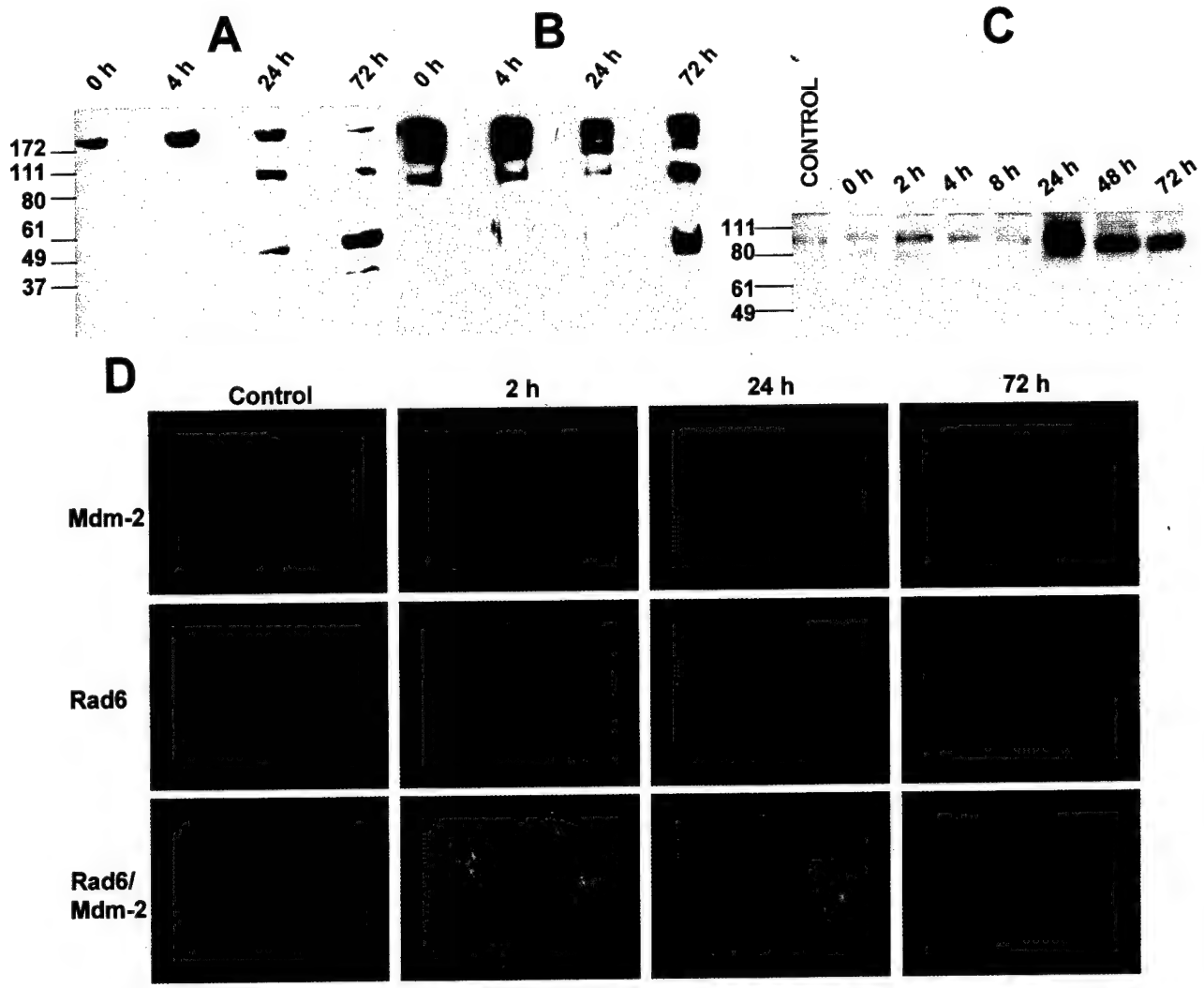

FIG. 6. ADR treatment induces Hdm2 degradation. MCF10A cells were treated with ADR for 1 h, and cultures were rinsed and incubated with drug-free medium. Cell extracts prepared at indicated periods of recovery were subjected to immunoprecipitation with Mdm2 antibody, and immune complexes resolved by SDS-PAGE under nonreducing conditions were analyzed by Western blot analysis with anti-Mdm2 (A) or antiubiquitin (B) antibody. (C) Steady-state levels of Hdm2 were measured by Western blot analysis of extracts prepared at the indicated times from control and ADR-treated MCF10A cells pretreated with MG132 to stabilize Hdm2. (D) Distribution and colocalization of Rad6 and Hdm2 were visualized in control and ADR-treated MCF10A cells at 2, 24, and 72 h of recovery by immunofluorescence staining with FITC-conjugated or Texas red-conjugated secondary antibody for Rad6 and Mdm2, respectively.

able in control cells (data not shown). At 24 h, a reduction in the signal of the 172-kDa band and the emergence of Mdm2-immunoreactive 110- and 55-kDa bands were observed. By 72 h, the intensities of the 172- and 110-kDa bands decreased >90% and were replaced by a proportional increase in a band at 55 kDa and a smaller band at 40 kDa. When the same blot was stripped and reprobed with antiubiquitin antibody, a similar pattern of immunostaining was observed (Fig. 6B). Intense ubiquitin-immunoreactive Mdm2-immunoprecipitable bands were observed at ~172 and 150 kDa during 0 to 4 h of recovery, followed by decreases in the 172- and 150-kDa bands at 24 h and subsequent increases in bands at ~110 and 55 kDa at 72 h posttreatment (Fig. 6B). These data suggest that ADR treatment may facilitate Hdm2 degradation via the ubiquitination pathway.

To obtain further evidence that ADR-induced Hdm2 ubiquitination and degradation occur via the 26S proteasome, MCF10A cells were treated with ADR prior to treatment with MG132, a 26S proteasome inhibitor, and lysates were analyzed for Hdm2 steady-state levels by Western blot analysis with Mdm2 antibody. The results of Fig. 6C show that exposure of ADR-treated cells to MG132 resulted in the accumulation of >25-fold-higher levels of intact Hdm2 by 24 h compared to those in untreated control samples or during early periods of recovery. These data suggest that the ADR-induced degradation of Hdm2 in MCF10A cells occurs at least in part via the ubiquitin-proteasome pathway since the decrease in intact Hdm2 levels induced by ADR (Fig. 6A and B) can be rescued by treatment with a proteasome inhibitor (Fig. 6C).

To determine whether the stabilization of Rad6-p53 complex formation observed in MCF10A cells parallels a corresponding decay of Hdm2, we examined the distribution of

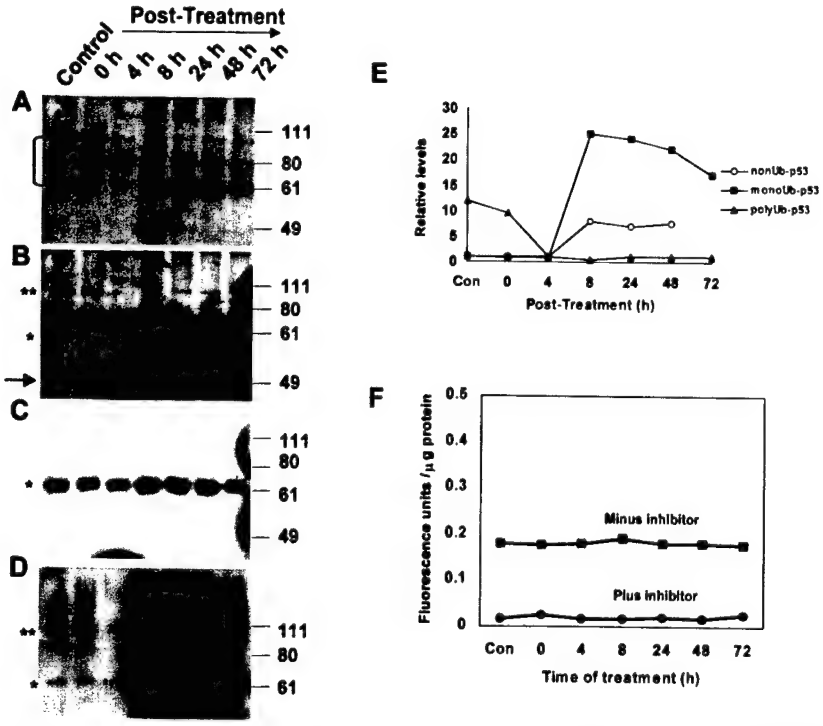

FIG. 7. ADR enhances monoubiquitination of p53. Control and ADR-treated cultures were pretreated with MG132, and extracts prepared at the indicated time points were subjected to immunoprecipitation with p53 pAb421 antibody. Immune complexes were subjected to SDS-PAGE and analyzed by Western blotting with polyubiquitin-specific FK1 (A), p53 CM-1 (B and C), or ubiquitin-protein conjugate-specific FK2 (D) antibodies. Panels B and C show an overexposure and a brief exposure, respectively. The positions of unubiquitinated (→), monoubiquitinated (✱), and polyubiquitinated (✱✱) p53 are indicated. (E) Graphic representation of relative levels of nonubiquitinated and monoubiquitinated p53 versus polyubiquitinated p53 detected by p53 CM-1 or polyubiquitin-specific FK1 antibodies, respectively. (F) Deubiquitinating enzyme activity in control and ADR-treated cells. (G) Colocalization of Rad6 and p53 was visualized in control MCF10A cells (subpanels A to C) and at 72 h of recovery post-ADR treatment of MCF10A cells (subpanels D to F) by immunofluorescence staining with FITC-conjugated or Texas red-conjugated secondary antibody for Rad6 and p53, respectively. (Subpanels G to I) Colocalization of Rad6 and ubiquitin were visualized in ADR-treated MCF10A cells with FITC-conjugated or Texas red-conjugated secondary antibodies for Rad6 and ubiquitin, respectively. (Subpanels J to L) Colocalization of ubiquitin and p53 were visualized in ADR-treated MCF10A cells with FITC-conjugated or Texas red-conjugated secondary antibodies for ubiquitin and p53, respectively. Note the colocalization of Rad6 and p53, Rad6 and ubiquitin, or p53 and ubiquitin in the nucleoli (thick arrows) and nucleoplasm (thin arrows).

Hdm2 and Rad6 by immunofluorescence microscopy in control and ADR-treated MCF10A cells. Hdm2 was localized in the nucleus and excluded from nucleoli in untreated MCF10A cells (Fig. 6D). After exposure to ADR, i.e., at 2 h of recovery, Hdm2 levels were significantly elevated and Hdm2 immunoreactivity was localized both to nuclear bodies and nucleoli (Fig. 6D). Consistent with immunoblotting experiments (Fig. 2), a 60% decline in Hdm2 immunoreactivity was observed in the nuclei at 24 h posttreatment, and by 72 h >90% of nuclei exhibited only diffuse staining in the nucleoplasm and substantial staining in the cytoplasm (Fig. 6D). Immunofluorescence localization of Rad6 in control MCF10A cells revealed diffuse staining in the cytoplasmic and nuclear compartments. However, treatment with ADR induced a preferential redistribution of Rad6 from the cytoplasm to the nucleus that was reflected by detection of elevated levels of Rad6 in the nucleus at least until 72 h posttreatment (Fig. 6D). These results suggest that ADR exerts opposing effects on the stability of Rad6 and Hdm2 in MCF10A cells.

ADR-stabilized p53 is ubiquitinated and colocalizes with Rad6 in the nucleus. Since treatment of MCF10A cells with ADR enhances both the steady-state levels of p53 and Rad6 and prolongs the stability of Rad6-p53 complexes, we investigated the effects of ADR on in vivo p53 ubiquitination status. Lysates prepared from MCF10A cells treated with ADR prior to treatment with MG132 were immunoprecipitated with pAb421 antibody. Immune complexes were resolved by SDS-PAGE and subjected to Western blot analysis with antibodies specific to polyubiquitinated protein conjugates (Fig. 7A), p53 CM-1 (Fig. 7B and C), or ubiquitin-protein conjugates (Fig. 7D). Analysis of p53 with CM-1 antibody in control and ADR-treated MCF10A cells exposed to MG132 revealed that the majority of p53 immunoprecipitated with the p53 antibody was ubiquitinated since overexposure of the blots was necessary to visualize the presence of normal nonubiquitinated p53 (Fig. 7B and C). Quantitation of relative intensities of nonubiquitinated p53 showed that samples at 8, 24, 48, and 72 h after ADR treatment contained ~8-fold-higher levels of p53 compared to control and earlier periods of post-ADR treatment (Fig. 7B). Short-time exposure revealed that ca. 15- to 25-fold-higher levels of monoubiquitinated p53 were present in ADR-treated samples at 8, 24, 48, and 72 h posttreatment compared to controls or at 0 and 4 h after ADR treatment (Fig. 7C). In addition to the 62-kDa p53 immunoreactive band, a prominent

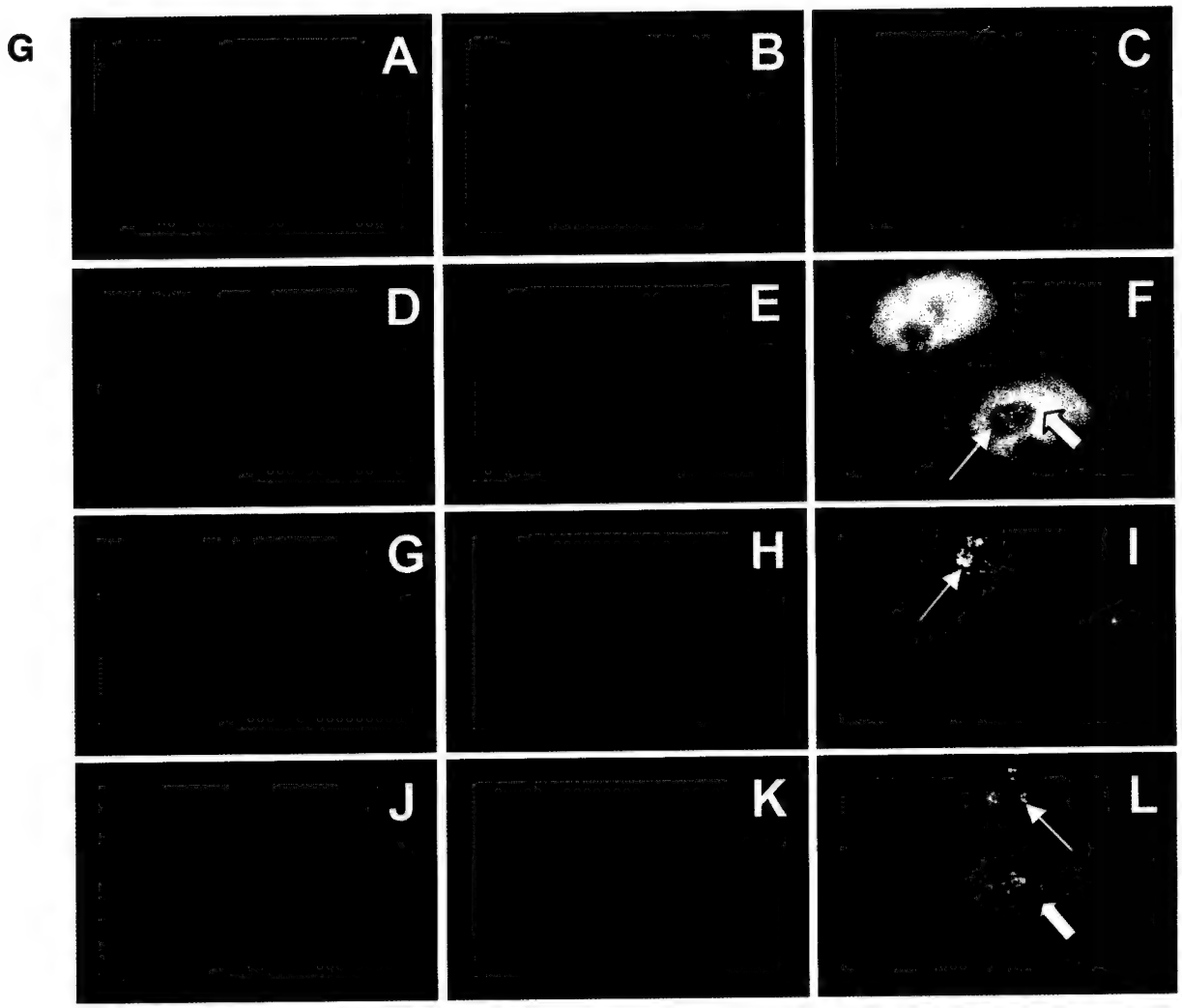

FIG. 7—*Continued.*

p53-immunoreactive band with a molecular size of ~100 kDa was also detected, the latter probably comprising p53 molecules carrying five molecules of ubiquitin (Fig. 7B). The levels of polyubiquitinated p53 in control and at 0 h after ADR treatment were ~8-fold higher than in samples at 4 and 8 h posttreatment and ~5-fold higher than in samples at 24, 48, and 72 h posttreatment (Fig. 7B).

Reprobing the blots with polyubiquitinated protein-specific FK1 antibody further substantiated that the 100-kDa p53-immunoreactive band indeed represented polyubiquitinated p53 and was most prominent in control samples and in samples at 0 h post-ADR treatment (Fig. 7A). It is interesting that although nonubiquitinated p53 was not detected with polyubiquitin-specific antibody, faint bands corresponding to 62, 70, 80, and 90 kDa were detected in most samples. It is not clear whether these bands represent nonspecific immunoreactivity to p53 molecules with limited ubiquitination or multimonoubiquitination. Densitometric analysis of the FK1-reactive 100-kDa band indicated its presence at ~10-fold-higher levels in control samples and in samples at 0 h post-ADR treatment compared to samples at 4, 8, 24, 48, and 72 h posttreatment. Immunoblotting with FK2, an antibody that recognizes all ubiquitin-protein conjugates, showed the presence of >50-fold-higher levels of monoubiquitinated p53 in ADR-treated samples at 8, 24, 48, and 72 h posttreatment compared to those in control samples or in samples at 0 and 4 h post-ADR treatment (Fig. 7D). The relative levels of unubiquitinated p53, monoubiquitinated p53, and polyubiquitinated p53 detected with p53 CM-1 and FK1 antibodies, respectively, are graphically summarized in Fig. 7E. These data indicate that p53 is polyubiquitinated in control samples and during the initial periods of ADR treatment. However, the drug-induced response is accompanied by a decrease in polyubiquitinated p53 that is coupled with a dramatic and concomitant increase in the levels of monoubiquitinated p53.

In order to determine whether the increase or decrease in monoubiquitinated p53 versus polyubiquitinated forms, respectively, reflected an increase in deubiquitinating enzyme activity in ADR-treated cells, we measured the ubiquitin-hydrolyzing activity in control and ADR-treated cells at 0, 4, 8, 24, 48, and 72 h of recovery according to the assay described by Dang et al. (13). The results in Fig. 7F show that there was no

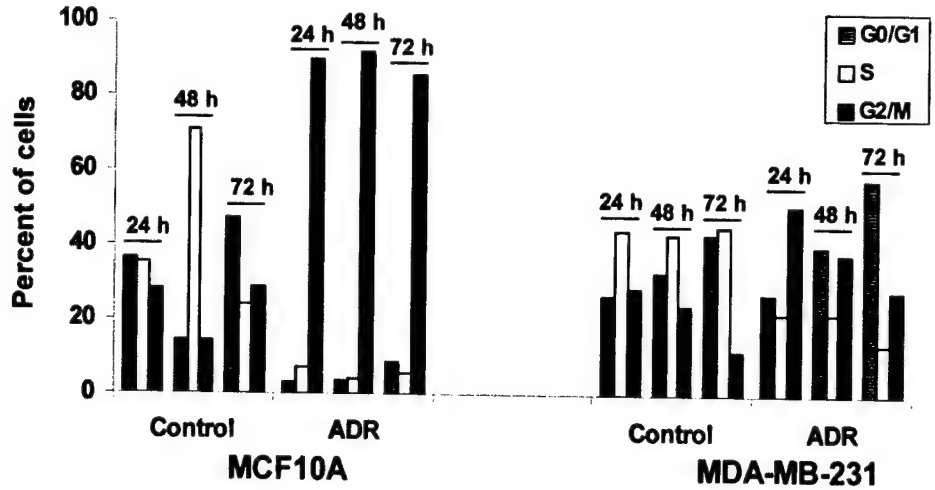

FIG. 8. ADR treatment induces differential effects on cell cycle arrest in MCF10A and MDA-MB-231 cells. Cell cycle progression was analyzed in control or ADR-treated MCF10A and MDA-MB-231 cells at 24, 48, and 72 h by using a FACScan.

significant difference in Ub-AMC-hydrolyzing activity between control and ADR-treated samples that can account for the high levels of polyubiquitinated p53 or monoubiquitinated p53 in control and ADR-treated samples, respectively. Inclusion of ubiquitin hydrolase inhibitor, ubiquitin aldehyde, abolished the Ub-AMC-hydrolyzing capacity of the extracts by >90%, thus confirming the specificity of ubiquitin hydrolase (Fig. 7F). These data suggest that alterations in the ratio of monoubiquitinated p53 to its polyubiquitinated forms is not a result of an increase in deubiquitinating activity but rather is due to alterations in Hdm2 E3 ligase activity that is required for the polyubiquitination of p53.

To determine the cellular localization of Rad6 and p53 and to confirm whether the Rad6 complexed p53 is indeed ubiquitinated, we probed control and ADR-treated (at 72 h of recovery) MCF10A cells with antibodies to Rad6, p53, or ubiquitin. Whereas negligible immunoreactivity to p53 was observed in untreated cells (Fig. 7GB), exposure to ADR caused a dramatic appearance of pAb421-immunoreactive p53 in the nucleoplasm and nucleoli of MCF10A cells (Fig. 7GE and GK). Similarly, treatment with ADR induced preferential accumulation of Rad6 in the nuclei of MCF10A cells (Fig. 7GD and GG and Fig. 6D) compared to untreated cells that displayed diffuse Rad6 staining in the cytoplasm and nucleus (Fig. 7GA and Fig. 6D). Double immunofluorescence labeling and image-merging experiments demonstrated the colocalization of Rad6 with p53 (Fig. 7GF), p53 with ubiquitin (Fig. 7GL) and Rad6 with ubiquitin (Fig. 7GI) in the nucleoplasm and nucleoli of ADR-treated cells when Hdm2 was undetectable (Fig. 6D). These data not only confirm the results from coprecipitation studies but also provide further evidence for ADR-induced effects on p53 ubiquitination, colocalization of p53 with Rad6, and the stability of Rad6-p53 complexes.

We next examined the effects of ADR on cell cycle progression in MCF10A and MDA-MB-231 cells since both cell lines show Rad6-p53 complex formation but with distinctly different stabilities. Treatment of MCF10A cells with 0.1 μg of ADR/ml induced G_2/M cell cycle arrest by 24 h in ~90% of cells that persisted at least up to 72 h of treatment, whereas similar analysis of untreated MCF10A cells at corresponding time points revealed normal cell cycle progression (Fig. 8). Similar flow cytometric analysis of MDA-MB-231 cells revealed that 51% of the cells arrested in G_2/M at 24 h, and at 72 h a majority of the cells (58%) were found to arrest in G_0/G_1 compared to only 28% in the G_2/M phase (Fig. 8).

Demonstration in vitro of Rad6- and Mdm2-mediated effects on p53 ubiquitination. Since our data showed that (i) a significant amount of p53 is associated with Rad6 in ADR-exposed MCF10A cells, (ii) ADR induces physical colocalization of Rad6 with p53 in MCF10A nuclei, (iii) a substantial amount of the p53 present in the nuclei of ADR treated MCF10A cells is ubiquitinated under conditions when Hdm2 is undetectable, and (iv) the majority of the posttranslationally stabilized p53 in ADR-treated MCF10A cells is indeed monoubiquitinated, we tested the effects of Rad6 singly or in combination with Mdm2 on p53 ubiquitination in a cell-free system. Recombinant Rad6 was incubated with GST-p53 in the presence or absence of GST-Mdm2 as indicated (Fig. 9). Under nonreducing conditions, E1-Ub thioesters are detectable both in the presence and in the absence of p53, and E1 per se has no effect on p53 ubiquitination (Fig. 9D). Interestingly, although thioester intermediates of E1-Rad6 are readily detectable in reactions lacking p53 (data not shown), E1-Rad6 thioester intermediates were not observed in reactions containing p53. These data suggest that inclusion of a suitable ubiquitination substrate such as p53 may promote rapid transfer of activated ubiquitin to the substrate. The molecular sizes of ubiquitinated p53 correspond with the presence of one or two ubiquitin molecules (Fig. 9A). The effects of Rad6 on p53 ubiquitination are specific since assay mixtures not containing Rad6 are unable to mediate transfer of ubiquitin to p53. Inclusion of GST-Mdm2 into reactions containing E1 and Rad6 induced polyubiquitination of p53, as confirmed by its immunoreactivity to ubiquitin (Fig. 9A), polyubiquitin (Fig. 9B), and p53 CM-1 (Fig. 9C) antibodies. These data suggest that, whereas Rad6 mediates restrictive ubiquitination of p53, Mdm2 functions by extending ubiquitin chains.

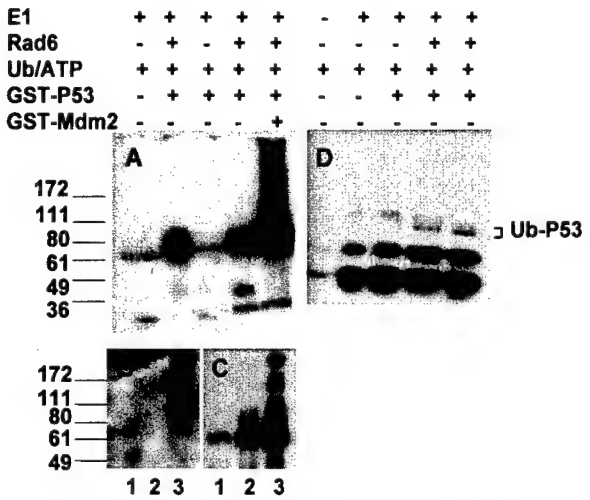

FIG. 9. Effects of Rad6 and Mdm2 on p53 ubiquitination. GST-p53 was incubated with ATP, ubiquitin, and E1 in the absence or presence of Rad6 or in the presence of both Rad6 and GST-Mdm2 as indicated. Reactions were terminated after 2 h at 30°C and then analyzed by SDS-PAGE under reducing (A to and C) or nonreducing (D) conditions and by Western blot analysis with ubiquitin (A and D), polyubiquitin (B), or p53 CM-1 (C) antibody. The positions of ubiquitinated p53 are indicated. The commercial preparation of ubiquitin contained significant levels of diubiquitin (D). The reactions and panels B and C contained E1, Rad6, Mdm2, ubiquitin, ATP, and p53 (lane 3); lacked Mdm2 (lane 2); or lacked Rad6 and Mdm2 (lane 1). Note the formation of fewer ubiquitin- or p53-immunoreactive bands in the presence of Rad6 as opposed to the formation of ubiquitin (A)-, polyubiquitin (B)-, or p53 CM-1 (C)-immunoreactive bands extending to the top of the gel in reactions containing Rad6 and Mdm2.

DISCUSSION

The catalytic activity of Rad6 as a ubiquitin-conjugating enzyme is essential for its functions in DNA repair since Rad6 with a defective catalytic site confers hypersensitivity to a variety of DNA-damaging agents (36, 42, 56). However, proteins relevant to DNA repair that are ubiquitinated by Rad6 besides histone H2b have remained unknown until recently. While this study was in review, Hoege et al. (20) demonstrated that proliferating cell nuclear antigen (PCNA), a DNA polymerase involved in DNA replication and repair, is a substrate of Rad6-mediated monoubiquitination and that damage-induced PCNA ubiquitination is essential for DNA repair. The results from the present study provide evidence for the first time that Rad6 may function in vivo during DNA damage-induced response by undergoing stable associations with proteins of the p53 pathway that ultimately result in restrictive ubiquitination of p53. Based on coimmunoprecipitation, surface plasmon resonance, and GST pull-down assays (unpublished data), we have demonstrated that Rad6 physically interacts with p53 and that this interaction is not dependent on Rad6's ubiquitination status. Thus, Rad6 can exist in complexes with p53 in the cells both before and after treatment with ADR. However, since ADR treatment induces quantitative and/or qualitative effects on Rad6, p53, p14ARF, and Mdm2 proteins, the levels and stability of Rad6-p53 complexes formed in vivo may be subject to regulation by ADR-induced posttranslational modifications. The results presented here are also more relevant to the clinical situation since the markers of drug-induced response are measured at various times of recovery or repair after a single exposure to the damaging agent rather than at different time points of treatment.

Rad6 is known to attach ubiquitin directly to a substrate protein either with or without the help of a ubiquitin ligase (54). Results from in vitro ubiquitination assays clearly show that p53 ubiquitination is a regulated process, wherein Rad6 mediates limited addition of ubiquitin moieties to p53 and further addition of ubiquitin molecules for extension of ubiquitin chains is dependent upon the presence of Mdm2-mediated E3 ligase activity. The physiological relevance of these in vitro data is underscored by results from in vivo experiments that demonstrated that the majority of ADR-stabilized p53 in MCF10A cells is not only monoubiquitinated and physically complexed with Rad6 but that the increase or decrease in levels of mono- versus polyubiquitinated p53 species, respectively, correlates with the decline in intact Hdm2 levels. Thus, p53 protein degradation, but not its monoubiquitination, is impaired during the ADR-induced p53 response. Unlike other ubiquitin-conjugating enzymes, such as UbcH5 (22) and UbcH7 (29), that efficiently ubiquitinate p53 in vitro, Rad6 expression is inducible by a variety of DNA-damaging agents. These results suggest a unique role for Rad6 in p53 ubiquitin modification and DNA damage signaling that are distinct from other known ubiquitin-conjugating enzymes that participate in the generation of degradation signal required for recognition by the 26S proteasome (21).

It is interesting that the chemotherapeutic drug ADR influences the stability of p53 by (i) enhancing p53 monoubiquitination, (ii) interfering with the cocompartmentalization of p53 and Mdm2 (62), and (iii) inhibiting p53 polyubiquitination that is required for nuclear export by Mdm2 and degradation by the proteasome (57). Thus, DNA damage-induced p53 ubiquitin modification may serve specific function(s) in the recovery process rather than simply be a tag for directing proteasome degradation. These findings are consistent with previous reports that have described ubiquitin modifications of histone H2B (45), p53 (34), and histone H1 (40) that do not lead directly to degradation. Since Hdm2 is not detectable and since high levels of ubiquitinated p53 are found to colocalize with Rad6 in the nuclei of ADR-treated MCF10A cells, it remains to be determined how ubiquitinated p53 is regulated in damaged cells.

Although expression of p14ARF is not linked to DNA damage (51), our data show that ADR exerts similar inductory effects on p14ARF protein expression as on p53 and Rad6. Results from our de novo metabolic-labeling studies clearly demonstrate that p14ARF recruitment into Rad6-p53 complexes is dependent on the presence of cisplatin-induced damage. Since Hdm2 is degraded at least in part via the ubiquitin-proteasome pathway in ADR-treated MCF10A cells, it is not clear whether p14ARF functions in p53 stabilization (44) by inhibiting E3 ubiquitin ligase activity of Hdm2 (23) or by facilitating Hdm2 destabilization, as proposed by Zhang et al. (63). ADR-induced downregulation of Mdm2 via mechanisms independent of the proteasome has been reported (33); however, these results conflict with the present data, indicating variations in anthracycline-induced responses that may be attributable to cell-specific differences. In this regard, it can be

noted that proteasome-mediated proteolysis of Mdm2 has been reported to play an important role in etoposide-induced early downregulation of Mdm2 in HL-60 cells since Mdm2 levels could be partially restored by proteasome inhibitors lactacystin and LLnL (11). Although the precise nature and regulation of interactions between Rad6, p53, p14ARF, and Hdm2 remain to be determined, our findings from both coimmunoprecipitation (endogenous Rad6 and p53 proteins) and plasmon resonance (recombinant Rad6 and GST-p53) studies suggest that Rad6 interacts directly with p53 in the absence of Hdm2 or p14ARF and that the stability of Rad6-p53 complexes in vivo are perhaps subject to regulation by drug-mediated effects on p14ARF and Hdm2 levels.

Although the region(s) of Rad6 molecule interacting with p53 is currently being determined, the present study represents the first demonstration of an in vivo correlation between ADR-induced p53 response, p53 ubiquitination status, p14ARF recruitment, Hdm2 decay, and stabilization of interactions between Rad6, a ubiquitin-conjugating enzyme and DNA repair protein, and p53. Thus, the longevity and functionality of the DNA damage-induced p53 response may be subject to regulation by the levels and activity of Rad6, proteins of the p53 pathway, and/or by the mutational status of p53. In this context, it is interesting that, in contrast to normal MCF10A cells that express wild-type p53 and exhibit stable Rad6-p53 complex formation and prolonged G_2/M arrest, metastatic MDA-MB-231 human breast cancer cells express mutant R280K p53, form complexes with Rad6 with transient stability, and exhibit short-lived G_2/M arrest. DNA damage has been believed to stabilize p53 by inducing posttranslational modifications such as phosphorylation, acetylation, sumoylation, or ubiquitination (1). Although phosphorylation of p53 is likely to be an important determinant of p53 stability, phosphorylation of amino and carboxy terminus sites of p53 is not absolutely required for p53 stabilization in response to certain DNA-damaging agents. In fact, p53 mutated in all potential amino and carboxy terminus phosphorylation sites remained susceptible to stabilization induced by UV irradiation and actinomycin D (2, 6). These data suggest that stabilization of p53 in response to various DNA damaging agents is not likely to occur through a single pathway but instead may involve multiple mechanisms that are unique to the cell and individual DNA-damaging agents. These mechanisms may include regulation of Hdm2 expression and stability, interaction of Hdm2 with enzymes of the ubiquitin system, regulation of Hdm2 E3 ligase activity, p53-Hdm2-p14ARF complex formation, Rad6-p53-p14ARF-Hdm2 complex formation, p53 ubiquitination, nuclear export of p53, and degradation of ubiquitinated p53 by the proteasome. Based on our data, it appears that the chemotherapeutic drug ADR elicits DNA damage-induced p53 response by influencing several of these steps in normal MCF10A and metastatic MDA-MB-231 breast cells.

Rad18 has been proposed to act to load or target Rad6 to sites of DNA damage where its ubiquitin-conjugating activity could subsequently modify the stalled DNA replication complex (3). In the yeast, complex formation between Rad6 and Rad18 is believed to be important during error-free and error-prone lesion bypass; however, the mechanism by which this complex participates in lesion bypass processes remains to be determined. Residues 141 to 149 at the carboxyl terminus of Rad6 are essential for Rad18 binding (5); thus, immunoprecipitation with a Rad6 antibody directed to the carboxyl end appears to have impeded Rad6-Rad18 binding. Since ADR exerts similar inductory effects on Rad6 and Rad18, studies utilizing different Rad6 antibodies are necessary to determine whether Rad18 is a significant component of the supramolecular complexes formed between Rad6 and proteins of the p53 pathway.

In summary, our findings suggest that ubiquitin modification mediated by Rad6 may be an important regulator of p53 activity. RNAi experiments are under way to confirm whether Rad6 is a major regulator of p53 ubiquitination in drug-treated cells. Although very little is known about the mechanisms regulating error-free versus error-prone postreplication repair, our data suggest that maintenance of stable Rad6-p53 interactions and monoubiquitinated p53 resulting in the prolonged presence of the DNA damage sensor, may be one such mechanism. Thus, alterations in Rad6 levels and/or activity or mutations in p53 that can potentially disrupt or influence the stability of Rad6-p53 interactions can lead to transitory G_2 arrest and increased promiscuous repair. Modulation of this interaction during DNA damage-induced cellular response, such as by Rad6-mediated p53 monoubiquitination, may serve to regulate and guarantee the fidelity of postreplication repair.

ACKNOWLEDGMENTS

This work was supported by U.S. Army Medical Research and Materiel Command grant DAMD17-99-I-9443 to M.P.V.S.

We thank K. Shavorskaya (BIAcore Facilities, Swedish University of Agricultural Sciences, Uppsala, Sweden) for performing biomolecular interaction experiments, A. Iakovenko (Max-Planck Institute for Molecular Biology, Germany) for calculating dissociation constant, H. Yasuda (School of Life Science, Tokyo University of Pharmacy and Life Science, Tokyo, Japan) for generously providing GST-p53 and GST-Mdm2 fusion proteins, and Gloria Heppner for critically reading the manuscript. We thank Noelle Kondrat for technical assistance and two anonymous reviewers for suggesting experiments shown in Fig. 7A and F.

REFERENCES

1. **Appella, E., and C. W. Anderson.** 2001. Post-translational modifications and activation of p53 by genotoxic stresses. Eur. J. Biochem. **268:**2764–2772.
2. **Ashcroft, M., and K. H. Vousden.** 1999. Regulation of p53 stability. Oncogene **18:**7637–7643.
3. **Bailly, V., J. Lamb, P. Sung, S. Prakash, and L. Prakash.** 1994. Specific complex formation between yeast RAD6 and RAD18 proteins: a potential mechanism for targeting RAD6 ubiquitin-conjugating activity to DNA damage sites. Genes Dev. **8:**811–820.
4. **Bailly, V., S. Lauder, S. Prakash, and L. Prakash.** 1997. Yeast DNA repair proteins Rad6 and Rad18 form a heterodimer that has ubiquitin conjugating, DNA binding, and ATP hydrolytic activities. J. Biol. Chem. **272:**23360–23365.
5. **Bailly, V., S. Prakash, and L. Prakash.** 1997. Domains required for dimerization of yeast Rad6 ubiquitin-conjugating enzyme and Rad18 DNA binding protein. Mol. Cell. Biol. **17:**4536–4543.
6. **Blattner, C., E. Tobiasch, M. Litfen, H. J. Rahmsdorf, and P. Herrlich.** 1999. DNA damage induced p53 stabilization: no indication for an involvement of p53 phosphorylation. Oncogene **8:**1723–1732.
7. **Bucchop, S., M. K. Gibson, X. W. Wang, P. Wagner, H. W. Sturzbecher, and C. C. Harris.** 1997. Interaction of p53 with the human Rad51 protein. Nucleic Acids Res. **25:**3868–3874.
8. **Cassier-Chauvat, C., and F. Fabre.** 1991. A similar defect in UV-induced mutagenesis conferred by the *rad6* and *rad18* mutations of *Saccharomyces cerevisiae*. Mutat. Res. **254:**247–253.
9. **Ciechanover, A.** 1994. The ubiquitin-proteasome proteolytic pathway. Cell **79:**13–22.
10. **Chau, V., J. W. Tobias, A. Bachmair, D. Marriott, D. J. Ecker, D. K. Gonda, and A. Varshavsky.** 1989. A multiubiquitin chain is confined to specific lysine in a targeted short-lived protein. Science **243:**1576–1583.
11. **Cho, J. W., J. C. Park, J. C. Lee, T. K. Kwon, J. W. Park, W. K. Baek, S. I.**

Suh, and M. H. Suh. 2001. The levels of Mdm2 protein are decreased by a proteasome-mediated proteolysis prior to caspase-3 dependent pRb and PARP cleavages. J. Korean Med. Sci. **16:**135–139.

12. **Coux, O., K. Tanaka, and A. L. Goldberg.** 1996. Structure and functions of the 20S and 26S proteasomes. Annu. Rev. Biochem. **65:**801–847.
13. **Dang, L. C., F. D. Melandri, and R. L. Stein.** 1998. Kinetic and mechanistic studies on the hydrolysis of ubiquitin C-terminal 7-amido-4-methylcoumarin by deubiquitinating enzymes. Biochemistry **37:**1868–1879.
14. **Finley, D., S. Sadis, B. P. Monia, P. Boucher, D. J. Ecker, S. T. Crooke, and V. Chau.** 1994. Inhibition of proteolysis and cell cycle progression in a multiubiquitination-deficient yeast mutant. Mol. Cell. Biol. **14:**5501–5509.
15. **Gottleib, T. M., and C. J. Sherr.** 1996. p53 in growth control and neoplasia. Biochim. Biophys. Acta **1287:**77–102.
16. **Haffner, R., and M. Oren.** 1995. Biochemical properties and biological effects of p53. Curr. Opin. Genet. Dev. **5:**84–90.
17. **Haupt, Y., R. Maya, A. Kazaz, and M. Oren.** 1997. Mdm2 promotes the rapid degradation of p53. Nature **387:**296–299.
18. **Hershko, A., and A. Ceichanover.** 1998. The ubiquitin system. Annu. Rev. Biochem. **67:**425–479.
19. **Hochstrasser, M.** 1995. Ubiquitin, proteasomes, and the regulation of intracellular protein degradation. Curr. Opin. Cell. Biol. **7:**215–223.
20. **Hoege, C., B. Pfander, G. L. Moldovan, G. Pyrowolakis, and S. Jentsch.** 2002. Rad6-dependent DNA repair is linked to modification of PCNA by ubiquitin and SUMO. Nature **419:**135–141.
21. **Hoffman, R. M., and C. M. Pickart.** 1999. Noncanonical MMS2-encoded ubiquitin-conjugating enzyme functions in assembly of novel polyubiquitin chains for DNA repair. Cell **96:**645–653.
22. **Honda, R., H. Tanaka, and H. Yasuda.** 1997. Oncoprotein Mdm2 is a ubiquitin ligase E3 for tumor suppressor p53. FEBS Lett. **420:**25–27.
23. **Honda, R., and H. Yasuda.** 1999. Association of p19(ARF) with Mdm2 inhibits ubiquitin ligase activity of Mdm2 for tumor suppressor p53. EMBO J. **18:**22–27.
24. **Jentsch, S., J. P. McGrath, and A. Varshavsky.** 1987. The yeast DNA repair gene RAD6 encodes a ubiquitin-conjugating enzyme. Nature **329:**131–134.
25. **Kastan, M. B., O. Onyekwere, D. Sidransky, B. Vogelstein, and R. W. Craig.** 1991. Participation of p53 protein in the cellular response to DNA damage. Cancer Res. **51:**6304–6311.
26. **Koken, M. H., P. Reynolds, I. Jaspers-Dekker, L. Prakash, S. Prakash, D. Bootsma, and J. H. Hoeijmakers.** 1991. Structural and functional conservation of two human homologs of the yeast DNA repair gene *RAD6*. Proc. Natl. Acad. Sci. USA **88:**8865–8869.
27. **Koken, M. H., E. M. Smit, I. Jaspers-Dekker, B. A. Oostra, A. Hagemeijer, D. Bootsma, and J. H. Hoeijmakers.** 1992. Localization of two human homologs, HHR6A and HHR6B, of the yeast DNA repair gene RAD6 to chromosomes Xq24-q25 and 5q23-q31. Genomics **12:**447–453–1992.
28. **Kubbutat, M. H., S. N. Jones, and K. H. Vousden.** 1997. Regulation of p53 stability by Mdm2. Nature **387:**299–303.
29. **Kumar, S., W. H. Kao, and P. M. Howley.** 1997. Physical interaction between specific E2 and Hect E3 enzymes determines functional cooperativity. J. Biol. Chem. **272:**13548–13554.
30. **Lawrence, C.** 1994. The RAD6 DNA repair pathway in *Saccharomyces cerevisiae*: what does it do, and how does it do it? Bioessays **16:**253–258.
31. **Lawrence, C. W., and D. C. Hinkle.** 1996. DNA polymerase zeta and the control of DNA damage induced mutagenesis in eukaryotes. Cancer Surveys **28:**21–31.
32. **Levine, A. J.** 1997. p53, the cellular gatekeeper for growth and division. Cell **88:**323–331.
33. **Ma, Y., R. Yuan, Q. Meng, I. D. Goldberg, E. M. Rosen, and S. Fan.** 2000. P53-independent downregulation of Mdm2 in human cancer cells treated with adriamycin. Mol. Cell. Biol. Res. Commun. **3:**122–128.
34. **Maki, C. G., and P. M. Howley.** 1997. Ubiquitination of p53 and p21 is differentially affected by ionizing and UV radiation. Mol. Cell. Biol. **17:**355–363.
35. **Midgley, C. A., J. M. Desterro, M. K. Saville, S. Howard, A. Sparks, R. T. Hay, and D. P. Lane.** 2000. An N-terminal p14ARF peptide blocks Mdm2-dependent ubiquitination in vitro and can activate p53 in vivo. Oncogene **19:**2312–2323.
36. **Montelone, S. Prakash, and L. Prakash.** 1981. Recombination and mutagenesis in rad6 mutants of *Saccharomyces cerevisiae*: evidence for multiple functions of the *RAD6* gene. Mol. Gen. Genet. **184:**410–415.
37. **Offer, H., M. Milyavsky, N. Erez, D. Matas, I. Zurer, C. C. Harris, and V. Rotter.** 2001. Structural and functional involvement of p53 in BER in vitro and in vivo. Oncogene **20:**581–589.
38. **Oliner, J. D., K. W. Kinzler, P. S. Meltzer, D. L. George, and B. Vogelstein.** 1992. Amplification of a gene encoding a p53-associated protein in human sarcomas. Nature **358:**80–83.
39. **Oliner, J. D., J. A. Pietenpol, S. Thialingam, J. Gyuris, K. W. Kinzler, and B. Vogelstein.** 1993. Oncoprotein MDM2 conceals the activation domain of tumour suppressor p53. Nature **362:**857–860.
40. **Pham, A. D., and F. Sauer.** 2000. Ubiquitin-activating/conjugating activity of TAFII250, a mediator of activation of gene expression in *Drosophila*. Science **289:**2357–2360.
41. **Prakash, L.** 1981. Characterization of postreplication repair in the yeast *Saccharomyces cerevisiae* and effects of the *rad6*, *rad18*, *rev3*, and *rad52* mutations. Mol. Gen. Genet. **184:**471–478.
42. **Prakash, S., P. Sung, and L. Prakash.** 1990. Structure and function of RAD3, RAD6, and other DNA repair genes of *Saccharomyces cerevisiae*, p. 275–292. *In* P. R. Strauss and S. H. Wilson (ed.), The eukaryotic nucleus. Molecular structure and macromolecular assemblies, vol. 1. Telford Press, Caldwell, N.J.
43. **Prakash, S., P. Sung, and L. Prakash.** 1993. DNA repair genes and proteins of *Saccharomyces cerevisiae*. Annu. Rev. Genet. **27:**33–70.
44. **Prives, C.** 1998. Signaling to p53: breaking the MDM2-p53 circuit. Cell **95:**5–8.
45. **Robzyk, K., J. Recht, and M. A. Osley.** 2000. Rad6-dependent ubiquitination of histone H2B in yeast. Science **287:**501–504.
46. **Shekhar, P. V. M., A. Lyakhovich, H. Heng, D. W. Visscher, and N. Kondrat.** 2002. Rad6 overexpression induces multinucleation, centrosome amplification, abnormal mitosis, aneuploidy, and transformation. Cancer Res. **62:** 2115–2124.
47. **Shekhar, P. V. M., R. Welte, R., J. K. Christman, H. Wang, and J. Werdell.** 1997. Altered p53 conformation: a novel mechanism of wild type p53 functional inactivation in a model for early human breast cancer. Int. J. Oncol. **11:**1087–1094.
48. **Shieh, S. Y., M. Ikeda, Y. Taya, and C. Prives.** 1997. DNA damage-induced phosphorylation of p53 alleviates inhibition by MDM2. Cell **91:**325–334.
49. **Smith, M. L., and A. J. Fornace, Jr.** 1996. The two faces of tumor suppressor p53. Am. J. Pathol. **148:**1019–1022.
50. **Soule, H. D., T. M. Maloney, S. R. Wolman, W. D., Peterson, Jr., R. Brenz, C. M. McGrath, J. Russo, R. J. Pauley, R. F. Jones, and S. C. Brooks.** 1990. Isolation and characterization of a spontaneously immortalized human breast epithelial cell line, MCF-10. Cancer Res. **50:**6075–6086.
51. **Stott, F., S. Bates, M. C. James, B. B. McConnell, M. Starborg, S. Brookes, I. Palmero, K. Ryan, E. Hara, K. H. Vousden, and G. Peters.** 1998. The alternative product from the human CDKN2A locus, p14(ARF), participates in a regulatory feedback loop with p53 and MDM2. EMBO J. **17:**5001–5014.
52. **Strous, G. J., and R. Govers.** 1999. The ubiquitin-proteasome system and endocytosis. J. Cell Sci. **112:**1417–1423.
53. **Sung, P., E. Berleth, C. Pickart, S. Prakash, and L. Prakash.** 1991. Yeast RAD6 encoded ubiquitin-conjugating enzyme mediates protein degradation dependent on the N-end-recognizing E3 enzyme. EMBO J. **10:**2187–2193.
54. **Sung, P., S. Prakash, and L. Prakash.** 1988. The RAD6 protein of *Saccharomyces cerevisiae* polyubiquitinates histones, and its acidic domain mediates this activity. Genes Dev. **2:**1476–1485.
55. **Sung, P., S. Prakash, and L. Prakash.** 1990. Mutation of cysteine 88 in *Saccharomyces cerevisiae* RAD6 protein abolishes its ubiquitin-conjugating activity and its various biological functions. Proc. Natl. Acad. Sci. USA **87:**2695–2699.
56. **Sung, P., S. Prakash, and L. Prakash.** 1991. Stable ester conjugate between the *Saccharomyces cerevisiae* RAD6 protein and ubiquitin has no biological activity. J. Mol. Biol. **221:**745–749.
57. **Tao, W., and A. J. Levine.** 1999. P19(ARF) stabilizes p53 by blocking nucleocytoplasmic shuttling of Mdm2. Proc. Natl. Acad. Sci. USA **96:**3077–3080.
58. **Torres-Ramos, C. A., S. Prakash, and L. Prakash.** 2002. Requirement of RAD5 and MMS2 for postreplication repair of UV-damaged DNA in *Saccharomyces cerevisiae*. Mol. Cell. Biol. **22:**2419–2426.
59. **Torres-Ramos, C. A., B. L. Yoder, P. M. Burgers, S. Prakash, and L. Prakash.** 1996. Requirement of proliferating cell nuclear antigen in RAD6-dependent postreplicational DNA repair. Proc. Natl. Acad. Sci. USA **93:** 9676–9681.
60. **Wang, X. W., A. Tseng, N. A. Ellis, E. A. Spillare, S. P. Linke, A. I. Robles, H. Seker, Q. Yang, P. Hu, S. Beresten, N. A. Bemmels, S. Garfield, and C. C. Harris.** 2001. Functional interaction of p53 and BLM DNA helicase in apoptosis. J. Biol. Chem. **276:**32948–32955.
61. **Xin, H., W. Lin, W. Sumanasekera, Y. Zhang, X. Wu, and Z. Wang.** 2000. The human *RAD18* gene product interacts with HHR6A and HHR6B. Nucleic Acids Res. **28:**2847–2854.
62. **Xirodimas, D. P., C. W. Stephen, D. P. Lane.** 2001. Cocompartmentalization of p53 and Mdm2 is a major determinant for Mdm2-mediated degradation of p53. Exp. Cell Res. **270:**66–77.
63. **Zhang, Y., Y. Xiong, and W. G. Yarbrough.** 1998. ARF promotes MDM2 degradation and stabilizes p53: ARF-INK4a locus deletion impairs both the Rb and p53 tumor suppression pathways. Cell **92:**725–734.

Chemosensitivity of human breast cells correlates with Rad6 expression and postreplication repair capacity

[1,2]Malathy P.V. Shekhar and [1]Alex Lyakhovich
[1]Breast Cancer Program, Karmanos Cancer Institute, [2]Department of Pathology, Wayne State University School of Medicine, 110 East Warren Avenue, Detroit, Michigan 48201, U.S.A.

Running Title: Rad6 influences drug sensitivity

Key words: postreplication repair, ubiquitin conjugating enzyme, cell cycle, adriamycin, cisplatin

Footnotes:
[2]Correspondence should be addressed to:
P.V.M. Shekhar
Breast Cancer Program, Karmanos Cancer Institute
110 East Warren Avenue, Detroit, Michigan 48201

Tel: (313) 833-0715, Ex. 2326/2259
Fax: (313) 831-7518
E-mail: shekharm@karmanos.org

Abstract

The HR6A and -B genes, homologues of the yeast Rad6 gene, encode ubiquitin conjugating enzymes that are required for postreplication repair (PRR) of DNA and damage-induced mutagenesis. We show here that consistent with its role as a PRR protein, HR6 protein (referred as Rad6) expression is cell-cycle regulated with maximal levels expressed in late S/G2 phases of the cell cycle. Exposure of MCF10A cells to adriamycin (ADR) causes enhancement in levels of Rad6 mRNA and protein that is accompanied by an increase in localization of Rad6 in the nucleus. Using *in vivo* cross-linking experiments, we demonstrate that the preferential nuclear localization of Rad6 protein observed in ADR-treated MCF10A cells is indeed associated with an increase in distribution of Rad6, Rad18, p53 and PCNA proteins to the DNA. Inclusion of actinomycin D abolished both basal and ADR-induced Rad6 transcription indicating that ADR-induced effects on Rad6 transcription resulted from an increase in transcriptional activity rather than from its effects on Rad6 mRNA stability. The increase in Rad6 protein expression observed in ADR-treated cells is dependent upon transcription and *de novo* protein synthesis as addition of actinomycin D and cycloheximide eliminated the induction effects. MCF10A cells engineered to overexpress ectopic Rad6 exhibit resistance to ADR and cisplatin whereas MCF10A cells stably transfected with antisense Rad6 display hypersensitivity to these DNA damaging drugs. Analysis of PRR capacities of parental MCF10A cells, MCF10A-Rad6 and MCF10A-antisense Rad6 cells following cisplatin treatment showed that the differences in sensitivity to the drug correlated with poor ability to tolerate DNA damage, as cells expressing antisense Rad6 displayed impaired ability to convert newly synthesized DNA to higher molecular weight species as compared to MCF10A and MCF10A-Rad6 cells. Although no human diseases have been linked to mutations in PRR pathway genes, these data suggest that Rad6 may play an

essential role in DNA damage tolerance and recovery via modulation of PRR, and that imbalances in levels of Rad6 could lead to changes in drug sensitivity and damage-induced mutagenesis.

Introduction

Many endogenous and exogenous agents are capable of damaging DNA. DNA lesions are subject to removal by DNA repair pathways. Many of the otherwise lethal replication-blocking lesions are typically repaired by nucleotide excision repair and base excision repair pathways. However, these mechanisms cannot often repair lesions in the genome due to limited repair capacity or poorly recognized damage. During DNA replication, unrepaired lesions can impose road blocks for the replication machinery. If these pathways are saturated or unable to repair such lesions prior to the onset of S phase, cell death could ensue. To prevent cell death in such circumstances, all cells contain DNA damage tolerance pathways. DNA damage tolerance acts to reinitiate replication in the presence of damage, without lesion removal. This better "safe than sorry philosophy" has apparently been adapted by all organisms and this genetic network is highly conserved throughout evolution (Broomfield *et al*, 2001).

In the yeast *Saccharomyces cerevisiae*, lesion bypass is composed of error-free and error-prone repair processes that are jointly regulated by Rad6 and designed to promote the completion of DNA synthesis (Lawrence, 1994). Not only does the Rad6 pathway account for a substantial fraction of budding yeast's resistance to DNA-damaging agents, but is also responsible for the generation of mutations induced by such damage (Lawrence, 1982).

The Rad6 gene encodes a 17 kDa protein (Reynolds *et al*, 1985) which is one of a group of ubiquitin conjugating (E2, UBC) enzymes (Jentsch *et al*, 1987) that covalently adds ubiquitin to certain lysine residues. The yeast Cdc34 (UBC3) E2 is required for G1 to S phase transition of the cell cycle (Goebl *et al*, 1988) whereas the yeast Rad6/UBC2/E2 is involved in a variety of processes including DNA repair, mutagenesis and cell proliferation (Haynes and Kunz, 1981). The Rad6

pathway regulates posttranslational modification of target proteins with Ub, which commits them to rapid proteolysis. *rad6* mutants possess an extremely pleiotropic phenotype that includes slow growth, severe defects in induced mutagenesis, extreme sensitivity to UV, X-ray and chemical mutagens, and hypersensitivity to antifolate drug metabolites (Prakash *et al,* 1990). The diversity of the phenotypes of *rad6* mutants suggests that the Rad6 gene product is central to cell cycle regulation. All the functions performed by Rad6 protein appear to result from ubiquitination since replacement of the conserved Cys 88 with serine produces a totally null phenotype (Sung*et al*, 1990; Sung *et al*, 1991).

That DNA recovery processes analogous to yeast exist in humans is reinforced by the discovery of human homologs of the Rad6 gene (Koken *et al*, 1991). Unlike in yeast and Drosophila, the Rad6 human homolog is encoded by two genes HHR6A (Rad6A) and B (Rad6B) that complement the DNA repair and UV mutagenesis defects of the yeast *rad6* mutant (Koken *et al*, 1991). Rad6A and Rad6B share ~ 96% identical amino acid residues and are localized on human chromosome Xq24-q25 and 5q23-q31, respectively (Koken *et al*, 1992). The human and yeast RAD6 homologs share ~70% sequence identity. Both human Rad6 genes have overlapping constitutive functions related to chromatin conformation that involve ubiquitin-mediated histone degradation (Koken *et al*, 1996). In whole animal studies, loss of the mouse Rad6B gene results in male infertility due to impaired spermatogenesis (Roest *et al*, 1996) which is postulated to result from defects in histone ubiquitination and chromatin modification (Koken *et al*, 1996).

HR6B or Rad6B is overexpressed in mouse and human breast cancer lines and tumors, and constitutive overexpression of Rad6B induces formation of multinucleated cells, centrosome amplification, abnormal mitosis, aneuploidy and transformation (Shekhar *et al*, 2002). Following

exposure of human breast epithelial cells to DNA damaging drugs, Rad6 is found to exist in supramolecular complexes with p53 and p14ARF, and the stability of the complexes appears to correlate with p53 stability (Lyakhovich and Shekhar, 2003). Thus, Rad6 appears to be an important ubiquitin conjugating enzyme that may play a significant role in the maintenance of genomic integrity of mammalian cells. Imbalances in the levels and activity of Rad6 lead to chromosomal instability and transformation *in vitro* (Shekhar *et al*, 2002). To further elucidate the functional role of Rad6 in normal human breast cells, we have evaluated the regulation of its expression during cell cycle and DNA damage-induced responses, its recruitment to the chromatin following DNA damage, and the consequences of Rad6 overexpression or depletion on postreplication repair capacity and sensitivity to commonly used chemotherapeutic drugs. Our results show that, consistent with its role as a postreplication repair (PRR) protein, maximal levels of Rad6 are expressed during late S/G2 phase of cell cycle, and that adriamycin (ADR)-stimulated increases in Rad6B mRNA expression occur at the transcriptional level. The ability of MCF10A human breast epithelial cells to tolerate DNA damage induced by ADR and cisplatin correlates with Rad6 expression levels and PRR capacities in that cells stably transfected with antisense Rad6B expression vector are PRR-compromised and hypersensitive to the drugs. These findings suggest an important role for Rad6 in normal human breast cells and imply that Rad6 overexpression frequently found in human breast cancers could potentially impact the fidelity of PRR pathways and hence the chemosensitivity of cancer cells.

Results

Regulation of Rad6 expression during cell cycle. In order to determine the steady-state levels of Rad6 protein expression during cell cycle, MCF10A cells were synchronized by serum starvation followed by release into complete growth medium. Cells harvested at various periods following release were either prepared for analysis of cell cycle distribution or lysed for Western blot analysis of Rad6 protein levels. As shown in Fig. 1A, a significant increase in steady-state levels of Rad6 was first detected at 16 h and attained maximal levels by 24 h. Comparison of Rad6 protein steady-state levels with cell cycle distribution profile showed that peak expression of Rad6 occurred either in S or G2 phases of cell cycle (Fig. 1B). In order to verify this conclusion, MCF10A cells were made quiescent by growing in serum-deficient media and released from G0 phase by stimulating them with complete medium for 8-10 h, followed by overnight treatment with 5 mM 5-hydroxyurea, a G1/S blocking drug, in complete medium. Cells were washed to remove 5-hydroxyurea and further incubated in drug-free complete medium. Cells were harvested at various times for the analysis of cell cycle progression and Rad6 protein expression by flow cytometry and Western blot analysis, respectively. As shown in Fig.1C and D, Rad6 expression is low during the quiescent phase when >95% of cells are in G0/G1 phases. Stimulation of cells with complete medium resulted in a slight increase in Rad6 levels. However, negligible increase in Rad6 levels is observed in cells arrested in G1/S phase by hydroxyurea treatment. Release from G1/S block by removing hydroxyurea and allowing cells to progress through cell cycle caused gradual but discernible increase in Rad6 protein levels that reached maximal levels only during late S/G2 phases of cell cycle (Fig. 1C and D). These data are consistent with those reported in *S. cerevisiae*, as yeast lacking Rad6 display defects in transit through the S/G2 phase of the cell cycle (Ellison *et al*, 1991) and suggest that Rad6 protein

expression profiles in human breast cells are consistent with its role as a postreplication repair protein.

Regulation of Rad6B mRNA expression by adriamycin. Semi-quantitative RT-PCR was performed to assess the effects of ADR, a potent anthracycline topoisomerase II inhibitor and one of the most widely used chemotherapeutic drugs, on Rad6B mRNA expression in normal MCF10A cells. Cells were treated with 0.1 μg/ml ADR for 1 h, rinsed and allowed to undergo recovery for various periods of time in drug-free media. After normalizing for GAPDH expression, a 2-fold increase in Rad6B cDNA products relative to untreated controls was observed as early as 2 h following ADR treatment, and levels increased to approximately 6-fold by 48 h post-ADR treatment (Fig. 2A). The ADR-induced profile of Rad6B mRNA transcription closely mirrored Rad6 protein expression observed in corresponding MCF10A cell lysates (Fig. 2B).

To determine whether the induction of Rad6B mRNA levels observed in ADR-treated MCF10A cells reflected enhanced transcription and/or increased stability of Rad6B transcripts, actinomycin D was added to prevent any new gene transcription. MCF10A cells were treated with ADR for 1 h followed by replacement with drug-free medium. Cells were allowed to recover for 4 h at which time both control and ADR-treated cells were incubated with actinomycin D, and Rad6B mRNA levels were monitored over the following 8 h period by the slot blot method using a Rad6B-specific cDNA probe. As shown in Fig. 3A, a linear increase in Rad6B transcription was observed in ADR-treated samples when compared to the corresponding untreated samples. Addition of the RNA pol II inhibitor actinomycin D abolished both basal and ADR-induced Rad6 transcription at similar rates (Figs. 3B and 3C). These data suggest that the higher levels of Rad6B transcripts

achieved by exposure to ADR arose primarily from enhanced transcription and not from effects on Rad6 mRNA stability. As the $t_{1/2}$ of Rad6B mRNA is ~ 70 min in both control and ADR-treated cells, these data suggest that continual transcription of the Rad6B gene may be required for maintenance of adequate levels of Rad6B and that once transcribed the mRNA is rapidly translated.

Posttranscriptional regulation of Rad6B by ADR. In order to determine if ADR influences translation and/or stability of the translated Rad6 protein, control and ADR-treated MCF10A cells were prepared as described above, and treated with actinomycin D or cycloheximide to inhibit *de novo* gene expression or protein synthesis, respectively. Levels of Rad6 protein were analyzed by Western blot analysis in cells harvested at 0, 2, 12 or 24 h following actinomycin D or cycloheximide treatment. As shown in Fig. 4A and B, Rad6 protein levels were slightly enhanced in control cells exposed to actinomycin D as compared to the corresponding untreated samples. In contrast, addition of actinomycin D to ADR-treated cells caused ~60% decrease in Rad6 protein levels when compared to the corresponding ADR-treated samples. It is not clear at present if the differences in actinomycin D effects observed in control and ADR treated cells reflect real differences in regulation of Rad6 protein synthesis during normal cell cycle versus that following DNA damage. Inclusion of cycloheximide dramatically reduced Rad6 protein levels in both control and ADR-treated cells. These data suggest that ADR enhances Rad6B expression levels primarily at the transcriptional levels, as inclusion of actinomycin D caused similar decreases in steady-state levels of ADR-induced Rad6 protein as those caused by cycloheximide.

The specificity of these data was tested by measuring p53 protein levels in the stripped blots (Fig. 4C and D). Analysis of p53 steady-state levels showed ~ 3-fold increase in p53 levels in ADR

treated samples as compared to untreated control samples (Fig. 4C and D). However, whereas addition of actinomycin D caused a dramatic (>60%) decrease in ADR-induced Rad6 protein levels (Fig. 4 A and B), similar addition of actinomycin D did not influence p53 steady-state levels in control or ADR-treated samples (Fig. 4 C and D). Addition of cycloheximide caused a dramatic reduction in p53 steady-state levels in control samples and only a modest decrease in ADR-treated samples (Fig. 4 C and D). These data are in agreement with previous reports and confirm that the ADR-stimulated increase in p53 protein levels reflects posttranslational stabilization rather than regulation at the transcriptional level (Kim *et al*, 2002).

Constitutive Rad6B overexpression induces resistance to DNA damaging agents. Since error-free lesion bypass has been suggested to account for most of Rad6-dependent resistance to DNA damaging agents, we examined the relative sensitivities to cisplatin (a chemotherapeutic drug that induces DNA damage by formation of intra- and inter-strand cross-links) and ADR of MCF10A cells stably transfected with Rad6B (clones 2 and 5), antisense Rad6B (AS2) or empty vector. MCF10A-Rad6B clone 2 and MCF10A-AS2 cells express similar or ~10-fold lower levels, respectively, of Rad6 as compared to the parental cells, and MCF10A-Rad6B clone 5 cells express ~ 20 or 40-fold higher levels of Rad6 as compared to vector-transfected or MCF10A-AS2 cells, respectively (Fig. 5A). As shown in Fig. 5B, MCF10A-Rad6B-overexpressing clone 5 displayed highest resistance to cisplatin (IC50 >1 μg/ml) when compared to empty vector-transfected MCF10A or MCF10A-Rad6B clone 2 (IC50 < 0.1 μg/ml), and MCF10A-AS2 cells (IC50 <0.05 μg/ml).

It is interesting to note that Rad6B-overexpressing clone 5 cells also exhibited highest resistance to ADR in that doses equivalent to ~ 0.75 μg/ml were required to cause 50% inhibition

of cell viability as compared to 0.1 μg/ml for MCF10A-Rad6 clone 2 or vector-transfected MCF10A cells, or 0.05 μg/ml for MCF10A-AS2 cells (Fig. 5C). Analysis of other clones showing similar levels of ectopic Rad6B expression as clone 5 cells (eg., clone 1) exhibited similar magnitudes of drug resistance as clone 5 cells (data not shown). Similarly, other MCF10A clones derived from antisense Rad6B transfection experiments displayed increased sensitivities to cisplatin and ADR (data not shown). These data reveal a correlation between Rad6B expression levels and relative sensitivities to cisplatin and ADR.

In order to determine if the differences in drug sensitivities reflected from alterations in cell proliferation rates, we monitored the growth rates of MCF10A-Neo, MCF10A-Rad6B clone 5, MCF10A-Rad6B clone 2 and MCF10A-AS2 cells. Although Rad6 transfectants displayed lower plating efficiencies as compared to vector controls, no differences in proliferation rates were observed as all three cell lines exhibited a doubling time of 20-23 h (Fig. 5D).

Treatment with DNA damaging drug induces recruitment and/or redistribution of Rad6 on the chromatin. Presence of Rad6 on the chromatin was determined by formaldehyde fixation which allows formation of *in vivo* cross-links between proteins or between protein and DNA. (Solomon and Varshavsky, 1985). Control and ADR-treated MCF10A cells were fixed with formaldehyde, and the sheared cross-linked chromatin subjected to isopycnic centrifugation on CsCl. As shown in Fig.6, phosphohistone H3, a marker that is positively associated with chromatin, was found to be exclusively associated with DNA in nuclear preparations of both control and ADR-treated MCF10A cells. Similarly, the majority of p53 and PCNA were found to be associated with DNA (fractions with higher density) in control MCF10A cells. In contrast, only a small proportion of Rad6 was found

to be associated with chromatin in control MCF10A cells, as the majority of Rad6 was present in the upper fractions, i.e., fractions with lower density. These data suggest that although Rad6 is present in the nucleus, only a small amount of it is physically associated with DNA in untreated MCF10A cells. However, following ADR treatment, a significant increase in Rad6 that is positively associated with chromatin was observed, and Rad6, PCNA, Rad18 and p53 were all found to colocalize with DNA as well as with phosphohistone H3 (Fig. 6). Treatment with ADR resulted in enhancement in the levels of p53 associated with the chromatin. This is consistent with ADR-induced posttranslational stabilization of p53 (Shieh *et al*, 1997) as evidenced by presence of a p53-immunoreactive doublet band (Fig. 6). No carboxypeptidase-immunoreactive bands were observed in the fractions, indicating the absence of contaminating cytoplasmic proteins in the nuclear fractions (data not shown). Exposure of MCF10A cells to cisplatin induced similar redistribution of Rad6 to the chromatin (data not shown). These findings suggest that although Rad6 protein is present in the nucleus, its recruitment to the chromatin appears to be modulated by DNA damage.

Post replication DNA Repair (PRR). DNA damage induced lesions are manifested as single strand DNA breaks that can be seen by separation of genomic DNA in an alkaline sucrose gradient (Lehman, 1972; Lehman *et al*, 1975). After a short incubation, the fragmented genomic DNA is converted into large molecular weight species, similar to DNA of untreated controls. This restoration process is defined as postreplication repair. In order to determine the role of Rad6 in normal human breast epithelial cells, we measured PRR capacity in MCF10A-Neo, MCF10A-Rad6B clone 5 and MCF10A-AS2 cells by the sedimentation velocity method. Figure 7 shows the results of a pulse and pulse-chase experiment with cells that were untreated or treated with cisplatin. Labeling times were

adjusted so that approximately equal amounts of DNA were labeled in untreated and cisplatin-treated cells. As shown in Fig. 7, striking differences in sedimentation profiles were observed between control MCF10A-Neo, MCF10A-Rad6B clone 5 and MCF10A-AS2 cells; however, the sedimentation profiles of pulse-labeled control MCF10A-Neo, MCF10A-Rad6B clone 5 and MCF10A-AS2 cells (Fig. 7A) are superimposable on their corresponding pulse-chased profiles (Fig. 7A'). The majority of DNA in control vector-transfected MCF10A-Neo and MCF10A-Rad6B clone 5 cells sedimented between 48 kb and 20 kb whereas DNA from control MCF10A-AS2 cells peaked close to the 20 kb marker. Examination of size of newly synthesized DNA in cisplatin-treated cells after a 45 min pulse with ^{3}H-thymidine showed similar sedimentation profiles in vector-transfected and Rad6B-transfected MCF10A cells, peaking near 20 kb, whereas DNA from MCF10A-AS2 cells was found near the top of the gradient near 5 kb. After a 90 min chase, DNAs from vector-transfected and Rad6B-transfected MCF10A cells were found to migrate between 48 and 20 kb markers whereas DNA from MCF10A-AS2 cells was observed as a broad band between 20 and 5 kb markers with a significant proportion of DNA close to the 5 kb marker (Fig. 7 B and B'). Profiles similar to those in Fig. 7 are highly reproducible and were obtained from three separate experiments. These data show that following exposure to cisplatin, MCF10A-AS2 cells, compared to controls, have decreased ability to convert the newly synthesized DNA to higher molecular weight species, a property indicative of poor DNA damage tolerance or impaired PRR capacity. These data are consistent with the data from Fig. 5B that show hypersensitivity of MCF10A-AS2 cells to cisplatin-induced cytotoxicity. The results of Fig. 7 also indicate that MCF10A-Rad6B clone 5 cells possess a moderately better capacity than parental MCF10A cells to convert the newly synthesized DNA

following cisplatin treatment to higher molecular weight species, and may explain the inherent resistance of Rad6B overexpressing cells to cisplatin-induced cytoxicity (Fig. 5B).

Discussion

Of the three major DNA damage repair pathways, the Rad6 pathway is the most complicated and least characterized (Friedberg *et al*, 1995). However, unlike Rad3 nucleotide excision repair pathway yeast mutants, which are extremely sensitive to UV but less to MMS and ionizing radiation, and Rad52 recombination repair pathway mutants that are extremely sensitive to MMS and ionizing radiation but less sensitive to UV, Rad6 pathway mutants are sensitive to a broad range of DNA damaging agents, suggesting a shared feature that inhibits DNA synthesis. Genetic analysis in yeast has indicated the importance of lesion-bypass in response to DNA damage. The present study characterizes the regulation and consequence of overexpression or lack of HHR6B, the human homolog of the yeast Rad6 protein, on cell proliferation, sensitivity to commonly used chemotherapeutic drugs and PRR capacity of normal human breast cells.

In contrast to the report by Koken *et al* (1996) that both mRNA and protein levels of Rad6A and B remain unchanged throughout the cell cycle in HeLa cells, our data show a cell cycle periodicity in Rad6 protein levels in normal MCF10A human breast epithelial cells, with maximal expression in late S/G2 phase. These results are consistent with Rad6 function as a postreplication repair protein and coincides with the cell cycle period at which yeast defective for *rad6* are arrested (Kupiec and Simchen, 1984; Ellison *et al*, 1991). Treatment of MCF10A cells with ADR causes G2/M arrest and increases in Rad6B mRNA and protein levels (Lyakhovich and Shekhar, 2003). Our

present data show that ADR-mediated increase in Rad6B gene expression occurs primarily via mechanisms involving transcriptional regulation rather than posttranscriptional control of Rad6B mRNA and protein stability. Rad6B mRNA in MCF10A cells has a short half-life, approximately 70 min, that is not altered by ADR treatment. These data suggest that ADR-induced increase in Rad6B mRNA and protein levels is dependent upon sustained transcription and efficient translation.

Our data from *in vivo* cross-linking experiments further demonstrate that the preferential nuclear localization of Rad6 protein observed in ADR-treated MCF10A cells (Lyakhovich and Shekhar, 2003) is indeed associated with an increase and/or redistribution of Rad6, Rad18, p53 and PCNA proteins to the DNA. Although these data do not confirm, they do suggest that damage may enable or promote assembly of these proteins, perhaps as complexes, at the sites of DNA damage. Rad18-Rad6A and Rad18-Rad6B complexes have been implicated in both error-free and error-prone lesion bypass (Xin *et al*, 2000; Cejka *et al*, 2001). Similarly, we have demonstrated the formation of supramolecular complexes between Rad6 and proteins of the p53 pathway in response to DNA damage and have shown that the stability of these complexes appears to correlate with the length of damage-induced G2/M arrest in so far as metastatic MDA-MB-231 human breast cancer cells display short-lived Rad6-p53 complexes and transient G2/M arrest whereas normal MCF10A cells display stable Rad6-p53 complexes and prolonged G2/M arrest (Lyakhovich and Shekhar, 2003).

rad6 null mutants of yeast exhibit extreme sensitivity to various DNA damaging agents, enhanced spontaneous and impaired mutagenesis, lower growth rate, and decreased viability under stress conditions (Lawrence, 1994). MCF10A cells with compromised Rad6B function display a phenotype reminiscent of the corresponding yeast mutant in terms of drug sensitivity (Gibbs *et al* 1998; Johnson *et al* 1999: Masutani *et al*, 1999). Although no human diseases have been linked to

mutations in PRR pathway genes, these results suggest that Rad6B may play an essential role in DNA damage tolerance and recovery. Since the Rad6 human homolog is encoded by two genes Rad6A and B that share >90% amino acid sequence identity and functional redundancy, the severe drug sensitivities and impaired PRR capacities observed in MCF10A cells stably transfected with the antisense Rad6B construct may be attributed to the complete loss of lesion-bypass as a result of neutralization of both Rad6A and B activities. However, the effects on MCF10A cell proliferation are not as dramatic as on yeast *rad6* mutants (Ellison *et al*, 1991) as MCF10A cells with compromised Rad6 function display similar proliferation rates as parental cells. These data suggest that whereas Rad6 plays an essential role in growth and proliferation of rapidly dividing organisms such as yeast, it is not essential for MCF10A cell proliferation but assumes an important role upon DNA damage. In this regard, it is interesting to note that MCF10A cells engineered to constitutively overexpress Rad6B exhibit resistance to cisplatin and ADR and are PRR proficient. Since Rad6 is required for both error-free and error-prone modes of PRR as shown by its epistatic relationship with Rad18, Rad5, Rad30, Rev3 and Rev7 (Xiao *et al*, 2000), it is conceivable that much of the repair activity in Rad6B-overexpressing MCF10A cells is error-prone. This is consistent with their transformed behavior as evidenced by abnormal mitosis, multinucleation, aneuploidy and ability for anchorage independent growth (Shekhar *et al*, 2002).

In summary, we have shown that Rad6 is not essential for normal human breast cell proliferation and growth, but that it plays a vital role following DNA damage via modulation of postreplication repair and hence sensitivity/resistance to chemotherapeutic drugs. Since Rad6 overexpression is detected in human breast tumors and constitutive overexpression of exogenous Rad6B induces aneuploidy and transformation, understanding mechanisms regulating Rad6-mediated

DNA damage tolerance pathway will shed light on cancer development and response to chemotherapy.

Materials and methods

Cell culture.

Culture conditions for cell lines used in this study have been described before (Shekhar *et al*, 2002). MCF10A is a human breast epithelial cell line that arose by spontaneous immortalization from cell cultures established from the subcutaneous mastectomy of a woman with fibrocystic disease. MCF10A cells are pseudodiploid, lack tumorigenicity in nude mice and are unable to support anchorage independent growth (Soule *et al*, 1990). Briefly, MCF10A cells were maintained in DMEM/F-12 medium supplemented with 5% horse serum, 0.02 μg/ml EGF, 0.5 μg/ml hydrocortisone, 10 μg/ml insulin, 0.1 μg/ml cholera toxin, 100 units/ml penicillin and 100 μg/ml streptomycin. Cell lines derived from MCF10A stable transfections with wild type human Rad6B in sense direction (MCF10A-Rad6 clones 2 and 5), antisense direction (MCF10A-a/s Rad6B, AS2), or corresponding vector (MCF10A-neo) were cultured in the same medium except it also contained 500 μg/ml of G418 (Life Technologies; Shekhar *et al*, 2002).

Western blot analysis.

Cell lysates were prepared as previously described in 10 mM Tris-HCl, pH 7.5/150 mM NaCl/1% Triton X-100/1 mM phenyl methylsulfonyl fluoride, 1 μg/ml each of leupeptin, pepstatin, antipain and 1 mM sodium orthovanadate, and proteins (50 μg) from each lysate separated by SDS-PAGE and transblotted onto Immobilon P membranes. The blots were stained with anti-Rad6 antibody.

Loading of protein was monitored by reprobing stripped membranes with mouse anti-β actin antibody (Oncogene Science). Rad6 and β-actin protein bands were visualized with anti-rabbit or anti-mouse IgG coupled to horseradish peroxidase, respectively, using ECL kit (Amersham, Arlington Heights, Illinois). The Rad6 antibody was generated by multiple immunization of New Zealand white rabbits with a synthetic peptide (K plus amino acid residues 131-152; Accession # NM_009458) that is conserved 100% in mouse and human HR6B, and 91% in human HR6A (Shekhar *et al*, 2002).

Analysis of Rad6 expression during cell cycle. MCF10A cells were synchronized by serum starvation for 72 h followed by release into complete growth medium. Cells were lysed at 0, 8, 16, 24, 32, 48 and 72 h following release and analyzed for Rad6 protein levels by Western blot analysis. Aliquots of cells harvested at the corresponding times were also analyzed for cell cycle progression by flow cytometry. In order to confirm Rad6 protein expression at specific phase of cell cycle, quiescent MCF10A cells were released from G0 phase by stimulating them with complete medium for 8-10 h, followed by overnight treatment with 5 mM 5-hydroxyurea (a G1/S blocking drug) in complete medium. Cells were washed to remove hydroxyurea and further incubated in drug-free complete medium. Cells were harvested during quiescent phase, following treatment with hydroxyurea and at various times after release from hydroxyurea for the analysis of cell cycle progression and Rad6 protein expression by flow cytometry and Western blot analysis, respectively.

Flow cytometry.

MCF10A cells (quiescent, 5-hydroxyurea-treated or post-release from 5-hydroxyurea) were trypsinized into single cell suspension, fixed in ice-cold 70% ethanol and stored at 4°C until required. Before analysis, cells were resuspended in 100 μg/ml RNase A (Promega Corp., Madison, WI), 40 μg/ml propidium iodide and sodium phosphate buffered saline. Analysis was performed on a Becton Dickinson fluorescence activated cell sorter (FACScan).

RT-PCR.

Rad6B mRNA expression was measured by semi-quantitative RT-PCR. MCF10A cells were either untreated or treated with 0.1 μg/ml ADR for 1 h, cells rinsed and replaced with drug-free media. At various times of recovery following ADR treatment, total RNA was isolated and treated with RNase-free DNase I. Two μg of DNase I-treated total RNA was reverse transcribed with SuperScriptII and 2 μl aliquot was used for PCR amplification of Rad6B cDNA. The PCR reactions contained Rad6B-primers +18/+38 and +420/+399 (Accession # M74525) as forward and reverse primers, respectively, and conditions that yielded a detectable PCR product using the minimum number of amplification cycles. Amplification of GAPDH cDNA was included as an internal control for the amount of cDNA tested. The GAPDH-specific primers were +186/+206 and +320/+302 (Accession # XM_006959) as forward and reverse primers, respectively. PCR was conducted for 22 cycles as it yielded products within the linear range of amplification of Rad6B cDNA. The PCR products were separated on agarose gels and ethidium bromide stained bands analyzed by densitometry (Model 300A densitometer, Molecular Dynamics, Sunnyvale, CA). The authenticity of the amplified sequences was verified by nested PCR using Rad6B specific primers and sequence analysis.

Measurement of mRNA decay.

MCF10A cells were treated with 0.1 μg/ml ADR for 1 h, cells rinsed and allowed to recover for 4 h at which time both control and ADR-treated cells were incubated with transcriptional inhibitor actinomycin D (5 μg/ml). Total RNA was extracted, DNase I-treated, and Rad6B mRNA levels were monitored at various times by slot blot method. Filters were hybridized overnight with a random-primed ^{32}P-labeled Rad6B-specific cDNA probe in buffer containing 6 X SSC, 50% formamide and 0.5% SDS. Filters were washed with 1 X SSC and subjected to autoradiography. Rad6B specific cDNA was amplified from DNAse I-treated MCF10A RNA using +18/+38 and +420/+399 as forward and reverse primers, respectively (Accession # M74525). The intensities of Rad6B-hybridizing bands from parallel experiments performed in the presence and absence of actinomycin D were quantitated by densitometry (Molecular Dynamics).

Measurement of protein stability.

Control and ADR-treated MCF10A cells were prepared as described above, and treated with actinomycin D (5 μg/ml) or cycloheximide (10 μg/ml) to inhibit new gene expression or protein synthesis, respectively. Levels of Rad6 protein were detected by Western blot analysis from cell lysates prepared at 0, 2, 12 or 24 h following actinomycin D or cycloheximide treatment. Blots were stripped and reprobed with p53 CM-1 polyclonal antibody (Novocastra Laboratories Ltd., Newcastle upon Tyne, United Kingdom) to validate the efficacy of actinomycin D and cycloheximide treatments.

Amounts of Rad6 (HR6A/HR6B) and p53 protein(s) were quantitated with a scanner densitometer (Molecular Dynamics).

In vivo cross-linking.

Control and ADR-treated MCF10A cells prepared as described above were fixed with 1% formaldehyde for 30 min at 37°C, and fixing stopped by addition of 0.125M glycine (Solomon and Varshavsky, 1985). Cells were washed, pelleted and lysed with buffer containing 0.5% NP-40. Nuclei were sedimented and nuclei lysed with buffer containing 0.25% Triton X-100 and 1 mM EGTA. The cross-linked chromatin was sheared by sonication, adjusted to 0.5% sarkosyl, and centrifuged at 7000 x g. Supernatants were overlaid onto 5 ml of 1.42 g/cm^3 CsCl in the same sarkosyl buffer and subjected to isopycnic ultracentrifugation at 40,000 rpm for 72 h at 15°C. Fractions of 0.5 ml were collected from the bottom of the tube, concentrated using Centricon filters, and CsCl was eliminated by consecutive dilution with 10 mM Tris-HCl, pH 7.5. Presence of DNA in the nuclear fractions was determined by agarose gel electrophoresis and ethidium bromide staining. The presence of Rad6, p53, Rad18, PCNA and phosphohistone H3 (a DNA marker) in fractions were determined by SDS-PAGE and Western blot analysis using antibodies specific for Rad6 (1), p53 (pAb421, Oncogene Science), human Rad18 (Imgenex, San Diego, CA), PCNA (Dako Corp.) and phosphohistone H3 (Upstate Biochemicals). Blots were also probed with anti-carboxypeptidase A antibody (Sigma-Aldrich Company, St. Louis, MO), a cytoplasmic protein to verify absence of contaminating cytoplasmic proteins in nuclear extracts.

Cytotoxicity assays.

The sensitivities of MCF10A cells stably-transfected with control vector (pCMV-neo), vector containing the full length Rad6B cDNA (pCMV-neo-Rad6), or vector containing antisense Rad6B cDNA (AS2), to commonly used chemotherapeutic drugs cisplatin or ADR were tested. MCF10A-

Rad6 clones 2 and 5 express similar or ~ 20-fold higher levels of Rad6 protein, respectively, as compared to the parental vector transfected MCF10A cells. 10 x 10^3 cells were plated in 24-well tissue culture dishes in DMEM/F12 medium as discussed above, and were treated on the following day with varying doses of ADR (0.01 - 2 μg/ml) or cisplatin (0.05 - 10 μg/ml) for 3 or 5 days, respectively. At the end of treatment period, the number of viable cells were determined by trypan blue exclusion in a hemocytometer.

Assessment of newly synthesized DNA (postreplication DNA repair assay, PRR).

PRR capacity was measured in vector-transfected MCF10A, MCF10A-Rad6 clone5, and MCF10A-AS2 cells by the sedimentation velocity method. Actively growing cells, control or cisplatin-treated (0.5 μg/ml, 30 min) were rinsed, allowed to recover for 6 h, and pulse-labeled with 200 μCi ^{3}H-thymidine (10 Ci/mmol, Perkin Elmer) for 45 min. In pulse-chase experiments, the pulse-labeled cells were further incubated for 90 min in fresh medium containing 10 μM thymidine. The cells were lysed, lysates irradiated with 20 Gy of X-rays on ice, cell suspension layered on top of 5-20% alkaline sucrose density gradients and centrifuged at 50,000 rpm for 2 h. Fractions were collected from the bottom, and amounts of TCA-precipitable radioactivity determined. Effects of Rad6 levels on PRR capacity were determined by comparing the sedimentation profiles of replicated DNA in pulse-labeled versus pulse-chased samples from corresponding control and cisplatin-treated MCF10A cells. Labeling times were adjusted so that approximately equal amounts of DNA are labeled in control and treated cells in order to eliminate or minimize labeling artifacts.

Statistical Analysis. Specific differences in sensitivities to cisplatin or adriamycin between MCF10A-Neo, MCF10A-AS2, MCF10A-Rad6B clone 2, and MCF10A-Rad6B clone 5 cells were examined by Student's t test with $P<0.01$ considered as statistically significant.

Acknowledgements.

This work was supported by grants DAMD17-99-I-9443 and DAMD17-02-I-0618 (to MPVS) from the U.S. Army Medical Research and Materiel Command. We thank Dr. Gloria Heppner for critical reading of the manuscript.

References

Broomfield S, Hryciw T and Xiao W. (2001). DNA postreplication repair and mutagenesis in *Saccharomyces cerevisiae*. *Mut. Res.*, **486**,167-184 (Review).

Cejka P, Vondrejs V and Storchova Z. (2001). Dissection of the functions of the *Saccharomyces cerevisiae* Rad6 postreplicative repair group in mutagenesis and UV sensitivity. *Genetics*, **159**, 953-963.

Ellison KS, Gwozd T, Prendergast JA, Paterson MC, and Ellison MJ. (1991) A site-directed approach for constructing temperature-sensitive ubiquitin conjugating enzymes reveal a cell cycle function and a growth function. *J Biol. Chem.*, **266**, 24116-24120.

Gibbs PE, McGregor WG, Maher VM, Nisson P and Lawrence CW. (1988). A human homolog of the *Saccharomyces cerevisiae* REV3 gene, which encodes the catalytic subunit of DNA polymerase zeta. *Proc. Natl. Acad .Sci. USA*, **95**, 6876-6880.

Goebl MG, Yochem J, Jentsch S, McGrath JP, Varshavsky A and Byers B. (1988). The yeast cell cycle gene CDC34 encodes a ubiquitin conjugating enzyme. *Science*, **241**,1331-1335.

Haynes RH and Kunz BA. (1981). The Molecular Biology of the yeast *Saccharomyces cerevisiae*: Life cycle and inheritance. Strathern J, Jones E and Broach J (eds.). Cold Spring Harbor Laboratory, Cold Spring Harbor, pp. 371-414.

Jentsch S, McGrath JP and Varshavsky A. (1987). The yeast DNA repair Rad6 encodes a ubiquitin conjugating enzyme. *Nature,* **329**, 131-134.

Johnson RE, Kondratick CM, Prakash S and Prakash L. (1999). hRAD30 mutations in the variant form of xeroderma pigmentosum. *Science*, **285**, 263-265.

Kim H, You S, Farris J, Foster LK, Foster DN. (2001). Post-transcriptional inactivation of p53 in immortalized murine embryo fibroblast cells. *Oncogene*, **20**, 3306-10.

Koken MH, Hoogerbrugge JW, Jasper-Dekker I, de Wit J, Willemsen R, Roest HP, Grootegoed JA and Hoeijmakers JH. (1996). Expression of the ubiquitin conjugating enzymes HHR6A and B suggests a role in spermatogenesis and chromatin modification. *Dev. Biol.*, **173**,119-132.

Koken MHM, Reynolds P, Jaspers-Dekker I, Prakash L, Prakash S, Bootsma D and Hoeijmakers JHJ. (1991). Structural and functional conservation of two human homologs of the yeast DNA repair gene Rad6. *Proc. Natl. Acad. Sci. USA*, **88**, 8865-8869.

Koken MH, Smit EM, Jaspers-Dekkers I, Oostra BA, Hagemeijer D, Bootsma D and Hoeijmakers JH. (1992). Localization of two human homologs, HHR6A and HHR6B, of the yeast DNA repair gene Rad6 to chromosomes Xq24-q25 and 5q23-q31. *Genomics*, **12**, 447-453.

Kupiec M and Simchen G. (1984). Cloning and integrative deletion of the Rad6 gene of *Saccharomyces cerevisiae*. *Curr. Genet.*, **8**, 559-566.

Lawrence C. (1994). The Rad6 DNA repair pathway in*Saccharomyces cerevisiae*: What does it do, and how does it do it? *BioEssays*, **16**, 253-258.

Lawrence CW. (1982). Mutagenesis in *Saccharomyces cerevisiae*. *Adv. Genet.*, **21**,173-254.

Lehman AR. (1972). Postreplication repair of DNA in ultraviolet-irradiated mammalian cells.*J Mol. Biol.*, **66**, 319-337.

Lehman AR, Kirk-Bell S, Arlett CF, Paterson MC, Lohman PH, de Weerd-Kastelein EA, Bootsma D. (1975). Xeroderma pigmentosum cells with normal levels of excision repair have a defect in DNA synthesis after UV irradiation. *Proc. Natl. Acad. Sci. USA*, **72**, 219-223.

Lyakhovich A and Shekhar, PVM..(2003). Supramolecular complex formation between Rad6 and proteins of p53 pathway during DNA damage-induced response. *Mol. Cell. Biol.*, .

Masutani C, Kusumoto R, Yamada A, Dohmae N, Yokoi M, Yuasa M, Araki M, Iwai S, Takio K and Hanaoka F. (1999). The XPV (xeroderma pigmentosum variant) gene encodes human DNA polymerase eta. *Nature*, **399**, 700-704.

Prakash S, Sung P and Prakash L. (1990). The Eukaryotic nucleus. Straus PR and Wilson SH (eds). Telford Press: Caldwell, NJ, Vol. 1, pp. 275-292.

Reynolds P, Weber S and Prakash L. (1985). Rad6 gene of*Saccharomyces cerevisiae* encodes a protein containing a tract of 13 consecutive aspartates. *Proc. Natl. Acad. Sci. USA*, **82**,168-172.

Roest Roest HP, van Klaveren J, de Wit J, van Gurp CG, Koken MH, Vermey M, van Roijen JH, Hoogerbrugge JW, Vreeburg JT, Baarends WM, Bootsma D, Grootegoed JA, Hoeijmakers JH. (1996). Inactivation of the HR6B ubiquitin-conjugating DNA repair enzyme in mice causes male sterility associated with chromatin modification. *Cell*, **86**, 799-810.

Shekhar PVM, Lyakhovich A, Heng H, Visscher DW and Kondrat N. (2002). RAD6 overexpression induces centrosome amplification, abnormal mitosis, aneuploidy and transformation. *Cancer Res.*, **62**, 2115-2124.

Shieh SY, Ikeda M, Taya Y, and Prives C. (1997). DNA damage-induced phosphorylation of p53 alleviates inhibition by MDM2. *Cell*, **91**, 325-334.

Solomon MJ and Varshavsky A. (1985). Formaldehyde-mediated DNA-protein cross-linking: a probe for *in vivo* chromatin structures. *Proc. Natl. Acad. Sci. (USA)*, **82**, 6470-6474.

Soule HD, Maloney TM, Wolman SR, Peterson WD Jr., Brenz R, McGrath CM, Russo J, Pauley RJ, Jones RF and Brooks SC. (1990). Isolation and characterization of a spontaneously immortalized human breast epithelial cell line, MCF-10. *Cancer Res.*, **50**, 6075-86.

Sung P, Prakash S and Prakash L. (1990). Mutation of yeast cysteine 88 in the *Saccharomyces cerevisiae* Rad6 protein abolishes its ubiquitin conjugating activity and its various biological functions. *Proc. Natl. Acad. Sci. USA*, **87**, 2695-2699.

Sung P, Prakash S and Prakash L. (1991). Stable ester conjugates between the *Saccharomyces cerevisiae* Rad6 protein and ubiquitin has no biological activity. *J. Mol. Biol.*, **221**, 745-749.

Xiao w, Chow BL, Broomfield S and Hanna M. (2000). The Saccharomyces cerevisiae Rda6 group is composed of an error-prone and two error-free postreplication repair pathways. *Genetics*, **155**, 1633-1641.

Xin H., W. Lin, W. Sumanasekera, Y. Zhang, X. Wu, and Z. Wang. (2000). The human RAD18 gene product interacts with HHR6A and HHR6B. *Nucleic Acids Res.*, **28**, 2847-2854.

Fig.1. Rad6 protein is maximally expressed in late S/G2 phase of cell cycle. MCF10A cells were made quiescent by serum starvation and released by stimulation with complete medium. A and B, Cells were harvested at various periods of release and analyzed for steady-state levels of Rad6 protein (A) and cell cycle progression (B). C and D, Quiescent cells (Q) were released by stimulation with complete medium for 8 h (Q.8h), and then treated with 5-hydroxyurea overnight (HU). Cells were rinsed, incubated in drug-free media and harvested at 4 (HU, 4h), 8 (HU, 8h) or 16 h (HU, 16h) of release from hydroxyurea treatment for analysis of Rad6 protein levels by Western blot analysis (C) and cell cycle phase distribution by flow cytometry (D).

Fig. 2. Regulation of Rad6 mRNA and protein expression by adriamycin (ADR). MCF10A cells were treated with 0.1 μg/ml of ADR for 1h, and cells allowed to recover in drug-free media for 0-72 h. A, steady-state levels of Rad6 protein in control (C) and at various periods of recovery. B, RT-PCR analysis of Rad6B and GAPDH mRNA expression.

Fig. 3. Effect of actinomycin D on ADR-induced Rad6B mRNA transcription and decay. A, MCF10A cells were either untreated (control) or treated with ADR for 1 h, rinsed and replaced with fresh drug-free medium, and Rad6B mRNA levels determined by slot blot analysis at 0-48 h of recovery. B, At 4 h of recovery (0*) cells from ADR and control groups were treated with actinomycin D and Rad6B mRNA levels were measured at 0.5 to 8 h following actinomycin D treatment. C, Percent of Rad6B mRNA remaining was determined by densitometry and expressed relative to actinomycin D treated control (0*) and ADR-treated (0*) samples.

Fig. 4. Effect of actinomycin D and cycloheximide on ADR-induced Rad6 and p53 protein expression. MCF10A cells were either untreated (control) or treated with ADR for 1 h and allowed to recover in drug-free media for 0-24 h. Untreated or ADR-treated cells at 0 h of recovery were also treated with actinomycin D (5 μg/ml) or cycloheximide (10 μg/ml), and Rad6B (A) protein levels determined by Western blot analysis at indicated time points. Blots were stripped and reprobed with p53 CM-1 polyclonal antibody (C). Levels of Rad6B (B) or p53 (D) protein levels were determined by densitometry and results expressed relative to those at 0 h in the respective groups.

Fig. 5. Rad6B overexpression confers resistance to cisplatin and ADR. A, Steady-state levels of Rad6 protein in selected MCF10A clones stably expressing empty vector (MCF10A-Neo), antisense-Rad6B (AS2), or wild type Rad6B (Rad6 clones 2 and 5). B, Cells were treated with various doses of cisplatin (B) or ADR (C) for 5 or 3 days, respectively, and number of viable cells determined by trypan blue exclusion. D, Proliferation rates of MCF10A-Neo, AS2, Rad6 clone 2 and Rad6 clone 5 cells.10 $X10^{-3}$ cells were seeded in 24-well plates and number of viable cells determined at indicated times by counting trypan blue excluded cells. Results are expressed as mean of three independent experiments; bars, ± S.E. ($P<0.01$).

Fig. 6. Adriamycin treatment enhances distribution and localization of Rad6 protein to the chromatin. MCF10A cells, untreated (control) or treated with ADR (0.1 μg/ml, 1h and allowed to recover for 6 h) were treated with formaldehyde at 37°C for 30 min to allow for *in vivo* cross-linking of proteins or protein-DNA complexes as described in Materials and Methods. Nuclei were isolated, lysed, sonicated and subjected to isopycnic centrifugation on CsCl cushions. Fractions were collected

from the bottom and analyzed for DNA by agarose gel electrophoresis or for the presence of Rad6, p53, Rad18, PCNA, phosphohistone H3 (a chromatin marker) and carboxypeptidase (a cytoplasmic marker) proteins by Western blot analysis. Since no carboxypeptidase-immunoreactive bands were observed in the fractions, the negative strips are not shown. Note the increase in localization of Rad6 protein in DNA containing high density fractions in ADR-treated cells. Also, note the presence of p53-immunoreactive doublet bands and co-localization of Rad6, p53, Rad18, PCNA and the positive chromatin marker phosphohisone H3 in DNA-containing fractions in ADR-treated cells.

Fig. 7. Postreplication DNA repair capacities of MCF10A-Neo, AS2 and Rad6B clone 5 cells by sedimentation velocity method. Actively growing cells, control or cisplatin-treated (0.5 μg/ml, 30 min), were rinsed and replaced with fresh drug-free media to allow recovery for 6h. Control and cisplatin-treated cells were pulsed labeled with ^{3}H-thymidine for 45 min or chased with 10-fold excess of cold thymidine for 90 min following pulse labeling. Cells were lysed, irradiated briefly and then subjected to ultracentrifugation on alkaline sucrose gradients. Fractions were collected from the bottom and aliquots of fractions subjected to TCA precipitation for determination of acid precipitable radioactivity. Results are expressed as a percent of total TCA precipitable radioactivity in the samples prior to ultracentrifugation. A and B, sedimentation profiles of control and cisplatin-treated cells, respectively. A' and B', sedimentation profiles of control and cisplatin-treated cells that were chased with unlabeled thymidine following pulse-labeling. Closed arrowhead, open arrowhead and arrow indicate positions of λ DNA, Hind III-cut λ DNA and linearized pGL-3 Basic Vector, respectively.

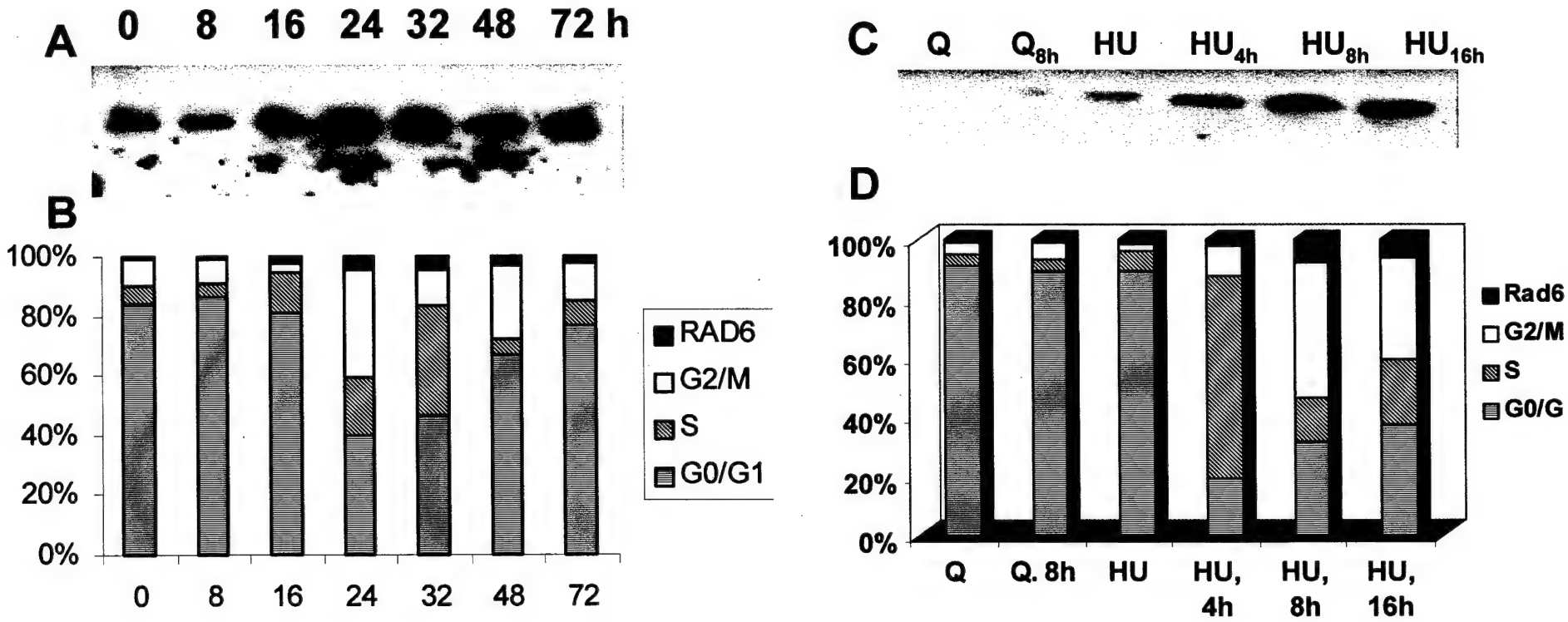
A
0 8 16 24 32 48 72 h
B
100%
80%
60%
40%
20%
0%
0 8 16 24 32 48 72
RAD6
G2/M
S
G0/G1
C
Q
Q8h
HU
HU4h
HU8h
HU16h
D
100%
80%
60%
40%
20%
0%
Q
Q. 8h
HU
HU, 4h
HU, 8h
HU, 16h
Rad6
G2/M
S
G0/G

Fig. 1

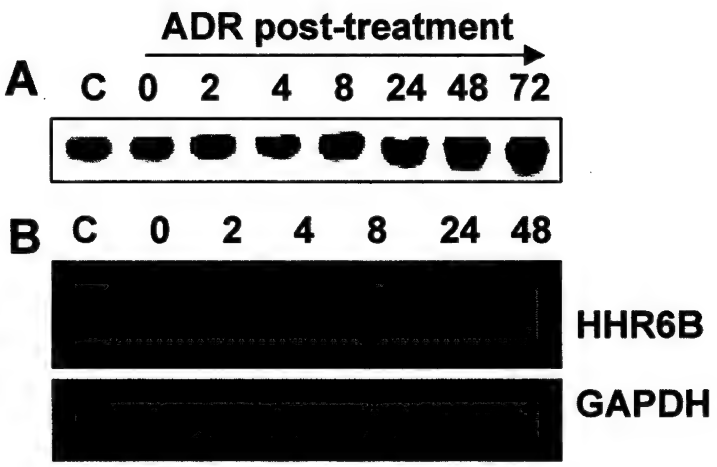

Fig. 2

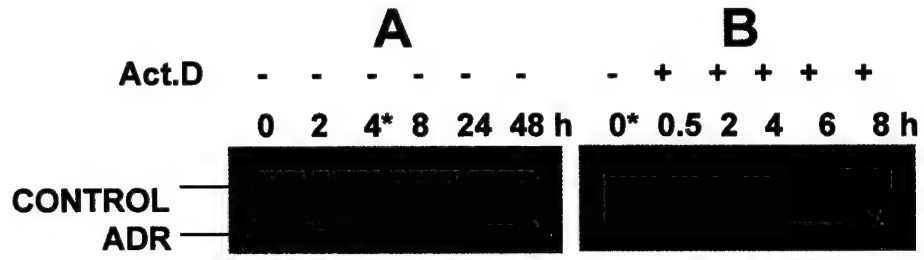
A
B
Act.D
- - - - - -
- + + + + +
0 2 4* 8 24 48 h
0* 0.5 2 4 6 8 h
CONTROL
ADR

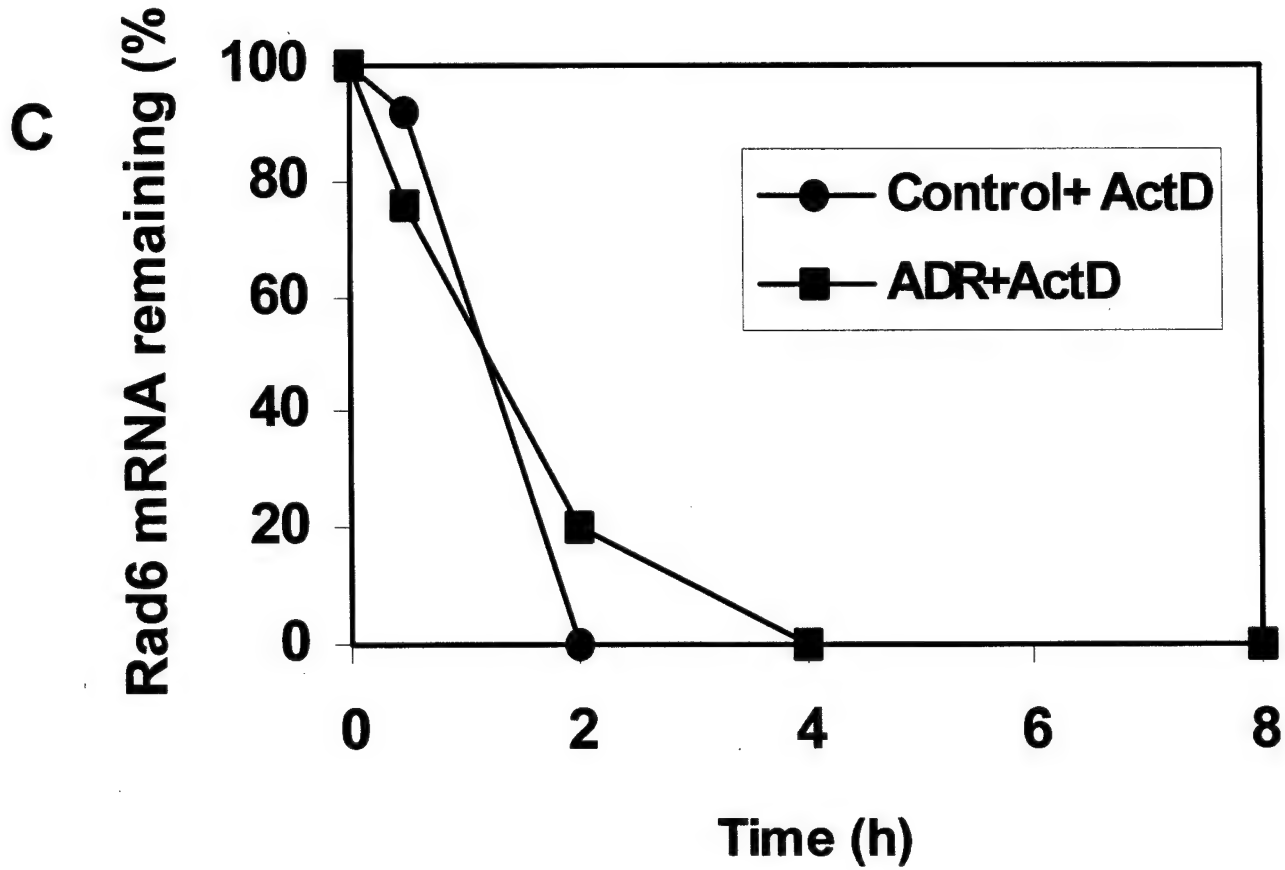
C
Rad6 mRNA remaining (%
100
80
60
40
20
0
0
2
4
6
8
Time (h)
Control+ ActD
ADR+ActD

Fig. 3

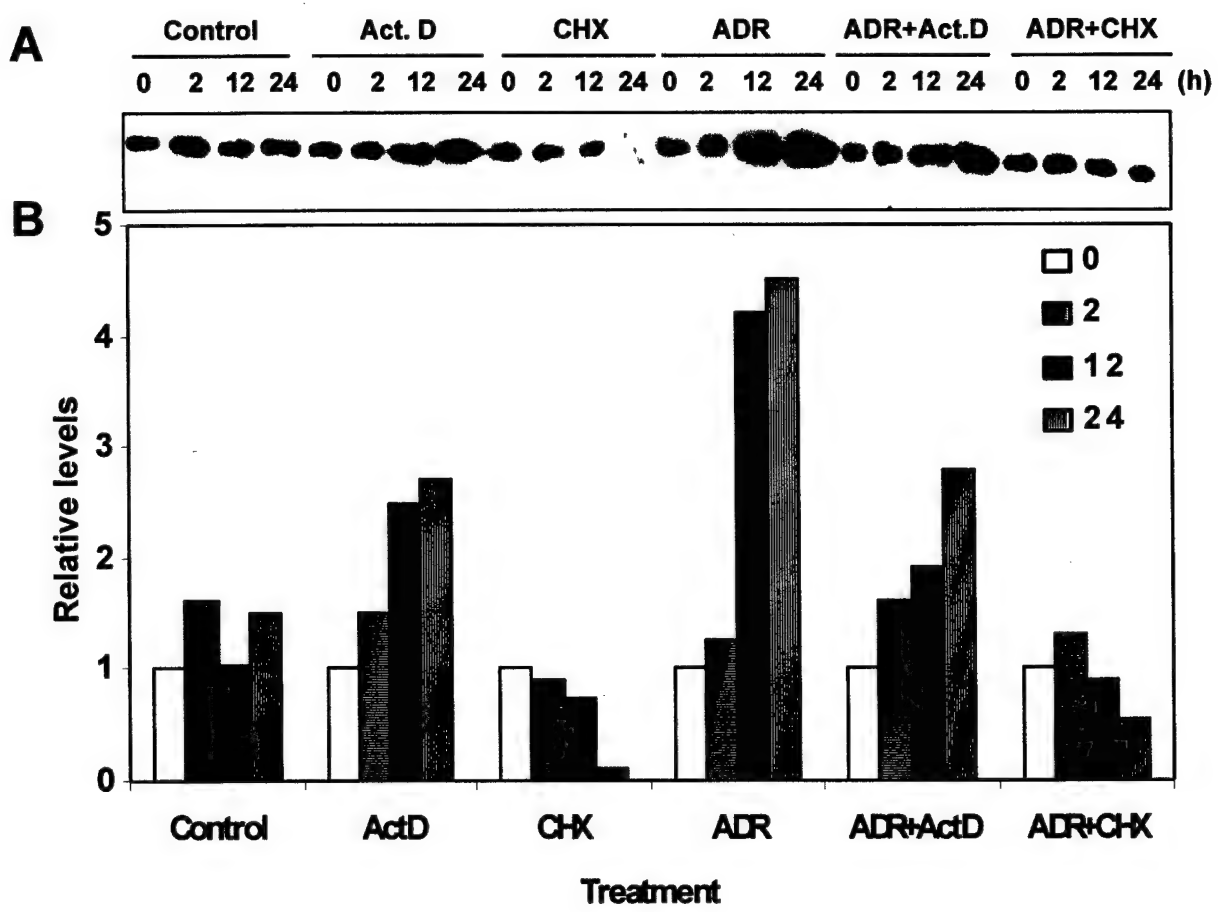
A
Control
Act. D
CHX
ADR
ADR+Act.D
ADR+CHX
0 2 12 24 0 2 12 24 0 2 12 24 0 2 12 24 0 2 12 24 0 2 12 24 (h)
B
Relative levels
0
1
2
3
4
5
0
2
12
24
Control
ActD
CHX
ADR
ADR+ActD
ADR+CHX
Treatment

Fig. 4

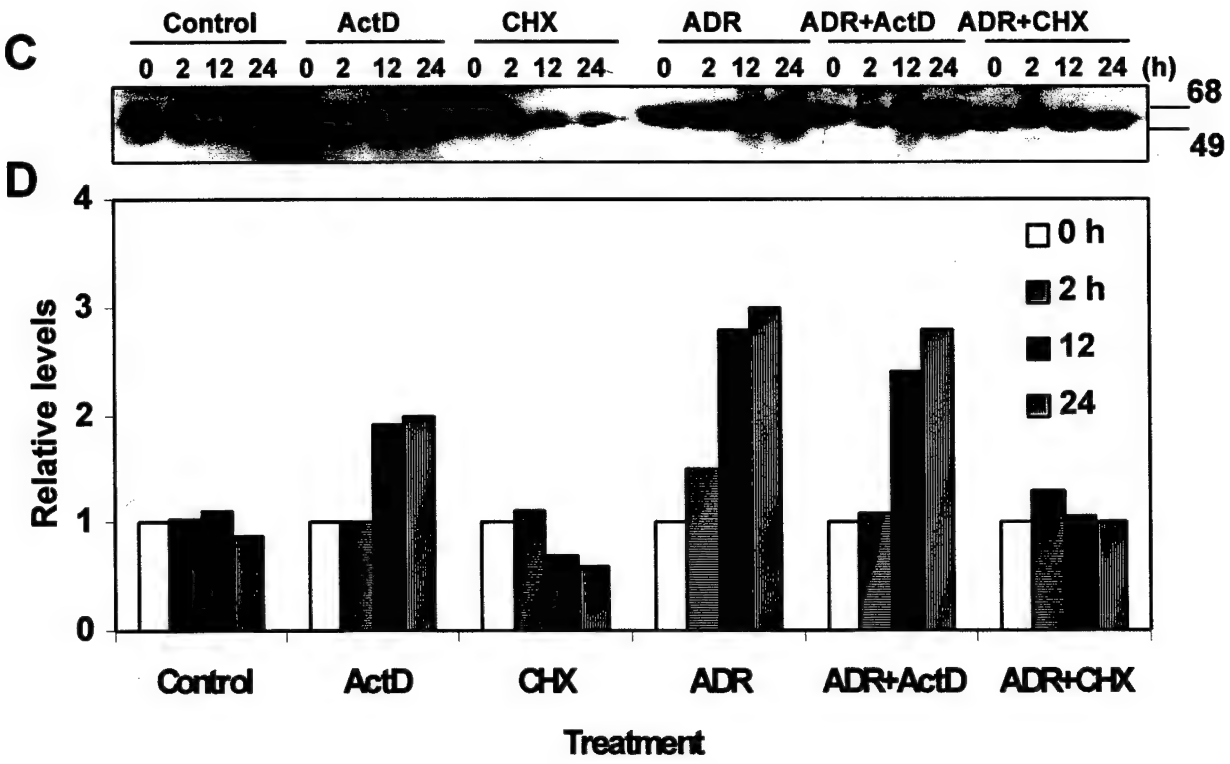
C
Control
ActD
CHX
ADR
ADR+ActD
ADR+CHX
0 2 12 24 0 2 12 24 0 2 12 24 0 2 12 24 0 2 12 24 0 2 12 24 (h)
68
49
D
Relative levels
0
1
2
3
4
0 h
2 h
12
24
Control
ActD
CHX
ADR
ADR+ActD
ADR+CHX
Treatment

Fig. 4

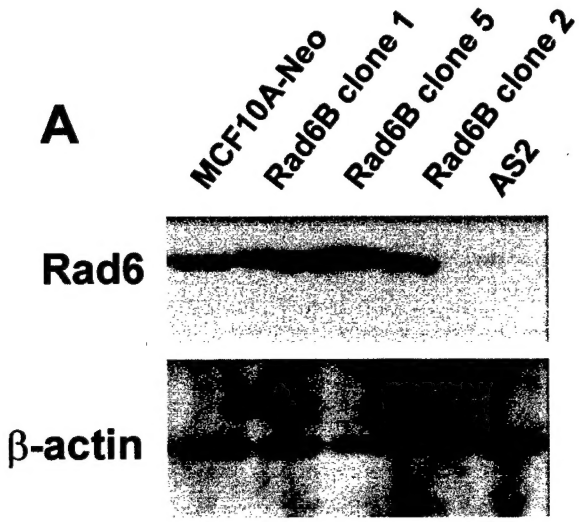
A
MCF10A-Neo
Rad6B clone 1
Rad6B clone 5
Rad6B clone 2
AS2
Rad6
β-actin

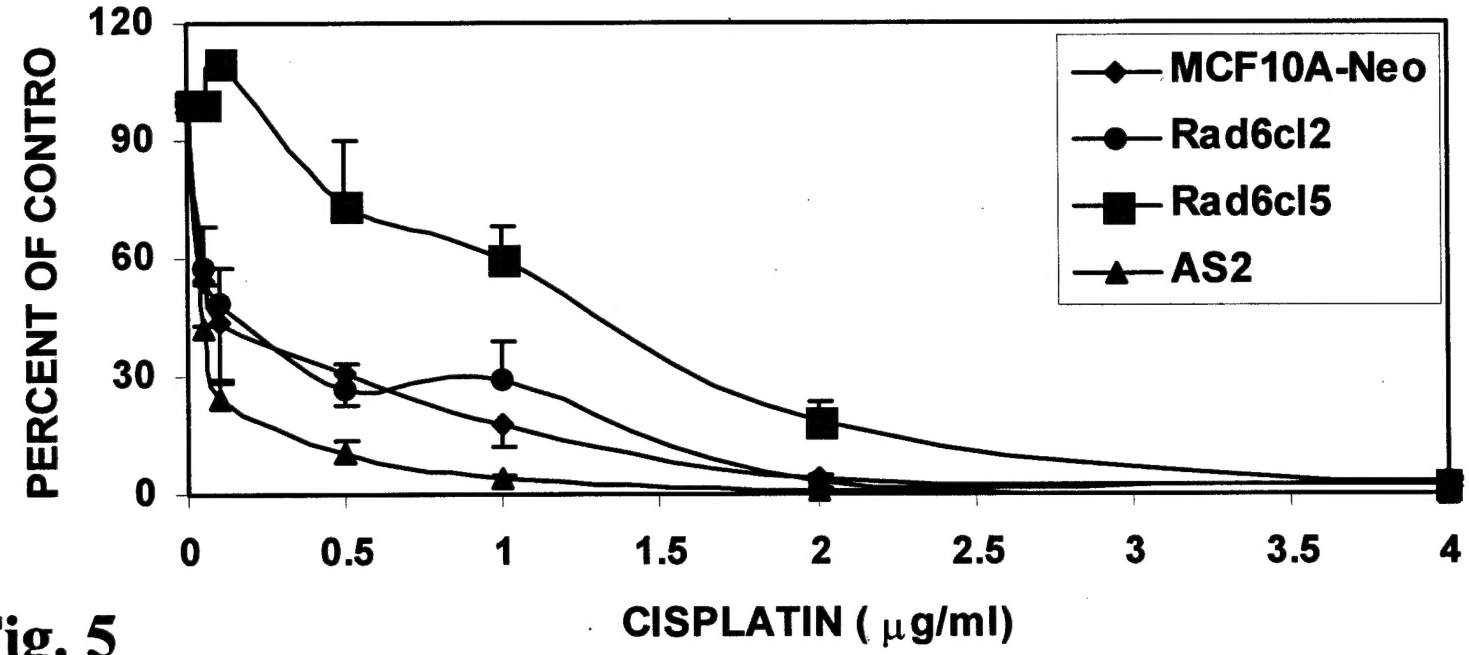
B
PERCENT OF CONTRO
120
90
60
30
0
0
0.5
1
1.5
2
2.5
3
3.5
4
CISPLATIN (μg/ml)
MCF10A-Neo
Rad6cl2
Rad6cl5
AS2

Fig. 5

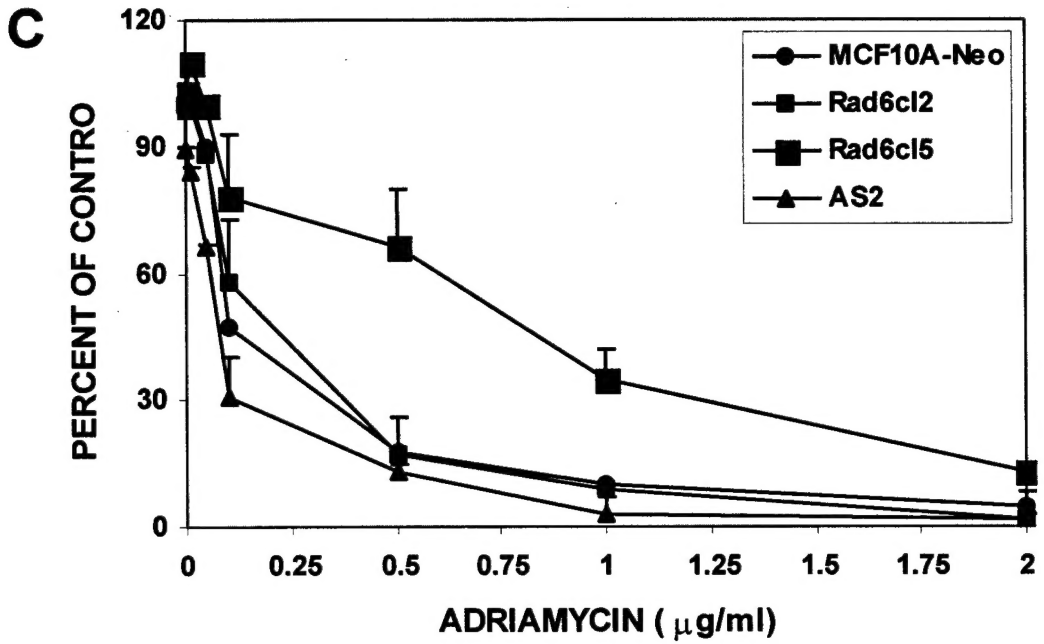
C
120
90
60
30
0
PERCENT OF CONTRO
0
0.25
0.5
0.75
1
1.25
1.5
1.75
2
ADRIAMYCIN (μg/ml)
MCF10A-Neo
Rad6cl2
Rad6cl5
AS2

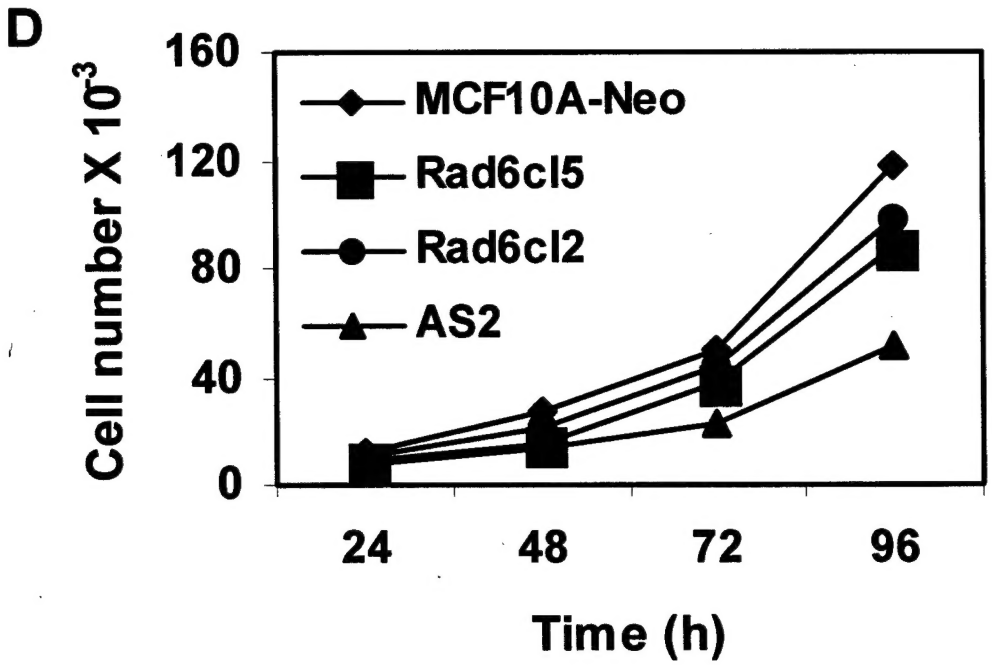
D
160
120
80
40
0
Cell number X 10-3
24
48
72
96
Time (h)
MCF10A-Neo
Rad6cl5
Rad6cl2
AS2

Fig. 5

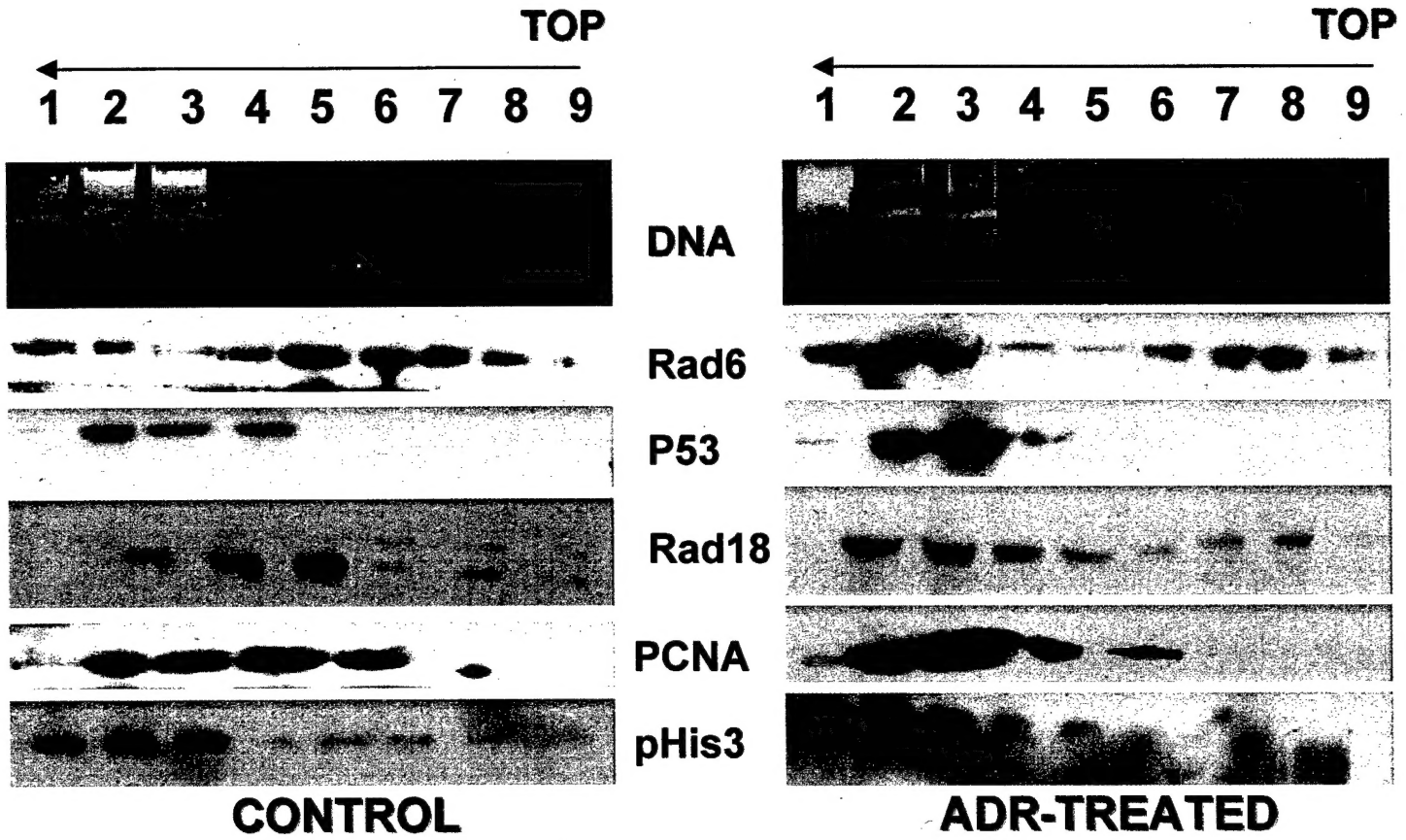
TOP
1 2 3 4 5 6 7 8 9
TOP
1 2 3 4 5 6 7 8 9
DNA
Rad6
P53
Rad18
PCNA
pHis3
CONTROL
ADR-TREATED

Fig. 6

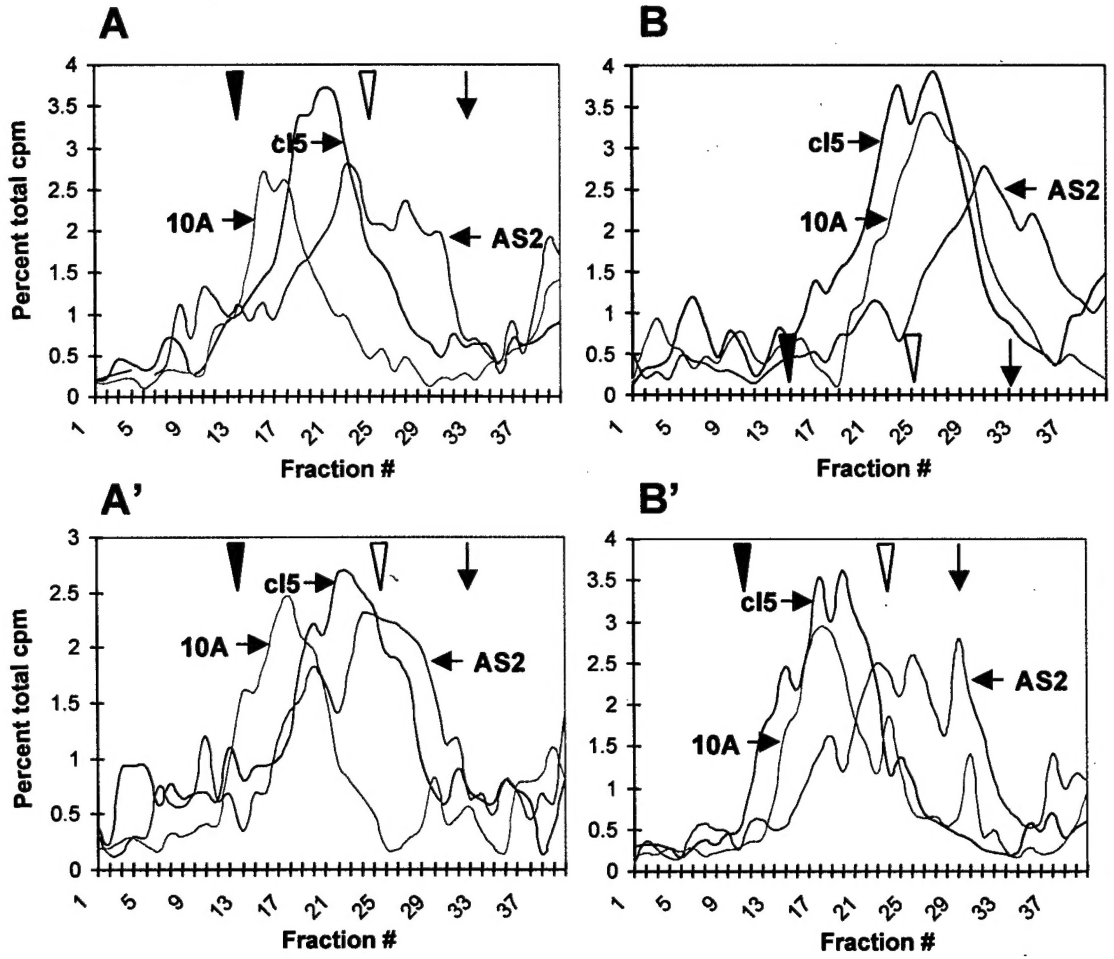

Fig. 7